UC San Diego

UC San Diego Electronic Theses and Dissertations

Title

Uncovering Opposing Roles of Shp2 in Myc-driven Hepatocellular Carcinoma

Permalink

https://escholarship.org/uc/item/1tz6x0h8

Author

Chen, Wendy Shuwen

Publication Date

2021

Peer reviewed|Thesis/dissertation

eScholarship.org Powered by the California Digital Library
University of California

UNIVERSITY OF CALIFORNIA SAN DIEGO

Uncovering Opposing Roles of Shp2 in Myc-driven Hepatocellular Carcinoma

A dissertation submitted in partial satisfaction of the requirements for the degree

Doctor of Philosophy

in

Biology

by

Wendy Shuwen Chen

Committee in Charge

Professor Gen-Sheng Feng, Chair
Professor Diana Hargreaves
Professor Lifan Lu
Professor Tannishtha Reya
Professor Karl Willert

2021

Copyright

Wendy Shuwen Chen, 2021

All rights reserved

The dissertation of Wendy Shuwen Chen is approved, and it is acceptable in quality and form for publication on microfilm and electronically.

University of California San Diego

2021

TABLE OF CONTENTS

LIST OF FIGURES

LIST OF SCHEMA

LIST OF TABLES

LIST OF ABBREVIATIONS

AAV: Adeno-associated virus

AFP: α-fetoprotein

Akt: protein kinase B

ALB: Albumin

ANOVA: analysis of variance

β-catenin: catenin beta 1, encoded by CTNNB1

bHLHZip: Basic-helix-loop-helix-leucine zipper domain

BKO: hepatocyte-specific β-catenin knockout

CCL#: Chemokine (C-C motif) ligand. Family: CCL2, CCL4, CCL5, CCL9, CCL17

CCL4 treatment: Carbon tetrachloride treatment

CCL4: Macrophage inflammatory protein 1β (MIP-1 β)

CCR: chemokine receptor

CDK: Cyclin-dependent Kinases

CDK4: Cyclin dependent kinase 4

c-Jun: Transcription factor AP-1

CK19: Keratin 19

Clec4f: C-type lectin domain family 4 member F

c-Met: tyrosine-protein kinase Met, Also: HGFR (hepatocyte growth factor receptor)

Cre: Cre recombinase

CT: Computed Tomography (scan)

CXCL10: CXC Motif Chemokine Ligand 10

CXCR3: CXC Motif Chemokine Receptor 3

DDC: N,N'-Dicyclohexylcarbodiimide

DEN: diethylnitrosamine

E-box: enhancer box

EGF: Estrogen growth factor

ERK: mitogen-activated protein kinase 1

F4/80: EGF module-containing mucin-like receptor, ADGRE1 gene

FBS: fetal bovine serum

FBXW7: F-Box and WD repeat domain containing 7

Gab1: GRB2-associated binding protein 1

Gab2: GRB2-associated binding protein 2

Gapdh: glyceraldehyde 3-phosphate dehydrogenase

GLOBOCAN: Global Cancer Observatory, World Health Organization

GRB1: growth factor receptor-bound protein 1

GRB2: growth factor receptor-bound protein 2

GS: Glutamine Synthetase

GSEA: gene set enrichment analysis

GSK3β: Glycogen Synthase Kinase 3 beta

H&E: Hematoxylin and Eosin, staining method

HB: Hepatoblastoma

HBV: Hepatitis B Virus

HCC: Hepatocellular Carcinoma

HCV: Hepatitis C Virus

HGF: Hepatocyte growth factor

HNF4α: Hepatocyte nuclear factor 4 alpha

HTVi: Hydrodynamic tail vein injection

ICC: Intrahepatic cholangiocarcinoma

IR: insulin receptor

KO: Knockout

Lect2: leukocyte cell derived chemotaxin 2

MAPK: mitogen-activated protein kinase

Max: Myc associated factor X

MDM: Monocyte-derived macrophage

MIF: Macrophage migration inhibitory factor

MRI: Magnetic Resonance Imaging (scan)

MTORC: mammalian target of rapamycin

Myc (MYC): cellular myelocytomatosis oncogene

NAFLD: non-alcoholic fatty liver disease

NASH: Non-alcoholic steatohepatitis

NF-kB: nuclear factor kappa-B

NPC: Non-parenchymal cell

OmoMyc: a 91-residue c-Myc dominant negative mini-protein

PCNA: Proliferating cell nuclear antigen

PDGFR: Platelet-derived growth factor receptor

PD-L1: Programmed death-ligand 1

PI3K: phosphatidylinositol 3-kinase

PIK3CA / PI3K: Phosphoinositide 3-kinase

Pten: phosphatase and tensin homolog

PTPN11: tyrosine-protein phosphatase non-receptor type 11, encodes Shp2 protein

Raf: Rapidly accelerated fibrosarcoma

Ras: Rat sarcoma

RTK: Receptor tyrosine kinase

RxRα: Retinol x receptor alpha

SB: Sleeping Beauty Transposase

SBKO: Hepatocyte-specific Shp2 and β-catenin knockout

scRNA-seq: Single cell RNA-sequencing

SH2: Src homology region 2

Shp2: SH2 containing protein tyrosine phosphatase-2 (Gene: PTPN11)

SKO: hepatocyte-specific Shp2 knockout

SOS – Sone of Sevenless

TCF4: Transcription factor 4. Also: TCF, TCF7l2

TCGA: The Cancer Genome Atlas network

TNFα: Tumor necrosis factor alpha

TRP53: tumor protein 53

tSNE: t-distributed stochastic neighbor embedding

VEGFR: vascular endothelial growth factor receptor

Wnt: Wingless-related integration site

WT: wild type TCGA: The Cancer Genome Atlas

YAP: Yes-associated protein 1

ACKNOWLEDGEMENTS

This work was guided from its beginnings by my advisor, Dr. Gen-Sheng Feng. Thank you for guiding me through my graduate school experience and for assisting me in furthering my scientific thinking and rigor. I am deeply grateful for your constructive advice. Thank you to my lab members, both past and present: for answering all of my inquisitive questions and patching up all the holes in my scientific knowledge and logic. Your support has been invaluable throughout the years.

A special thank you to my committee members who helped guide and support my scientific work over these years: Drs Li-fan Lu, Diana Hargreaves, Karl Willert, and Tannishtha Reya. All of you have provided extremely helpful advice and discussion on the direction, scope, and details of my project. Thank you.

I would not have gotten to where I am without the guiding hands of my previous mentors. Thank you to Dr. Ke Zhang, my undergraduate PI who taught me techniques and provided advice that I use to this day. Thank you to Dr. Holger Wesche at Amgen, for a fleeting summer insight into the workings of Biotechnology and challenges in therapeutic development of cancer field. Thank you to Dr. Anil Bhushan for the opportunity to acquire so many mouse-related techniques and a wider perspective on disease-based research.

My friends throughout my graduate student career, I thank you for all the amazing adventures that have again and again renewed my creativity and motivations. Your emotional and moral supports have been indispensable throughout this experience. Jacey Liu, thank you for being an amazing lab mate and even better friend. Amy Pribadi (and Ollie!) thanks for being an amazing housemate and friend. The above, along with

Ye Zhang and Youtong Huang, we had some of the best little adventures around San Diego. All of your insights on life and the pursuit of all of our little hobbies and foodie adventures have made me better-rounded as a person. Also thanks to my DND group, who have managed to successfully sustain 6+ years of campaigning, snacking, and the pursuit of the nerdiest gaming hobby. And finally to my cat, Evie, for your existence, reminding me of the importance of eating and sleeping on time, and the simple happy things in life. I owe all of you infinite gratitude.

Thank you to family. Thanks Dad, for supporting me through a field of which you have little knowledge. You started to read scientific material for us to discuss, and I see your supportive confidence in my ability to succeed. Thanks Mom for your support in my wellbeing, encouraging me to develop as a person, and find myself outside of work. My little brother, Daniel, you do you. Thanks for being there for me.

Chapters 1-4 are adapted from material that has been submitted for publication: Chen, Wendy S.*; Liang, Yan*; Zong, Min*; Liu, Jacey L.; Kaneko, Kota; Hanley, Kaisa L.; Zhang, Kun; Feng, Gen-Sheng. (2021) “Single Cell Transcriptomics Reveals Opposing Roles of Shp2 in Myc-driven Liver Tumor Cells and Microenvironment.” (In Press, *Cell Reports*) Single-cell RNA sequencing data was generated by Yan Liang, upon request by dissertation advisor or myself. The dissertation author was a primary investigator and the first author of this material.

Funding and training opportunities were provided by NCI grants R01CA236074, R01CA176012 and R01CA239629 to G.S.F.; NIH “Growth Regulation and Oncogenesis” Training Grant T32CA009523 to W.S.C. Special thank you to Drs. X. Chen (UCSF), G. Lemke (Salk), N. Varki and K. Willert (UCSD) for reagents and histopathological

analysis. We also thank the Genomics, Histology, Flow Cytometry, and Animal Facility at UCSD for technical assistance.

VITA

2011-2014	Research Assistant I, University of California Los Angeles
2012	Undergraduate intern, Amgen Inc. (South San Francisco, California)
2010-2014	Bachelor of Sciences, University of California Los Angeles
2014-2015	Research Associate II, University of California San Francisco
2015-2021	Doctor of Philosophy, University of California San Diego

PUBLICATIONS

Chen WS*, Liang Y*, Zong M*, Liu JJ, Kaneko K, Hanley KL, Zhang K, & Feng GS. (2021) Single Cell Transcriptomics Reveals Opposite Roles of Shp2 in Myc-driven Liver Tumor Cells and Microenvironment. (In Press, *Cell Reports*)

Kaneko K, Liang Y, Liu Q, **Chen WS**, & Feng GS. (2021) CD133+ Intercellsome Mediates Direct Cell-Cell Communication to Offset Intracellular Signaling Deficit. (Manuscript under Revision: *Nature Cell Biology*) BioRxiv, doi:10.1101/2021.07.14.451852

Luo Y, **Chen WS**, Lee J, Feng GS, & Newton I. (2019) Stress Conditions induced by locoregional therapies stimulate enrichment and proliferation of liver cancer stem cells. *J. of Vascular and Interventional Radiology*. 10.1016/j.jvir.2019.02.026

Liu J*, Li Y*, **Chen WS**, Zong M, Kaneko K, Xu R, Karin, M, & Feng GS. (2018) Ptpn11/Shp2 Is Required for Liver Tumorigenesis Driven by c-MET, b-Catenin and PIK3CA. *J. of Hepatology*, S0168-8278 (18) 30131-4.

Zhang K, Liu J, Truong T, Zukin E, **Chen W**, & Saxon A. (2017) Blocking allergic reaction through targeting surface-bound IgE with low affinity anti-IgE antibodies. *J. Immunol.* 198(10):3823-3834.

Chen, WS, Zhu, HH, & Feng, GS (2016). Treating leukemia at the risk of inducing severe anemia. *Experimental Hematology*, 44(5), 329-331.

FIELD OF STUDY

Major Field: Biological Sciences

Studies in Molecular Biology

Professor Gen-Sheng Feng

ABSTRACT OF DISSERTATION

Uncovering Opposing Roles of Shp2 in Myc-driven Hepatocellular Carcinoma

by

Wendy Shuwen Chen

Doctor of Philosophy in Biology

University of California San Diego, 2021

Professor Gen-Sheng Feng, Chair

Hepatocellular Carcinoma is a complex cancer with little available targeted therapeutics, in part due to the recently uncovered paradoxical roles of previously defined proto-oncogenes. Our lab and others have identified overexpression and ablation of several proto-oncogenes sensitizes the liver towards HCC development. Previously, our lab demonstrated hepatocyte deletion of *Shp2/Ptpn11* in mice (SKO) ablates HCC driven by cMET/Δ90-β-catenin or cMET/PIK3CA mutant yet greatly accelerates chemical carcinogen-induced HCC. To clarify the complex mechanisms of Shp2 function in HCC, we examined the contribution of the proto-oncogene Myc, which acts downstream of Shp2. The aim of my dissertation research is to elucidate the novel

murine model of Myc-driven tumorigenesis in SKO background, examining cell-intrinsic and extrinsic factors driving tumor development. Original work in this dissertation shows that Myc-driven hepatocellular carcinoma (HCC) is dramatically aggravated in mice with hepatocyte-specific *Ptpn11/Shp2* deletion. Using single-cell RNA-sequencing coupled with functional assays, we show Shp2-knockout livers exhibit defective clearance of tumor-initiating cells by altering macrophage polarization and reducing macrophage phagocytic activity, resulting in an immune-suppressive environment. We uncover that Myc-induced tumors selectively develop from the rare Shp2-positive hepatocytes in Shp2-deficent liver. Myc-driven oncogenesis depends on intact Ras-Erk signaling, driven by Shp2, to sustain Myc stability. Basal Wnt/β-catenin signaling is upregulated in Shp2-deficient liver, which is further augmented by Myc transfection. Ablating *Ctnnb1* suppresses Myc-induced HCC in Shp2-deficient livers, revealing an essential role of β-catenin in assisting in Myc-driven HCC. Consistently, Myc overexpression and *CTNNB1* mutations are frequently co-detected in HCC patients with poor prognosis. Single cell RNA sequencing and functional *in vivo* / *in vitro* data together reveal the complex mechanisms of liver tumorigenesis driven by cell-intrinsic oncogenic signaling of Myc, supported by intrinsic Shp2 and β-catenin signaling, in cooperation with a tumor-promoting microenvironment generated by disruption of Shp2 proto-oncogenic signaling.

INTRODUCTION

1. Current state of Hepatocellular Carcinoma

Hepatocellular carcinoma (HCC) represents a vast majority (75-85%) of primary liver cancer, a highly fatal disease with rising incidences and mortality worldwide. In 2018, GLOBOCAN reported 841,080 new cases of liver cancer worldwide, accounting for 4.7% of all cancers with a fatality count of 781,631, or 8.2% of cancer deaths that year (Bray et al., 2018). Incidences arise predominantly in older male populations with highest rates in Eastern Asia regions and northern Africa (Bray et al., 2018).

Liver cancer results from a series of proliferative, metabolic and architectural alterations over chronic hepatic disorders (El-Serag, 2011; Llovet et al., 2016). The main risk factors include chronic infection with hepatitis B virus (HBV), hepatitis C virus (HCV), aflatoxin exposure, increased alcohol intake, and type II diabetes. The rise in obesity prevalence and subsequent chronic fatty liver disease strongly contributes to the rising incidences of liver cancer predicted over the next decade in previously low-risk HCC regions worldwide.

Rarer types of liver cancer include intrahepatic cholangiocarcinoma (ICC) and hepatoblastoma (HB). ICC is cancer arising from cells in the bile ducts of the liver and is staged and treated through other options. It differs from HCC due to the rarity (10-20%) and the origin, from non-parenchymal cells or hepatocytes converted to biliary cells. Therefore, ICC has different genetic and metabolic dysregulations from hepatocyte-based cancers. Hepatoblastoma, on the other hand, is a rare form of liver cancer arising

primarily in child populations under 4 years of age (Kim et al., 2005; Russell and Monga, 2018). Hepatoblastoma has a characteristic “Blue” appearance on tissues dyed with hematoxylin and eosin (H&E) , the preferred histopathological staining, with small dedifferentiated cells and aggressive growth and invasion into surrounding liver tissue (Zheng et al., 2017b). Hepatoblastoma is treated with surgery and chemotherapy.

HCC, characteristically resistant to chemotherapy, is often diagnosed at late stages with limited treatment options. Patients with chronic alcohol abuse, hepatitis viral infection, or toxin-induced liver damage often progress to advanced liver scarring (cirrhosis). 3-5% of patients will advance to hepatosteatosis, characterized by increased liver inflammation, and a lesser percentage of those patients to liver cancer (Bray et al., 2018). Other individuals with chronic fatty liver disease (NAFLD) may progress to non-alcoholic steatohepatitis (NASH), advanced liver scaring (cirrhosis), and further to co-incidence with liver cancer.

Patients with these pre-malignant conditions are at increased risk for liver cancer and ideally undergo surveillance screening every 6 months, with ultrasound or for the serum biomarker alpha-fetoprotein (AFP). Increased levels of AFP remain the most prominent serum biomarker, with ~50% co-incidence with liver cancer; leaving many HCC patients undiagnosed through blood detection methods. Other serum biomarkers such as des-gamma-carboxy prothrombin (DCP) and Glypican-3 (GPC3) have been suggested as new blood biomarkers; however these targets are not widely accepted due to inadequate detection rates (Lawton, 2020). Liver ultrasound, the most common screening test, can detect tumors of comparable size but is hindered by interference in

patients with chronic liver diseases; interference due to increased adipose tissue, cirrhosis, and fibrosis.

Many patients forgo screening due to the asymptomatic nature of chronic liver damage. Chronic liver damage is often healed by efficient and persistent liver regeneration. Over time, chronic regeneration results in inflammatory fibrosis and build-up of proliferative DNA damage and ROS, but often does not yield visible symptoms until severe metabolic dysfunction. Patients with dramatically reduced liver function will have jaundiced membranes, yellowing of skin and mucosal membranes from bilirubin build-up. Therefore, a major contributing factor to HCC fatality is lack of early diagnosis and co-incidence with chronic liver disease.

Once liver cancer is detected through ultrasound or the serum biomarker AFP, then confirmed through CT or MRI, histopathology is used to determine liver cancer stage and treatment options. HCC is identified primarily through histopathological means, by staining biopsies to identify cell and tissue pathological alterations. Many HCC types can be histopathologically identified, though clinical identification stages are not unified (Yang and Heimbach, 2020). BCLC (Barcelona Clinic Liver Center) is a clinical staging system prevalently used in Europe which ranks liver cancer from 0, and A-D (Forner et al., 2010; Llovet et al., 1999). Patients categorized as BCLC D have terminal stage HCC whereby cancerous cells show vascular invasion, distant metastasis, and patients are not candidates for transplantation surgery due to worsening liver function (Forner et al., 2010).

The primary treatment therapy for liver cancer patients is surgical resectioning, radiofrequency ablation, and cryotherapy. Historically, liver cancer was treated through

surgical resectioning, utilizing the liver's effective regeneration to restore liver mass and function after resecting tumor masses. However, liver cancer patients with concurrent chronic liver disease, itself a common precursor to liver cancer, often have impaired liver function and regeneration. Therefore a portion of resectioning efforts fail due to the poor condition of the non-cancerous liver regions being unable to sustain essential metabolic functions for life. A novel surgical technique recently developed, transarterial embolization (TACE) effectively ablates only tumor tissue, allowing for less liver removal than traditional surgical resectioning (Llovet et al., 2016; Yang and Heimbach, 2020). Because the liver is a detailed architecturally structured organ with high blood perfusion, transarterial embolization can place small beads into blood vessels to cut off blood flow to the tumor. New advances combine radiation therapy by using radioactive beads to not only block blood flow but also apply localized radiation therapy to the tumor and surrounding areas (Llovet et al., 2016). Surgeons and researchers are exploring ways to refine and enhance new surgical ablation therapies and combine these physical therapies with targeted therapeutic drugs and new immunotherapy efforts. Though surgical techniques are advancing, drug-based therapeutics are still necessary for a significant portion of patients presenting with late-stage inoperable disease.

2. Targeted therapeutics for HCC

Very few targeted therapeutics for HCC have been approved. Despite low therapeutic benefits, the multi-tyrosine kinase inhibitor Sorafenib (Nexavar®, Bayer) (multi-kinase VEGFR, PDGFR, and Raf/Mek/Erk inhibitor) had remained the frontline

drug for advanced HCC for a decade (Llovet et al., 2016). Sorafenib, in part, works to upregulate p53 and suppress FOXM1 to inhibit HCC growth and invasion, as well as alter tumor-associated macrophage growth factor secretion (Sprinzl et al., 2015; Wei et al., 2015). Unfortunately, Sorafenib has a reported average life extension of only 3 months, and the full mechanistic details of Sorafenib's therapeutic effect on HCC have not fully been identified.

Breakthroughs within the last 3 years have yielded FDA approval for several targeted inhibitors, originally developed for other cancers, in inoperable HCC. All are predominantly multi-kinase inhibitors where one major target is VEGFR2: lenvatinib, regorafenib, cabozantinib, and ramucirumab (Huang et al., 2020) (Figure 0.1). Spurred by the success of this recently identified VEGFR2 target, research efforts have been further motivated to discover new inhibitor treatments to better target HCC and extend patient survival.

Cancer immunotherapy for HCC is just starting to uncover the intricacies and vulnerabilities of HCC through immune targeting. In 2020, the FDA recently approved a new frontline treatment: The combination therapy of atezolizumab (VEGFA inhibitor) and bevacizumab (PD-L1 inhibitor) achieved significantly better overall and tumor progression-free survival rates than sorafenib in unresectable HCC (Finn et al., 2020). Currently, several ongoing phase III clinical trials involve combination therapy with immune checkpoint inhibitors, previously approved multi-kinase inhibitors, and surgical techniques (TACE) in the hopes of improving curative rates. Recent studies on combination treatments, of targeted inhibitors and immunotherapies, often show synergistic therapeutic efficacy (Wen et al., 2019). A more rigorous understanding of the

crosstalk between host immune system, liver cells and tumor cells will pave way for the future of effective treatments HCC.

Large-scale multi-platform analyses and data mining are leading the field in precision medicine and identification of therapeutic targets. The Cancer Genome Atlas (TCGA) network is a cancer genomics program characterizing primary cancer and normal cancer samples. Data mining of liver cancer (LIHC) and HCC sections of TCGA's pan-cancer atlas revealed common genetic alterations correlating to human patient data (Cancer Genome Atlas Research Network. Electronic address and Cancer Genome Atlas Research, 2017). The most commonly mutated genes in HCC are TRP53 (31%), CTNNB1 (27%), ALB (13%) and genes with significant DNA copy number alterations include RB1 del (deletion) (19%), CDKN3A del (13%), NCOR1 del (22%). Epigenetic analysis of gene hyper-methylation, in HCC tumor samples as compared to paired normal tissue, revealed distinct subgroups as related to clinical or molecular attributes such as HCV, HBV, CTNNB1 mutations, or TERT promoter mutations. The TCGA data set validated several commonly altered genes and essential pathways but also uncovered unique targets, such as the amplification of MET and VEGFA loci, indicating HCC sensitivity to multi-kinase inhibitors other than sorafenib. These data also suggested characteristics of low immune invasion may predict positive patient response to immunotherapy. Using these and other patient data sets, data mining can assist in precision medicine by indicating potential patient groups for future targeted therapeutics and clinical trials.

The high recurrence rate of HCC, in combination with often already present chronic liver disease and accumulation of inflammatory fibrosis, often hinders HCC

patient recoveries. Conclusively, future development of more efficacious mechanism-based therapeutics requires deeper understanding of cell-intrinsic and -extrinsic tumorigenic signals intertwined in the liver.

3. Shp2 (PTPN11) as a proto-oncogene

Shp2 (Src homology 2 domain-containing phosphatase 2) is a cytoplasmic SH2-containing tyrosine phosphatase encoded by *Ptpn11* signaling immediately downstream of several essential receptor tyrosine kinases and cytokine receptors (Feng and Pawson, 1994; Liu and Qu, 2011; Neel et al., 2003). Shp2 has two SH2 domains, a PTP phosphatase domain, and a C-terminal tail with phosphorylatable tyrosine residues (Tyr542 and Tyr580). At basal state Shp2 is autoinhibited in a ‘closed’ conformation whereby the PTP domain and SH2 domains associate using noncovalent bonds. With SH2-domain docking residues phosphorylated, Shp2 shifts into the ‘open’ active conformation, freeing the PTP domain for phosphatase activity.

Unlike typically inhibitory phosphatases, Shp2 uniquely promotes several MAPK signaling cascades involved in driving proliferation, extracellular signaling, etc. Shp2 transduces signal for Ras-Erk, Jak-Stat, PI3K-Akt, and NF-kB pathways, though the detailed mechanisms of Shp2 activity are not yet fully understood (Figure 0.2) (Bard-Chapeau et al., 2006; Han et al., 2015; Ran et al., 2016). While its phosphatase activity is important in signal transduction, Shp2 also has scaffolding activity interacting with GRB2, Gab1, and Gab2 (Bard-Chapeau et al., 2006; Ran et al., 2016). Notably, Shp2 phosphatase activity promotes the Ras/Erk proliferative pathway by inhibiting negative

signals such as Gab1, Paxillin and Sprouty, and drives signaling of RTKs such as cMet, Epidermal growth factor receptor (EGFR), and insulin receptor (IR) (Bard-Chapeau et al., 2006; Hanafusa et al., 2004). Despite extensive study, the identified interactive partners cannot fully explain all of Shp2's activities.

Shp2 nuclear functions are not as well studied. At low cell density, Shp2 can translocate to the nucleus through activity from non-phosphorylated YAP/TAZ and interact with binding partners such as paraformin and Stat5 (Takahashi et al., 2011). Shp2 can stimulate TCF/LEF and TEAD-induced genes, as well as dephosphorylate Stat1 and Stat3 to inhibit their transcriptional activity, as well as prevent nuclear export of TERT to promote telomerase activity (Liu and Qu, 2011; Takahashi et al., 2011; Tsutsumi et al., 2013; Wu et al., 2002).

Shp2's various functions were also identified in blood cell types. Shp2 deletion in embryonic stem cells inhibited development of these knock-out cells into erythroid and myeloid progenitors while Rag2-knockout blastocysts with Shp2 deletion were inhibited from lymphopoiesis to T and B cell stages. Thus Shp2 is required for establishment and differentiation of all blood cell lineages. In cytokine and immune signaling, Shp2 is an important mediator of inhibitory receptor signaling, recruited to T-lymphocyte-associated antigen (CTLA-4), programmed death-1 (PD-1), among others (Liu and Qu, 2011).

Shp2 was the first tyrosine phosphatase identified as a proto-oncogene, with dominant active mutations detected in leukemia and various solid tumors (Chan and Feng, 2007). Shp2-activating mutations are generally hyper-activating mutations; often destabilize the 'closed' formation to induce increased phosphatase activity and downstream Ras/Erk activation. Shp2 mutations have been identified in many human

diseases, such as Leopard syndrome, Noonan syndrome, hematological malignancies, and several solid tumors (Digilio et al., 2002; Tartaglia et al., 2004; Tartaglia et al., 2001; Tartaglia et al., 2003; Yuan et al., 2003). In solid tumors, Shp2 mutations are rarer and manifest alongside other oncogenic driver dysregulations. For example, the gain-of-function $Shp2^{E76K}$ mutant, found in colorectal cancer, leads to a persistently exposed PTP domain, allowing for constant phosphatase activity. This same $Shp2^{E76K}$ mutant supports glioblastoma multiforme and lung cancer through promoting tumors via the Erk pathway. In liver cancer, Shp2 overexpression correlates with poor patient prognosis and drives aggressive HCC progression (Han et al., 2015).

Our lab generated a murine knockout model of Shp2 with Albumin-cre mediated deletion of floxed Shp2 alleles in hepatocyte cell populations. Shp2 ablation in hepatocytes inhibits immediate-early liver regeneration in response to partial hepatectomy (Bard-Chapeau et al., 2006). Shp2-knockout livers induce metabolic alterations, such as dysregulation of bile acid synthesis through the suppression of FXR signaling, resulting in increase in bile acid levels, enlarged gallbladder phenotype, and chronic hepatobiliary complications (Li et al., 2014a).

Shp2 deletion in hepatocytes exacerbated HCC induced by the chemical carcinogen diethylnitrosamine (DEN), as well as dramatically accelerated liver tumorigenesis driven by non-alcoholic steatohepatitis (NASH) with additional Pten-deficiency (Bard-Chapeau et al., 2011; Luo et al., 2016). Aged SKO mice also develop hepatocellular adenoma, suggesting build-up of chronic liver damage from metabolic dysregulation in combination with a pro-tumorigenic microenvironment induced by hepatic deletion of Shp2 is tumorigenic (Bard-Chapeau et al., 2011). However, deleting

Shp2 in hepatocytes ablated HCC driven by oncogene pairs cMet / ΔN90β-catenin or cMet / PIK3CA^{H1047R} mutant in hydrodynamic tail vein injection (HTVi) models (Liu et al., 2018). Other proto-oncogenes, such as β-catenin, Jnk, Akt, and cMet also show these contradictory results, whereby both overexpression and knockout of proto-oncogenes sensitizes the liver to tumorigenesis (Das et al., 2011; Feng, 2012; Li et al., 2012; Nejak-Bowen et al., 2010; Takami et al., 2007). These results indicate unique circumstances in the liver and the paradoxical roles of classical proto-oncogenes acting as both proto-oncogenes and tumor suppressors in liver tumorigenesis.

Shp2 has been a promising therapeutic target due to its position as a significant transducing signal for multiple growth factor signals and regulatory control of MAPK signaling. Increased tyrosine phosphatase activity is a hallmark of a variety of cancers. Shp2 has recently become a druggable target, with the advent of allosteric Shp2 inhibitors. Early studies suggest chemical inhibition of Shp2 effectively suppressed proliferation of solid cancers driven by RTK oncogenic signals but without KRas activating mutations (Chen et al., 2016). Continuing studies indicate some cancers with KRAS^{G12C} mutation are also vulnerable to allosteric Shp2 inhibitors, broadening the effective range (Kerr et al., 2021). Several Shp2 inhibitors are in early stage clinical trials for MAPK- or RTK-driven solid cancers without activating KRas mutations, and in combination with other RTK and Ras targeting molecules (LaMarche et al., 2020; Liu et al., 2021). Drug resistance may come from Shp2 activating mutations, which resists allosteric inhibition via conformational changes and tilts the balance of activated Shp2 to allow for Ras/Erk activation in defiance of Shp2 inhibition.

Shp2 is an important phosphatase regulator of various cell signaling functions, including proliferation, survival, and various differentiations. The dual inhibiting and promoting effects of Shp2 on liver cancer is yet to be elucidated. Recent studies identified some Shp2 metabolic and proliferative functions in the liver, but also hints at further complex mechanisms that require further elucidation.

My dissertation project contributes to our understanding of the paradoxical nature of Shp2 signaling by identifying how Shp2 deletion in liver may contribute to tumor permissiveness while intrinsic Shp2 signaling assists in tumor development.

4. Introduction to c-Myc

C-Myc (MYC) is a master transcription factor in the basic-helix-loop-helix-leucine zipper (bHLHZip) protein family. Myc is a nuclear proto-oncogene which functions as a transcriptional regulator for cell proliferation, differentiation, metabolism, apoptosis, angiogenesis, immune response, protein translation, and stem cell de-differentiation (Felsher and Bishop, 1999; Gabay et al., 2014; Zheng et al., 2017b). Oncogenic Myc activation can override homeostatic cell growth and proliferation, causing unstoppable DNA replication, global changes in metabolism, activation of angiogenesis, and inhibition of innate immune responses (Dang, 2012; Miller et al., 2012; Zheng et al., 2017b). Changes in the tumor microenvironment, such as perturbances from normal regulation of either innate or adaptive immune systems, may also assist in accelerating or introducing permissiveness to tumorigenesis.

Myc functions by dimerizing with Max, which is ubiquitously expressed, and acts as a transcriptional regulator for E-Box regions, DNA sequences of CACGTG (or variations of the sequence) in enhancer regions. Myc binding to various DNA sites is strongly dependent on cell-type, intrinsic expression level, and epigenetic state of the cell. Other heterodimer partners of Max, such as Mxd family of proteins, can function as negative regulators of Myc transcriptional activity by competing for Max binding on E-box regions. For example, Max-Myc binding to TRRAP at E-box sites leads to histone H3 and H4 acetylation, recruitment of RNA Poly II and amplification in transcription for the target gene (Gomez-Roman et al., 2003).

The stable active form of Myc is p-Myc^{S62}, induced by phosphorylation of the serine-62 site by ERK, JNK, or CDK. Further phosphorylation on its T58 site (p-Myc$^{S62+T58}$) will trigger degradation events, binding to FBXW7 and leading to proteosomal degradation. Overexpression of oncogenic RAS and ERK can lead to increased Myc expression as a result of increased protein stability (Farrell and Sears, 2014; Sears et al., 1999). Presence of Shp2, signaling transducer for several upstream growth factors, can directly affect duration of Myc activity and degradation through Src and ERK activity as shown *in vitro* (Ren et al., 2010). Her4 can change cancer metabolic states by promoting Myc stabilization through CIP2a-induced increase in activated-Myc and GSK3b-mediated decrease in Myc^{T58}.

Oncogenic Myc is an essential hallmark gene of cancer. Aberrant expression of c-Myc (Myc), primarily in the form of deregulation (overexpression) and gene translocations, is implicated in ~50% of human cancers and a wide variety of experimentally induced animal cancer models (Dang, 2012; Schaub et al., 2018). With

amplification of Myc expression, Myc signaling loses specificity and increases binding activity at low-affinity E-box sites and enhancer regions.

Normal cell fate with Myc activation is strongly dependent on level and context of Myc expression, whereby strongly induced Myc is associated with apoptosis and accumulated DNA damage, while moderately high expression leads to proliferative arrest and senescence (Gabay et al., 2014; Grandori et al., 2003). Overexpression of Myc alone results in apoptosis due to the presence of checkpoints controlled by TRP53, PTEN, and ARF that respond to deregulated cell proliferation by inducing cell death or cell cycle arrest (Felsher and Bishop, 1999; Gomez-Roman et al., 2003; Grandori et al., 2003; Hoffman and Liebermann, 2008). Many cancer models utilized oncogenic Myc's synergy with TRP53 knock-out, which effectively drives tumorigenesis in organs such as liver, prostate, breast, colon, and melanoma (Dang, 2013).

Myc activity is crucial in growing and proliferating cells, but also essential in the metabolic reprogramming required for uncontrolled biomass build-up and proliferation noted in tumor cells. Myc controls glutaminolysis and glycolysis, and thus ATP production, by transcriptional regulation of nearly all enzymes and nutrient transporters along the process (i.e. SLC2A1, SLC1A5) (Gao et al., 2009). Myc can also directly activate cyclin-dependent kinase 4 (CDK4) and E2 factor (E2F) to advance cell cycle and DNA replication, and may also have transcriptionally independent roles in binding to DNA replication complex during early stages of S phase.

Myc has a pivotal role in cell growth and proliferation through its precise regulation of E-box binding sites. However, aberrant Myc transcriptional activity, the

uncontrolled binding and activation of E-box binding sites on nonspecific promotors, makes Myc a dangerous oncogene in tumorigenesis.

5. Myc's roles in Liver Cancer

Despite the wide-breadth of research on Myc regulation several details still need elucidation. Myc overexpression and amplification is commonly detected in aggressive HCC with poor prognosis, pediatric HB, and in liver diseases such as Alcoholic liver disease (Abou-Elella et al., 1996). In the liver, Myc can promote hepatocyte proliferation, as an immediate-early response gene in response to liver injury. Development of neonatal liver requires Myc expression; however, postnatal hepatocyte proliferation and liver regeneration after partial hepatectomy can be Myc-independent (Sanders et al., 2012).

Several murine liver cancer models involve overexpression of Myc coupled with oncogenic growth factors (EGF, HGF, TGFa), knockout of checkpoint regulator p53, or in addition to chronic chemically-induced liver injury (DDC, CCL4 treatments) (Beer et al., 2008; Heindryckx et al., 2009; Klocke et al., 2001; Ohgaki et al., 1996; Thorgeirsson and Santoni-Rugiu, 1996; Zheng et al., 2017b). The crosstalk between Myc and growth factors accelerates tumor progression, where mice with overexpression of Epithelial growth factor (EGF) and Myc lead to rapid HCC occurrence in 12-18 weeks due to selection and subsequent growth of neoplastic cells (Heindryckx et al., 2009). In contrast, co-expression of Hepatocyte growth factor (HGF) and Myc surprisingly delays tumorigenesis, whereby HGF selectively inhibits proliferation of neoplastic cells, while

stimulating normal hepatocyte proliferation (Thorgeirsson and Santoni-Rugiu, 1996). Addition of hepatotoxins severely accelerates Myc-driven HCC; DDC or CCl4-treated mice have HCC occurrence in 4-5 weeks, compared to non-treated models at 180 days. Myc alone is inefficient to drive HCC in transgenic C57BL/6 mice, which required co-expression of another oncogene or simultaneous deletion of a tumor suppressor (Murakami et al., 1993; Ruiz de Galarreta et al., 2019). In my dissertation, we generated a Myc-driven HCC model in the Shp2 knockout background, uniquely inducing HCC using overexpression of Myc oncogene with knockout of a canonically upstream oncogene (Shp2).

Remarkably, genomic analysis has revealed frequent co-occurrence of Myc amplification and *CTNNB1*/β-catenin mutations in HCC and hepatoblastoma patients as well as in mouse HCC models (Bisso et al., 2020; Cairo et al., 2008; Calvisi et al., 2001; Network., 2017; Ruiz de Galarreta et al., 2019). β-catenin is a well-known driver of Myc expression and activity. B-catenin binds to the Myc promoter and drives Myc-induced proliferation and metabolic control (Yochum et al., 2008). Epistatic analysis in the intestines indicate Myc was positioned downstream of APC/β-catenin (Sansom et al., 2007; Wong et al., 2015). However, Myc deletion did not suppress the effect of APC loss in the liver, although β-catenin removal did (Reed et al., 2008). Hepatic zonation of ammonia metabolizing enzymes controlled by Wnt/β-catenin signaling was also found independent of Myc (Burke et al., 2009). Recent studies proposed several cooperative mechanisms for Myc and β-catenin in driving liver tumorigenesis, including YAP/TAZ activation (Bisso et al., 2020) or immune suppression (Ruiz de Galarreta et al., 2019).

Therefore, the mechanisms of cooperativity between Myc and β-catenin may be unique in the liver-specific context and require further investigation.

Myc-dependent cancers often suffer “oncogene addiction”, whereby withdrawal of Myc drastically reduces tumor growth and increases hepatocyte re-maturation by inhibiting proliferation, remodeling metabolic processes, inducing senescence, and altering microenvironment (Dauch et al., 2016a; Jain et al., 2002; Li et al., 2014b; Shachaf et al., 2004). Myc-induced liver tumorigenesis, if assisted by other genetic events such as loss of p53 or mutant Ras, can relieve Myc-addiction temporarily by sustaining tumorigenesis until the reoccurring tumors reactivate Myc expression (Choi et al., 2011; Gabay et al., 2014). Recurring Myc-driven HCC are more aggressive than primary tumors before Myc withdrawal (Dolezal et al., 2017).

The state of Myc-addiction within cancers, along with the prevalence of Myc amplification in various cancers, makes Myc an attractive therapeutic target. However, Myc is considered a high risk target due to potential serious side effects from inhibition of a master regulator protein essential for various aspects of cell metabolism, survival, and proliferation. Recent advances in Myc inhibitors yielded very few molecules with efficacy. A recent success, OmoMYC, has been shown to block Myc transactivational activity and shows efficacy in inhibiting Myc-driven tumor growth, with minimal side effects (Savino 2011, PLOS One).

Despite this singular recent success, historically, inhibiting Myc has been a struggle due to Myc’s lack of enzymatic activity, nuclear localization, and lack of hydrophobic pockets for small-molecule drug targets to bind. Just as Shp2 inhibitors have proven efficacious in treating MAPK- or RTK-driven solid cancers, similar

alternative- therapeutics for indirect suppression of Myc may prove highly advantageous. Efforts have also focused on disruption of the Myc-Max tetradimer, thus disrupting downstream target genes but critically do not address Myc's independent transcriptional activity. Myc directly regulates components of both Glucose and Glutamine metabolic processes and Myc-dependent HCC are metabolically addicted (Miller et al., 2012; Zheng et al., 2017b). Due to these metabolic vulnerabilities, inhibitor studies have targeted key enzymes and transporters in glycolysis and glutaminolysis in therapeutic research efforts, to screen for synthetically lethal inhibitors (Carroll et al., 2015). Recent successes in combination therapies of small molecule inhibitors with immunotherapies, to utilize both genetic and immune-based vulnerabilities of Myc-driven cancers, may also prove fruitful for advancing clinical therapeutics against the wide variety of Myc-driven cancers.

In my dissertation, I uncover targetable vulnerabilities in Myc-driven carcinogenesis, intrinsically linked to the Shp2-Ras-Erk signaling pathway, to innate immune-related tumor clearance abilities, and explore organ-specific interactions with Wnt/β-catenin signaling.

6. Single-Cell RNA-sequencing to dissect intra-organ interactions

Single-Cell RNA-sequencing (scRNA-seq) is considered the successor to traditional bulk RNA-sequencing. Previously bulk RNA-sequencing was performed on samples of multiple cell types and were unable to distinguish individual cell interactions. scRNA-seq allows for precise detection of gene expression profiles of individual cells,

thus allowing for applications of large data analysis in fields such as temporal tracking of genetic mutations in patient samples, parenchymal ligand-receptor interactions, and new discoveries of transient or hard to detect cell identities and subtypes(Chen et al., 2020; Hou et al., 2016; van Dijk et al., 2018). Recent studies uncovered novel intrahepatic macrophage subpopulations within human liver (MacParland et al., 2018) and identified distinct characteristics of exhausted CD8+ T cells and regulatory mechanisms that may affect response to immunotherapy (Zheng et al., 2017a). Novel algorithms can utilize scRNA-seq data to reconstitute liver zonation and metabolic processes through transcriptome analysis of individual hepatocytes (Halpern et al., 2017). scRNA-sequencing is not without flaws and introduces sequencing bias in the form of artificially-low detection rates. In my dissertation project, we overcame this inherent flaw in scRNA-seq data with the utilization of MAGIC, a data imputation algorithm, to normalize gene expression utilizing data from neighboring cells. Unlike most scRNA-seq studies in the liver, my dissertation combines scRNA-sequencing analysis with functional techniques to effectively uncover, validate, and explain intricacies of our HCC model. Our application of single cell RNA-sequencing to characterize all hepatic cell types in mouse liver allowed us to uniquely uncover cell-specific mechanisms at critical points in tumor development.

7. Objective and experimental design of the dissertation project

Previously, we showed hepatocyte deletion of Shp2 in mice (SKO) ablated HCC driven by c-MET/Δ90-β-catenin or c-MET/PIK3CA mutant (Liu et al., 2018). These

results indicate the importance of Shp2 in promoting the Ras/Erk signaling cascade downstream of RTKs. However, the same also exacerbated HCC induced by chemical carcinogen diethylnitrosamine (DEN), as well as dramatically accelerated liver tumorigenesis driven by non-alcoholic steatohepatitis (NASH) with additional Pten-deficiency (Bard-Chapeau et al., 2011; Luo et al., 2016). These studies introduce the paradoxical role of proto-oncogene Shp2 in liver oncogenesis. In the c-Met/Δβ-catenin driven model of HCC, deletion of Shp2 is suspected to inhibit tumorigenesis by impairing signaling transduction, through Shp2, and thus inhibiting appropriate cell growth and proliferation. Therefore we bypassed the Shp2 signaling by utilizing Myc, an oncogene located further downstream Shp2.

Given these results, my PhD dissertation project focused on dissection of oncogenic signaling mechanisms by utilizing Myc-driven tumorigenesis. We examined a murine HCC model with overexpression of Myc, downstream of the Ras/Erk signaling cascade, and critical processes in how bypassing Shp2 signaling induces tumorigenesis in SKO mice.

Based on previous work in the lab, we predicted that oncogenic Myc, unlike previous cMet-driven tumor models would evade requirement of Shp2 expression and thus, coupled with the inflammatory microenvironment previously examined in SKO mice, be able to generate tumors. The murine model of Myc-driven HCC was generated uniquely in cancer-resistant C57BL/6 mice with Albumin-cre-driven hepatic deletion of Shp2/Ptpn11. By utilizing the recently developed Hydrodynamic tail vein injection (HTVi) method, we mimicked human cancers by transfection of Myc oncogene in selective

hepatocytes without further perturbing the background liver. This novel Myc model is fast (4 weeks), allowing for comparatively effective study of tumor development.

We combined single cell RNA-sequencing (scRNA-seq) with molecular and functional assays and deciphered complex mechanisms of Myc-driven liver tumorigenesis by analyzing mechanisms relating to tumor development intrinsic to Myc-driven tumor cells and crosstalk with immune tumor microenvironment. We first utilized scRNA-sequencing to characterize all hepatic cell types in mouse liver and uncover cell-specific mechanisms at critical time points in tumor development. Histopathology analysis and scRNA-seq data revealed altered macrophage polarization and defective phagocytosis in SKO liver, allowing for tumor permissive microenvironment. Genetic ablation of proto-oncogene Shp2 does not inhibit, but rather promotes Myc-dependent tumor development through establishment of a strongly tumor suppressive immune microenvironment.

We discovered that Shp2 was also required cell-autonomously for hepato-oncogenesis driven by a downstream nuclear oncogene Myc, by maintaining an intact Ras/Erk pathway upstream of Myc. Crosstalk of Myc and Shp2 involves Ras/Erk signaling, whereby Shp2 and Erk expression contribute to increased Myc protein stability. Our findings reveal, despite attempting to bypass Shp2 signaling by utilizing Myc, Myc-dependent tumor development still required intrinsic Shp2 signaling for tumor development.

Furthermore, we provide the first evidence here that Myc-induced HCC requires Wnt/β-catenin signaling, although Myc has been widely known as a downstream target

of β-catenin. Using this novel tumor development model, we revealed Myc-driven carcinogenesis is dependent on both Ras/Erk and Wnt/β-catenin signaling pathways.

These findings diagnosed targetable vulnerabilities in Myc-driven HCC, elucidated mechanisms in complexity of oncogenic signaling crosstalk distinct in the liver, and demonstrated cooperativity of scRNA-sequencing analysis and functional assays.

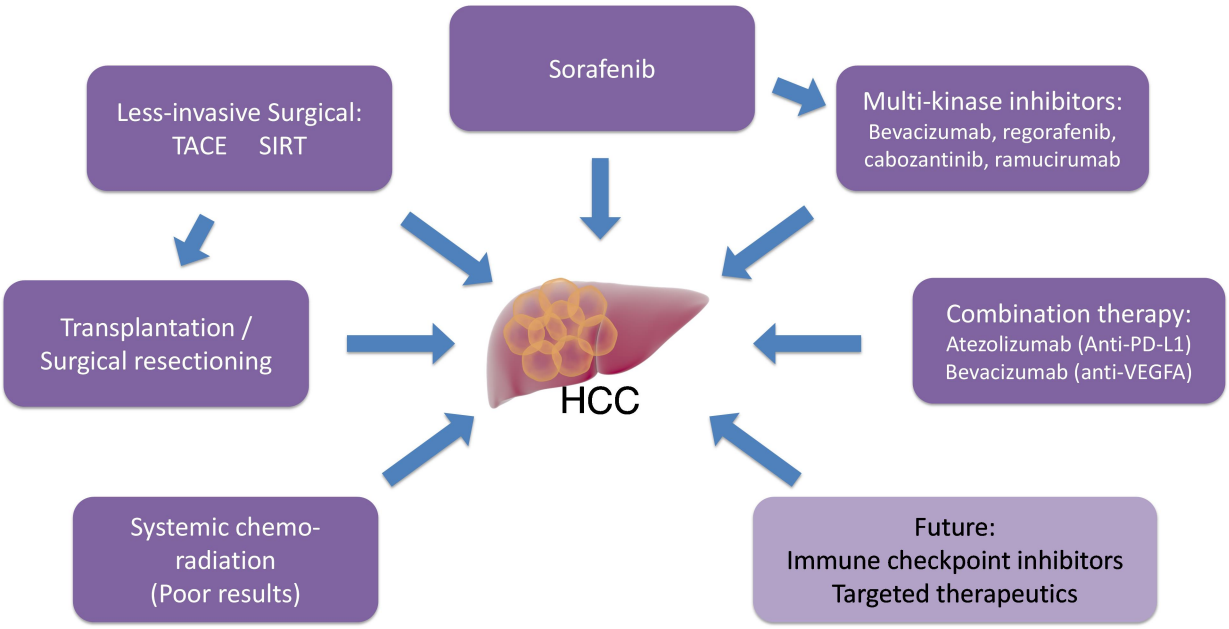

Figure 0.1: Therapeutics in treating liver cancer
Summary of possible therapeutics in treatment of liver cancer.

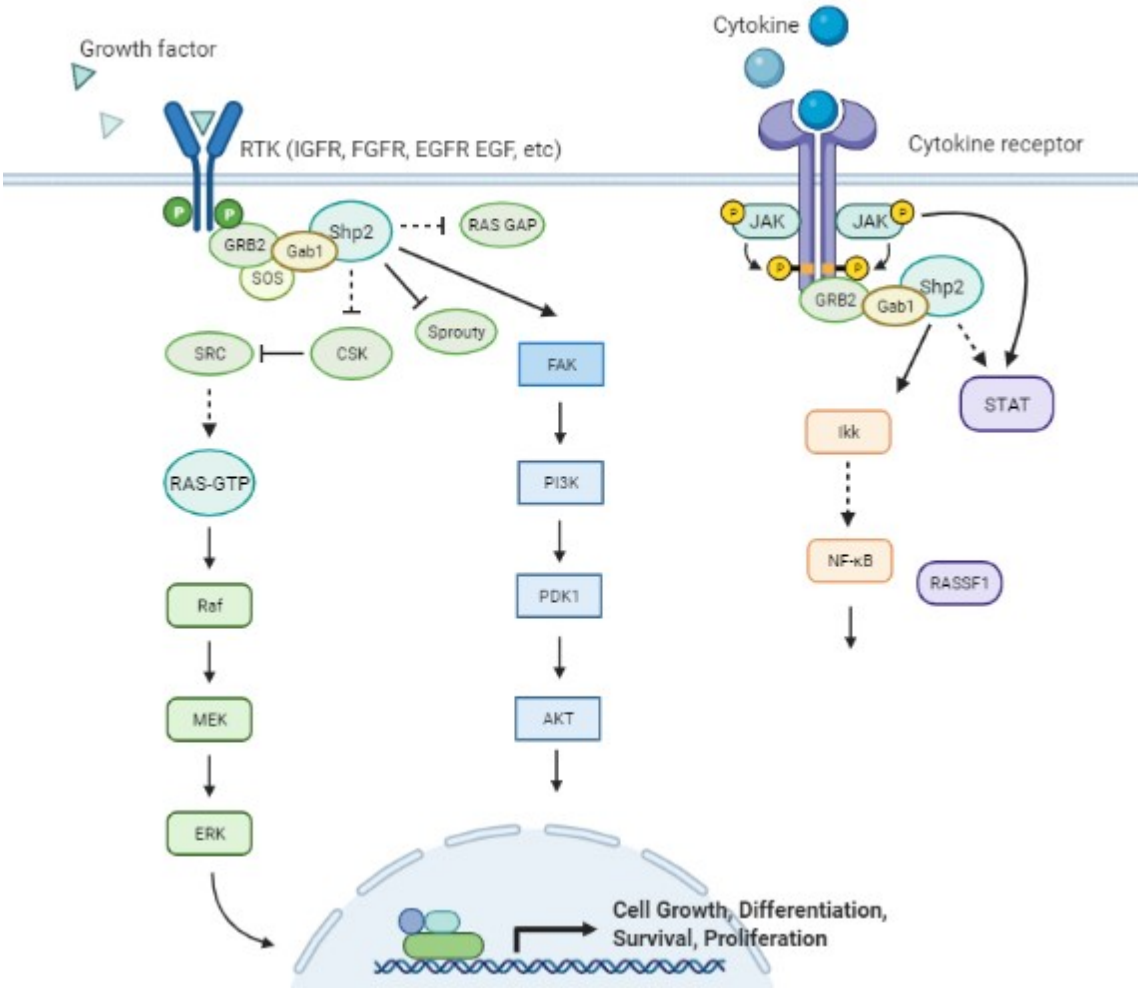

Figure 0.2: Shp2 signaling in various pathways
Summary of select Shp2 downstream signaling pathways that drive cell growth, differentiation, survival, and proliferation. Generated with the assistance of Biorender.com.

MATERIALS AND METHODS

Mouse strains

All animals used in this study were C57BL/6J background. All mouse husbandry and procedures were performed in compliance with protocols approved by the UCSD Institutional Animal Care and Use Committee (Protocol: S09108). The SKO ($Shp2^{hep-/-}$) and BKO ($B\text{-}catenin^{hep-/-}$) mouse lines were generated using Albumin-Cre as previously described (Bard-Chapeau et al., 2006). The SBKO line was generated by breeding SKO and BKO mouse lines together, maintaining heterozygous expression of Albumin-cre. Mice lacking the Albumin-cre transgene were used as wild-type controls (WT).

Genotyping was performed by PCR analysis of genomic DNA extracted from tail snips using the following primers (5'-3') to detect the presence of the transgene (Cre) or differences in length between wild-type and floxed alleles (Shp2, β-catenin):

Cre forward: GCG CGG TCT GGC AGT AAA AAC TAT C;

Cre reverse: TTG ATA GCT GGC TGG TGG GTG ATG;

Shp2 forward: ACG TCA TGA TCC GCT GTC AG;

Shp2 reverse: ATG GGA GGG ACA GTG CAG TG;

β-catenin forward: AAGGTAGAGTGATGAAAGTTGTT;

β-catenin reverse: CACCATGTCCTCTGTCTATTC;

Tumor Models

Tumor models were generated by hydrodynamic tail vein injection (HTVi) using a ratio of 10:1 for DNA plasmid to sleeping beauty transposase. For the Ras/Myc model,

$NRas^{G12V}$ and Myc were used at a ratio of 95:5 for a total 10 μg/ml. Plasmids (Bcat: PT3-EF1a-N90-β-catenin; PT3-EF1a-C-Myc; PT/Caggs-Nras-V12, pCMV/SB11) were kindly provided by Dr. Xin Chen at University of California San Francisco. Plasmid PCKO-dnTCF7l2 was kindly provided by Dr. Gregory Lemke at Salk Institute for Biological Sciences (Vacik et al., 2011). PT3-EF1a-eGFP and PT3-EF1a-dnTCF7l2 were cloned for use. Plasmid DNAs were diluted in phosphate-buffered saline (PBS) and injected at 0.1 mL/g body weight through the tail vein in 4-6 seconds. AAV-TBG-GFP (Addgene; 105535) and AAV-TBG-Cre (Addgene; 107787) were purchased from Addgene and injected at the titer of 2×10^{11} pfu/mouse.

Macrophage Depletion

Clondronate Liposome (C.L.) depletion was performed via intraperitoneal injection of C.L. (C09T0317, www.liposome.com) or control liposome (P08T0317, www.liposome.com) at 200ul per 20g mouse. C.L. was injected 3 days before HTVi to prime the liver, then injected 3 hours after HTVi injection of cMyc+SB and every 5 days after. Samples were collected 28 days after HTVi injection.

Immunoblotting

Protein was extracted from liver lysate or cells using RIPA buffer (30mg liver per 400ul RIPA) and denatured using an SDS-based sampling buffer with dithiothreitol (DTT) and bromophenol blue. Tumor, non-tumor tissues, hepatocytes, and non-parenchymal cells were extracted separately as noted. Cytosolic and Nuclear fractions were separated using nuclear extraction kit (ab113474). Denatured protein samples were

fractioned on SDS-PAGE gels and transferred to 0.45 μm nitrocellulose membrane (Bio-Rad; 1620115). Membranes were washed 3x for 10 minutes in TBST, blocked with 5% fat free milk, and incubated with primary antibodies at 4°C overnight. Next, membranes were washed 3x for 10 minutes and appropriate horseradish peroxidase conjugated secondary antibodies were applied for 2 hours at room temperature, before detection with Chemiluminescent Substrate on a BioRad Chemilluminescence Imager.

Immunohistochemistry and Immunofluorescence

FFPE sections and Hematoxylin and Eosin (H&E) stained sections were generated by the Tissue Technology Shared Resource and Histopathology division of the Comparative Phenotyping core at UCSD. Hematoxylin and eosin (H&E) stained liver sections were assessed by Dr. Nissi Varki (UCSD) at the above core, for histopathological evaluation of liver tissues. Immunohistochemical staining was performed on FFPE sections (5μm thickness) and counterstained with Hematoxylin (EMS; 2617303). FFPE sections were deparaffined using histoclear, blocked with 3% hydrogen peroxide for 10 minutes, steamed in antigen retrieval for 30 minutes (cooled for 10-20 minutes), blocked in 5% NGS in TBST, incubated with primary antibody at 4°C overnight, incubated with secondary antibody with HRP for 2 hours at room temperature, and exposed using DAB.

Immunofluorescence was performed on fresh frozen tissue sections fixed with 4% PFA at 4°C overnight. Slides were then washed 3x for 10 minutes using TBST, blocked in 3% BSA, incubated with primary antibody at 4°C overnight, washed 3x for 10 minutes each, incubated with secondary antibody for 2 hours at room temperature, and mounted

with VECTASHIELD mounting medium with DAPI (VWR; H-1200). Other staining kits include Pico-Sirius Red Stain Kit (American MasterTech; KTPSRPT), TUNEL kit (Takara; MK500), and RNAScope 2.5 HD Assay- Red (ACDBio; 322360, 3223650). Antibodies used for staining listed in Table 0.1.

Cell Culture and Assays

PLC/PRF/5 and NR-PDAC cells were cultured in DMEM (GIBCO SH30910.03) containing 10% Fetal Bovine Serum (Hyclone; 10313021), non-essential amino acid (Gibco; 11140050) and 0.1% Penicillin-Streptomycin (Gibco; 1514022). BXPC-3 cells were cultured in RPMI-1640 containing 10% Fetal Bovine Serum and Penicillin-Streptomycin. Cells were pre-treated with SHP099 (Chemietek; CT-SHP099) or Trametinib (APExBIO; A3018), followed by cycloheximide (Sigma-Aldrich; 239764) treatment. Batches of cells were harvested every 15 minutes after addition of cycloheximide, followed by cell lysis and immunoblotting to determine residual Myc protein level.

293T cells were cultured in DMEM containing 10% Fetal Bovine Serum and 0.1% Penicillin-Streptomycin. Cells were acquired from AATC and routinely tested for mycoplasma contamination. 293T cells were co-transfected in triplicate with Super 8x TopFlash in addition to Vector backbone or dnTCF plasmid (600ng DNA per well in 6-well plate) using Lipofectamine 3000. Super 8x TopFlash (Addgene #12456) was kindly provided by Dr. Karl Willert at the Sanford Consortium for Regenerative Medicine. Luciferase signal was detected using Tecan Spark 20M Multimode Microplate reader after 24hrs of LiCl (20mM) stimulation.

RNA extraction and real-time quantitative PCR

cDNA was acquired from fresh frozen liver through RNA isolation via Trizol reagent (Thermo Fisher Scientific; 15596018) and reverse transcription using High-Capacity cDNA Reverse Transcription Kit from Thermo Fisher Scientific (4368814). Real-time qPCR was performed using DyNAmo Flash SYBR Green qPCR Master Mix from Thermo Fisher Scientific (F415) on Stratagene mx3005p instrument. Relative expression of mRNA was calculated by $2^{-\Delta\Delta Ct}$ method and normalized to GAPDH or BACTIN. Primer list in Table 0.2.

In situ Hybridization

Fresh 5µm FFPE sections were treated using the "Formalin-Fixed Paraffin-Embedded (FFPE) Sample Preparation and Pretreatment" protocol (322452) from ACD Biotechne. Then stained for Shp2 in situ hybridization oligo probe using the RNAScope 2.5 HD Detection Reagent – Red User Manual (322360-USM) using reagents from the RNAScope 2.5 HD Detection Red Kit (ACD Biotechne: 322350, 322360). Sections were then mounted with glycerol, or counterstained using the immunohistochemistry protocol listed above.

Flow Cytometry Analysis

Non-parenchymal cells were isolated from the liver via two-step perfusion with Ca^{2+}-free HBSS buffer and then with collagenase H in HBSS buffer containing Ca^{2+}. Non-parenchymal cells were separated by centrifugation and cleared of erythrocytes by

ACK lysis buffer. Cells were first stained for L/D dye and then stained for panel antibodies for 30 minutes at 4°C. Cells were fixed using 1% PFA in PBS overnight at 4°C, resuspended in PBS, and analyzed on a BD LSRFortessa X-20 HTS flow cytometer at the Human Embryonic Stem Cell Core at UCSD. Data was analyzed using FlowJo 10.6.2 (BD). Antibodies list in Table 0.3.

Liver cell isolation for single-cell RNA-seq

Mouse liver was perfused with HBSS buffer, then with collagenase H (Roche; 11074059001) in HBSS buffer (0.8 mg/ml) until liver was digested. Next, the liver was dissociated and passed through a 100μm cell strainer. Cells were centrifuged at 70g for 5 minutes, in order to pellet hepatocytes from non-parenchymal cells. To remove dead cells and debris, the pelleted hepatocytes were re-suspended in 45% Percoll (Sigma-Aldrich) and centrifuged at 70g for 10 min, without brake. Meanwhile, the Dead Cell Removal Kit (Miltenyi Biotech; 130-090-101) was used to eliminate dead cells in non-parenchymal cells, after spinning down at 250g for 5 minutes. Hepatocytes and non-parenchymal cells were further washed with PBS and counted with hemocytometer. Of note, for tumor-bearing livers, after perfusion the tumors were first dissected out, minced, and incubated in perfusion buffer with collagenase H for 1 hour at 37℃. Uniquely, 30% Percoll was used to purify tumor cells, instead of 45%.

Single cell RNA library construction and sequencing

The isolated hepatocytes and non-parenchymal cells were loaded onto 10x Chromium Controller, separately, and then partitioned into nanoliter-scale Gel Beads-In-

Emulsion (GEMs). Cells in GEMs were lysed, and RNAs released from cells were immediately captured by barcoded beads in the same GEMs, followed by reverse transcription, amplification, fragmentation, adaptor ligation and index PCR. For each library, the volume of single cell suspension was calculated in order to generate 5000 GEMs per sample. Libraries were constructed using Chromium Single Cell 3' Reagent Kits (V2 chemistry, 10x Genomics). Sequencing was performed on Illumina HiSeq 4000 at IGM Genomics Center, University of California, San Diego, with the following read length: Read 1, 26bp, including 16bp cell barcode and 12bp unique molecular identifier (UMI); Read 2, 98bp transcript insert; i7 sample index, 8bp. The single cell RNA-sequencing data have been deposited into the GEO repository, with a GEO accession number assigned (GSE157561).

Single cell RNA-sequencing data preprocessing

Obtained reads were mapped to mouse reference genome GRCm38 using CellRanger package (v3.0.2). The human MYC sequence and annotation were manually added into GRCm38 genome, in order to track the expression of plasmid we injected. For each sample, an expression matrix was generated after mapping, UMI counting and cell barcode calling, with each row representing a gene and each column representing a cell. Next, low quality cells and genes were filtered for downstream analysis. In brief, for each sample, genes expressed in less than 3 cells were removed; cells failed to meet following criteria were removed: 1) the number of genes detected in each cell should be more than 200 but less than 5000; 2) the UMIs of mitochondrial genes should be less than 20% of total UMI; 3) the total UMIs of a cell should be less

than 30000 to avoid non-singlet (i.e. transcriptome representing more than one cell). The number of cells passing these filters was listed in Table 2.1. After filtering, the raw expression matrix was normalized by the total expression, multiplied by scale factor 10,000, and log-transformed. Next, we regressed on total number of UMIs per cell as well as mitochondrial gene percentage. The z-scored residuals calculated by normalization and scaling were stored for downstream analysis.

Datasets integration and subpopulation detection

We integrated all cells collected from the same time point or condition, i.e. 0 day, 10 days after vector injection, 10 days after Myc injection, and 4 weeks after Myc injection. For each time point or condition, the integrated datasets included hepatocytes and non-parenchymal cells from both WT and SKO liver. The single cell datasets integration was performed using Seurat R package (v2.4). In brief, canonical correlation analysis (CCA) was used to identify common source of variation between prepared datasets and generate vectors that projected each dataset into the maximally correlated subspaces. Aligning these CCA subspaces returned a dimension reduction for downstream analysis. Next, we performed SNN graph-based clustering and visualized integrated datasets with t-SNE. We used 30-40 CCs for these calculation and tuned resolution parameter in order to get reasonable number of subpopulations (Figures 2.1). The genes used for cell type assignment are well-known markers. We plotted their specific expression in corresponding subpopulations (Figure 2.2). Otherwise, for hepatocytes collected at time point or condition of interest, we extracted these cells out

from integrated datasets and re-clustered with higher resolution in order to further identify subpopulations within hepatocytes.

MAGIC data imputation

To study gene-gene relationship in our datasets, we used a data imputation method called Markov affinity-based graph imputation of cells (MAGIC). “Dropout” is the most challenging technique problem of single cell RNA-sequencing technique. Many expressed mRNAs cannot be captured by current protocols. Therefore, the gene-gene relationship is lost in raw datasets. MAGIC was developed to fill in missing transcripts, via sharing information across similar cells. We performed MAGIC and calculated Pearson correlation coefficient between two genes after data imputation.

Differential expression analysis and Gene-Set Enrichment Analysis

After cell type assignment, we performed differential expression analysis for specified comparison. 1) Identify subpopulation specific genes. We performed differential expression test for each gene between cells in subpopulation of interest and cells not in this subpopulation. 2) For each assigned cell type, identify differential expression genes between cells from WT and SKO. 3) For hepatocytes grouped by Shp2 and Myc expression, we first performed MAGIC imputation and set threshold based on expression density plots after imputation. Hepatocytes with higher Shp2 imputation levels than threshold were assigned as Shp2+ cells, while hepatocytes with lower Shp2 imputation levels were assigned as Shp2- cells. We assigned Myc+ cells and Myc- cells using the same strategy. We then performed differential expression test

between Shp2+ Myc+, Shp2- Myc+, and Shp2-Myc- hepatocytes. 4) Test for differential expressed genes between SKO tumor cells and non-tumor hepatocytes. Wilcoxon Rank Sum test was used in all comparisons described above. Next, Gene-Set Enrichment Analysis (GSEA) was applied to identify pathways that are significantly enriched in these differential expression gene lists. We first ordered genes by log fold-change of the average expression between two groups. Then gene sets collected by Msigdb (Subramanian et al., 2005), including Hallmark, BioCarta, KEGG, Pathway Interaction Database, and Reactome, were used for GSEAPreranked analysis.

Defining gene set signature score

We defined signature score per cell for gene set we are interested as:

$$s_{ij} = \frac{\#expressed\ genes\ in\ gene\ set\ j\ /\ \#genes\ in\ gene\ set\ j}{\#total\ expressed\ genes\ /\ \#total\ genes}$$

We calculated signature scores for gene sets: 1) Myc/β-catenin Signature, consisting of 125 genes defined by Bisso et al. (2020). 2) Wnt target, consisting of 155 genes collected from Wnt target database (https://web.stanford.edu/group/nusselab/cgi-bin/wnt/target_genes) and The Molecular Signatures Database (MSigDB) gene set HALLMARK_WNT_BETA_CATENIN_SIGNALING. 3) Hippo-Yap pathway, consisting of 32 genes collected from MsigDB gene sets REACTOME_YAP1_AND_WWTR1_TAZ_STIMULATED_GENE_EXPRESSION and REACTOME_SIGNALING_BY_HIPPO. 4) mTORC1 signaling pathway, consisting of 23 genes collected from MsigDB gene set REACTOME_MTORC1_MEDIATED_SIGNALLING. 5) Myc target, consisting of 243 genes collected from MsigDB gene sets HALLMARK_MYC_TARGETS_V1 and

HALLMARK_MYC_TARGETS_V2. After calculation, we made boxplot and performed Wilcoxon test to check significant difference of signature scores between groups. The heatmap of genes in these gene sets was made using scaled expression values of randomly selected 150 cells in each group.

TCGA data analysis

The TCGA dataset was downloaded from TCGA-LIHC project, including RNA-sequencing results and clinical information for 371 HCC patients. And the CTNNB1 mutation and MYC copy number variation for these patients were obtained from cBioPortal. We first divided all patients into three groups based on their MYC expression levels: Low (MYC expression level of the patient is lower than 30% percentile); High (MYC expression level of the patient is higher than 70% percentile); Mid (other patients). We plotted different types of CTNNB1 mutation in three groups respectively. For survival analysis, all patients were divided into four groups based on MYC and CTNNB1 activities: $MYC^{+}CTNNB1^{+}$ (both MYC and CTNNB1 activity of this patient are higher than third quantile); $MYC^{+}CTNNB1^{-}$ (only MYC activity of this patient is higher than third quantile); $MYC^{-}CTNNB1^{+}$ (only CTNNB1 activity of this patient is higher than third quantile); $MYC^{-}CTNNB1^{-}$ (other patients). The MYC or CTNNB1 activity for each patient was defined as aggregated expression levels of MYC downstream targets or CTNNB1 downstream targets. And the aggregated expression levels were calculated as:

$$a_i = \sum_{target\ gene\ j} FPKMUQ_{ij} * Weight_j$$

CTNNB1 downstream targets are described above. We used log2 fold change calculated based on the comparison between WT mice and β-catenin KO mice RNA-seq dataset (Liang et al., 2018) as weight for CTNNB1 target genes. MYC downstream targets included 158 genes collected from Msigdb DANG_MYC_TARGETS_UP and DANG_MYC_TARGETS_DN. We used log2 fold change calculated based on the comparison between Myc overexpression mice and WT mice as weight for MYC target genes (Bisso et al., 2020). Next, we performed survival analysis using survival and survminer R package. The similar patients clustering and survival analysis was done for tumor samples in GSE14520.

NicheNet Analysis

The potential interactions between hepatocytes and MDMs, or hepatocytes and Kupffer cells were predicted by NicheNet (Browaeys et al., 2020). NicheNet used 10D-Myc scRNAseq datasets generated in this study as input and combined with a prior model of ligand-receptor-target signaling paths to predict ligands secreted by sender cells and receptors expressed by receiver cells that together might drive target gene expression changes in receiver cells. Specifically, we defined WT hepatocytes, SKO Shp2- hepatocytes and SKO Shp2+ hepatocytes as sender cells; then defined MDMs or Kupffer cells as receiver cells, respectively. The gene set of interest was defined as the differentially expressed genes between SKO MDMs and WT MDMs, or SKO Kupffer cells and WT Kupffer cells, respectively, with p value < 0.01 and average log2 fold change > 0.25. And the background expressed gene set was defined as a list of genes expressed in at least 10% of receiver cells. Next, the ligand activities were calculated as

Pearson's correlation coefficients, based on the presence of their target genes in gene set of interest, compared to the background expressed gene set. Further, the receptors and target genes were inferred for top-ranked ligands. We performed analysis for MDMs and Kupffer cells separately, and for each cell type, we made and combined plots including top-ranked ligand activities, their corresponding expression levels in sender cells, interaction potential of ligand-receptor pairs, receptor expression levels in receiver cells, regulatory potential ligand-target pairs, as well as receptor expression levels in receiver cells.

Quantification and Statistical analysis

Statistical analysis was performed using GraphPad Prism 5.0. Cells with positive staining were scored in at least three fields at ×200 magnification per mouse using ImageJ/FIJI. Statistical significance between means of multiple groups was calculated by: two-way ANOVA with posttest Bonferroni (multiple paired groups), one-sided ANOVA with posttest Tukey (multiple groups), or students T-test (two groups) as required. Bar graph values are presented as means ± standard deviation. Dot plot values presented with median and quartile markers. Survival Curves were plotted by Kaplan-Meier analysis and compared using log-rank test.

Table 0.1 Antibodies used for immunoblotting and immunostaining

Antibody	Source	Identifier
AFP	Cell Signaling Technologies	4448
β-actin	Sigma	A5316
β-catenin	Santa Cruz	SC-7199
CD8	eBioscience	14-0032-81
c-Jun	Cell Signaling Technologies	9165
CK19	DSHB	Troma-III
Clec4f	BioLegend	156804
Cyclin D1	Life technologies	AHF0102
E-cadherin	Santa Cruz	sc-7870
Erk1/2	Cell Signaling Technologies	4695
F4/80	eBioscience	14-4801-82
Gapdh	Cell Signaling Technologies	5172
Glutamine Synthetase (IHC)	Cell Signaling Technologies	CST 3886
GSK3β	Cell Signaling Technologies	9315
Histone 3	Cell Signaling Technologies	4499P
HNF4a	Santa Cruz	sc-8987
Ki67	eBioscience	14-5698-80
MYC	abcam	ab32072
p-c-Jun	Cell Signaling Technologies	2361
p-c-Myc (S62)	abcam	ab51156
p-c-Myc (T58)	abcam	ab28842

Table 0.1, continued. Antibodies used for immunoblotting and immunostaining

Antibody	Source	Identifier
PCNA	Santa Cruz	7907
p-Erk1/2	Cell Signaling Technologies	4370
p-GSK3α/β	Cell Signaling Technologies	9336
p-β-catenin (S33/37/T41)	Cell Signaling Technologies	9561
Shp2	Santa Cruz	sc-7384

Table 0.2, QPCR Primer Sequences

Gene	Primer (5′ - 3′)
CCL2 Forward	GTTGGCTCAGCCAGATGCA
CCL2 Reverse	AGCCTACTCATTGGGATCATCTTG
CCL9 Forward	CCCTCTCCTTCCTCATTCTTACA
CCL9 Reverse	AGTCTTGAAAGCCCATGTGAAA
PD-L1 Forward	GCTCCAAAGGACTTGTACGTG
PD-L1 Reverse	TGATCTGAAGGGCAGCATTTC
CCL17 Forward	TACCATGAGGTCACTTCAGATGC
CCL17 Reverse	GCACTCTCGGCCTACATTGG
CXCL10 Forward	CCTGCCCACGTGTTGAGAT
CXCL10 Reverse	TGATGGTCTTAGATTCCGGATTC
CSF1 Forward	AGTATTGCCAAGGAGGTGTCAG
CSF1 Reverse	TTCCTGGTCTACAAATTCAAAGG
RXRα Forward	CCATGAACCCTGTGAGCAG
RXRα Reverse	CCTCTTGAAGAAGCCCTTGC
βactin Forward	TCCTGTGGCATCCACGAAACTACA
βactin Reverse	ACCAGACAGCACTGTGTTGGCATA

Table 0.3, Antibodies used for Flow Cytometry

FACS Antibodies	Source	Identifier
Life/Dead Aqua Stain	ThermoFisher	L34957
CD45 - PerCP	Biolegend	147706
Ly6c - PE	Biolegend	128008
F4/80 - BV421	Biolegend	123124
CD11c - APC	Biolegend	117309
MHCII - APC Cy7	Biolegend	107628
CD11b - BV605	Biolegend	101257
TCRβ - BV421	Biolegend	109226
NK1.1 - APC	Biolegend	108710
CD8 - PE Cy7	Biolegend	100722
CD19 - APC Cy7	Biolegend	115530
CD4 - BV605	Biolegend	100451
CD69 - BV711	Biolegend	104537

RESULTS

Chapter 1:

Characterization of Novel model of Myc-induced HCC

1.1 Myc-driven carcinogenesis is drastically exacerbated in Shp2-deficient liver

We recently demonstrated genetic ablation of Shp2 in hepatocytes abrogated liver tumorigenesis induced by c-MET (Liu et al., 2018). Through this study, we identified an essential role of Shp2 in the relay of proliferative oncogenic signals elicited by MET, a receptor tyrosine kinase (RTK) upstream of Shp2, in combination with other oncogenic pathways. Therefore, we sought to examine the effect of Shp2 removal on Myc, a nuclear oncoprotein that acts downstream in signaling transduction.

To generate the tumor model, we used the 'Hydrodynamic Tail Vein Injection' (HTVi) technique to uniquely transfect 2-10% of hepatocytes while retaining non-tumorigenic liver microenvironment (Chen and Calvisi, 2014). An expression plasmid carrying the human c-Myc (hereafter Myc or hMyc) cDNA, is introduced to only hepatocytes through increased intravascular pressure, which drives DNA solution into hepatic vein and increases hepatocyte transfection rates. The resulting tumor model mimics human liver cancer development, with controlled and selected oncogenic drivers,

lack of further liver-wide genetic alterations, and induces tumorigenesis only after full murine adult development.

Accordingly, we used HTVi to transfect Myc and the sleeping beauty (SB) transposase into wild-type (WT; $Shp2^{f/f}$) and hepatocyte-specific Shp2 knockout mice (SKO; $Shp2^{f/f}$: Albumin-Cre^{+}) (Figure 1.1A). Like previous reports, Myc alone was inefficient to induce liver tumor in WT mice of C57BL/6 background (Figure 1.1B) (Jia et al., 2020; Mendez-Lucas et al., 2017). Astonishingly, Myc transfection in SKO livers induced rapid and severe tumor development at a high frequency (86%) in only 4 weeks (Figures 1.1B-1.1C), with much larger and greater numbers of tumors, and increased liver weight as well as a splenomegaly phenotype (Figures 1.1C-1.1G). Due to aggressive tumor progression, the tumor-bearing SKO mice rarely survived 6 weeks. Tumor areas expressed high levels of exogenous Myc and Ki67 indicative of highly proliferative Myc-driven tumors (Figure 1.2A). Corresponding regions were also positive for HNF4α, a hepatocyte marker, but not CK19, a cholangiocyte marker, (Figure 1.2B), which identified the tumors as HCC rather than hepatocyte-transformed intrahepatic cholangiocarcinoma (CCA).

1.2 Myc-induced tumors are classified as trabecular hepatocellular carcinoma

We first examined the characteristics of Myc-driven tumors. Histopathological analysis, with consult by pathologist Dr. Nissi Varki, identified tumors as aggressive differentiated trabecular HCC, organized in pseudo-glandular growth with inflammatory cell invasion (Figure 1.3A, Table 1.1). Myc overexpression is also implicated in a large percentage of human hepatoblastoma samples, though β-catenin and YAP are the

essential oncogenic drivers (Russell and Monga, 2018). While Myc-induced tumors in FVB/N mice were classified as hepatoblastoma, we observed these tumors had hepatoblastoma-like high nucleus-to-cytoplasm ratios indicative of high proliferation yet maintained hepatocyte morphology and expression (Figure 1.3A, Table 1.1) (Chen and Calvisi, 2014; Liu et al., 2017). These cancer cells lacked the de-differentiated state of hepatoblastoma cells, organized with more aggressive edge regions arrayed in an unorganized sheet pattern, still identifiable as differentiated HNF4α+ hepatocytes (Figure 1.3A).

Inflammatory cell invasion was observed in a majority of tumors, identified primarily as F4/80+ tumor-associated macrophages (TAMs) (Figure 1.3B) with other immune cell types infrequently identified. TAMs are primarily derived from PBMCs, rather than organ-resident macrophages, which was reflected in our model where Clec4f+ resident liver Kupffer cells (liver-resident macrophages) were identified only outside tumor enclosed regions (Figure 1.3B) (Huang et al., 2021; Wu and Dai, 2017).

Myc activity was validated through immunoblot analysis, revealing strongly activated p-Myc ^{S62} in tumor regions, as compared to non-tumor regions (Figure 1.4A). Erk, which can phosphorylate Myc's S62 site and promote Myc transcriptional activity, was correspondingly highly expressed. Active GSK3β, a kinase promoting Myc degradation, was also increased in tumor tissues. Concomitant increase of β-catenin, which is also regulated by GSK3β, was also noted and explored later in the project (Figure 1.4A). C-Jun, important in immediate-early proliferative response to liver injury and downstream of Shp2 and Jnk signaling, but not liver-specific β-catenin signaling, was upregulated in tumor (Figure 1.4A). These results indicate tumors are all driven by

oncogenic Myc activity, with upregulation of genes across several pathways associated with liver proliferation.

This extremely aggressive HCC model driven by Myc alone in SKO liver was unanticipated, as mouse HCC models were often induced by Myc in combination with constitutively active mutant β-catenin or p53 deletion (Bisso et al., 2020; Dauch et al., 2016b; Liu et al., 2017; Ruiz de Galarreta et al., 2019). Previously, HTVi models with comparable tumor development required at least 8 weeks to develop and further required dual-oncogenic drivers; while HCC induced by chemo-carcinogen diethylnitrosamine (DEN) requires 5+ months in C57BL/6 mice (Liang et al., 2018; Liu et al., 2018). Our Myc-driven HCC model is comparatively faster, requiring only 4 weeks to develop tumors. Thus, hepatocyte-deletion of Shp2, while disrupting RTK-elicited tumorigenic signaling, dramatically aggravated hepato-oncogenesis driven by a nuclear oncoprotein Myc.

Acknowledgements:

Chapter 1 is adapted from material that is in press: Chen, Wendy S.; Liang, Yan; Zong, Min; Liu, Jacey L.; Kaneko, Kota; Hanley, Kaisa L.; Zhang, Kun; Feng, Gen-Sheng. “Single Cell Transcriptomics Reveals Opposing Roles of Shp2 in Myc-driven Liver Tumor Cells and Microenvironment.” *Cell Reports*. The dissertation author was a primary investigator and the first author of this material.

Chapter 2:

Microenvironment influence on Myc tumor Development

2.1 Shp2-deficient liver has impaired tumor clearance ability

With the model established, next we asked how Myc could induce tumors in SKO liver but not WT C57BL/6 liver. First we examined the tumor initiation stage by, histopathologically analyzing the development of Myc-transfected hepatocytes at the pre-neoplastic stage following the oncogene injection. The transfection efficiency was similar between WT and SKO livers, as examined on day 7 (Figure 1.5A). At day 7 and 10, both WT and SKO livers yielded Myc^{+} cells or colonies of comparable sizes and numbers (Figure 1.5A), populated by proliferative Myc^{high} rather than Myc^{low} hepatocytes (Figures 1.6A-B). However, the livers became noticeably different at day 14; Myc^{+} cells disappeared in WT liver whereas Myc^{+} colonies were expanding in SKO liver. Singular Myc^{low} hepatocytes were rarely detected in either genotype at day 14 (Figures 1.5A, 1.6B-C). These data suggest difference in Myc-transfected hepatocyte population whereby cells with high expression of Myc were more likely to achieve tumorigenesis, while cells with low expression of Myc did not proliferate efficiently and establish tumors. Our observations also provide explanation as to why previous attempts of Myc-driven liver cancer models could not induce tumorigenesis in wild-type C57BL/6 mice. Importantly, our findings reveal a critical time point exists at around 10 to 14 days whereby proliferation-capable Myc-transfected hepatocytes in WT liver disappear. Thus, one critical mechanism underlying the severe tumor phenotype in SKO liver is the impaired elimination of Myc-induced tumor-initiating cells at early stages.

H&E staining identified immune clusters near Myc-transfected cell clusters, so we investigated the potential of immune interference in this critical tumorigenesis period. Immunostaining of immune populations revealed co-localization of Myc+ hepatocytes with inflammatory clusters of $F4/80^+$ and $CD8^+$ cells, primarily in WT rather than SKO livers (Figure 1.7A). We next performed FACS analysis at the early stage, and identified significantly higher numbers of Kupffer ($CD11b^+$ $Ly6c^-$ $F4/80^+$) and B cell populations, while lower numbers of monocytes ($CD11b^+$ $Ly6c^{Hi}$ $F4/80^-$) and MDM ($CD11b^+$ $Ly6c^+$ $F4/80^+$), in WT than SKO livers (Figure 1.7B), with no significant difference observed for CD4, CD8, NKT and NK cells (Figures 1.7B). While the importance of the myeloid population is apparent through FACS and staining data, more detailed immune analysis was needed to examine the mechanism of immune microenvironment effect on Myc-driven tumorigenesis.

2.2 scRNA-seq analyses reveal a tumor-promoting environment in Shp2-deficient liver

In order to appropriately investigate tumor initiation and progression, we turned to scRNA-sequencing to dissect mechanisms underlying the aggressive HCC phenotype at single cell resolution. We established a new liver tissue processing protocol, which allowed isolation of all hepatic cell types at high quality suitable for scRNA-seq analysis (Materials and Methods) (Figure 2.1A). The novelty of our protocol utilizes techniques to ensure live cells from all cell types of the liver are sequenced, increasing the quality of our resulting data and reducing artifacts from dead or fragmented cells.

Hepatocytes and non-parenchymal cells (NPCs) were isolated and sequenced from WT and SKO livers, at day 0 before HTVi (0D-Ctrl), 10 days after Myc or empty vector injection (10D-Myc or 10D-Vector), and 4 weeks after Myc transfection (4W-Myc) (Figures 2.1A-E). The 10D-Vector data was selected to control for effects from the HTVi technique, which is known to induce acute liver damage and regeneration. We performed droplet-based scRNA-seq with the 10x Genomics Chromium platform. The data from 27,327 cells, after outlier filtering, were normalized and scaled for clustering and dimensional reduction and visualized using t-distributed stochastic neighbor embedding (tSNE) (Table 2.1) (Figures 2.2A-D). All cells from WT and SKO livers were integrated and clustered for comparison at the different time points using pre-selected clustering parameters (Figure 2.2A-H). In integrated WT and SKO liver data, we distinctly identified all major hepatic cell clusters in the 0D-Ctrl (Figure 2.1B), 10D-Vector (Figure 2.1C), 10D-Myc (Figure 2.1D) and the 4W-Myc data (Figure 2.1E).

First we focused on mechanisms of immune escape in SKO liver and tumor clearance in WT liver, as observed at 10 days in functional data. To dissect the hepatic microenvironment, we first observed differential immune cell populations in WT and SKO livers. In the 0D-Ctrl data, before oncogene injection, we detected higher numbers of almost all innate and adaptive immune cell types in SKO livers (Figure 2.3A), indicating increased basal levels of hepatic injuries and inflammation caused by Shp2 removal from hepatocytes, in agreement with shallower observations from previous publications (Bard-Chapeau et al., 2011). Next, we compared the 10D-Vector and 10D-Myc data to evaluate specific hepatic responses to the exogenous Myc expression by ruling out effects of the HTVi procedure. 10D-Myc data yielded lower numbers of

classical dendritic cells (cDC), Kupffer cells, monocyte-derived macrophages (MDM), neutrophils and B cells in SKO than WT livers, 10 days after Myc transfection (Figure 2.3B). These data suggest a generally impaired innate immune cell response to initiation of Myc-induced tumors in the SKO liver at the early stage. The 4W-Myc data showed that aggressive tumor growth in SKO liver was accompanied by modest increases in NK2, $CD11b^{+}$ cDC, neutrophil, MDM and Kupffer cells, relative to the WT liver (Figure 2.4A). In summary, at 10 days after HTVi of Myc, WT livers have increased innate immune cells – populations which decrease by the 4 week timepoint – which correlate with the critical tumor colony disappearance timepoint in WT liver. SKO livers have decreased innate immune cells which rebound at the 4 week timepoint, with mature tumor cells.

2.3 Clearance of Myc-transfected hepatocytes is impaired due to macrophage polarization

Due to the dramatic changes in macrophage populations between the 10D and 4W time points as well as the immunostained presence of F4/80+ cells near Myc+ cells at 10D, we decided to further characterize the macrophage populations. Differential expression analysis showed that inflammatory M1 macrophage markers, such as CD38, Irf7, and Saa3, were significantly upregulated in 10D-Myc WT livers but not at other time points (Figure 2.5A). Moreover, we detected higher expression of phagocytosis-related genes, including Fcgr4, Lyn, and Fcgr1 in MDMs and Kupffer cells in the 10D-Myc data, with no significant change detected in 0D-Ctrl and 10D-Vector data (Figures 2.6A-B). In 4W-Myc data, WT livers have reduced phagocytic gene expression and increased M2

macrophage markers, reversed from 10D-Myc data (Figures 2.4A, 2.5B). These results suggest a unique early hepatic response to Myc-transformed cells in the WT mice, which was markedly attenuated in SKO liver.

Indeed, we observed large microgranuloma structures in H&E sections of WT liver, indicating atypical increased macrophage phagocytosis activity in engulfing hepatocytes, thus corroborating with our scRNA-seq analysis (Figure 2.7A). As compared to SKO liver, WT liver at 9D and 14D had more and larger hepatocyte-engulfment-related microgranuloma per liver area (Figure 2.7A-D). SKO livers showed characteristic increased inflammatory clusters and fibrosis, but yielded only few microgranulomas. Quantified microgranulomas – involving hepatocytes – in SKO liver were sized appropriately for individual hepatocyte engulfment, indicating tumor colonies were not likely to be phagocytosed. We hypothesize that reduced tumor incidence in WT liver was a result of clearance of Myc-transfected hepatocytes in WT liver performed by macrophages, resulting in microgranuloma structures 9-14D after tumor induction. This innate immune response against Myc-driven cells was induced without use of additional inflammatory antigen as seen in other models (Ruiz de Galarreta et al., 2019). These data showed that macrophage function was impaired in Shp2- deficient liver resulting in defective elimination of Myc-transfected tumor-initiating cells.

We next asked how tumorigenesis may change in the absence of this innate immune response. Therefore, we sought to ablate macrophage populations using clodronate liposome (C.L.). Clodronate liposome consists of clodronate (dichloromethylene-bisphosphonate, Cl2MBP) artificially encapsulated in liposomes. C.L. is effectively targeted by phagocytic macrophage populations, which engulf and digest

the liposome phospholipid outer layer; accumulation of clodronate within the macrophage triggers apoptosis (Van Rooijen and Sanders, 1994). Thus, treatment with C.L. effectively depletes phagocytic cells in the treated animal, of which a majority of affected cells consists of macrophages throughout the animal, not limited to the liver. Pre-injection of C.L., or control empty (PBS-loaded) liposomes, before HTVi cleared macrophage populations before introduction of Myc plasmid, with additional C.L. injections throughout tumorigenesis to maintain clearance of a majority of macrophage populations during tumor development (Figure 2.8A). However, macrophage depletion by C.L. had no significant effect on tumor burdens (Figures 2.8B-C). C.L. efficiently cleared macrophage populations in C.L. injected livers with less efficient clearance in spleen due to reduction of phagocytic macrophage populations in the spleen (Figure 2.8D). Other immune populations, such as CD8+ T cell populations, were unaffected by C.L. or control liposome treatment. Lack of tumorigenesis in WT liver is likely due to clearance of both pro- and anti-tumor MDM/Kupffer cell sub-populations. In the absence of macrophages, oncogenic Myc still induced tumor initiation and development effectively in SKO liver, suggesting immune populations other than macrophages may also play a significant role in tumor development. C.L. was also unable to clear tumor-associated macrophage populations within the tumor area which may have influenced the innate immune system's lack of response to Myc-transfected cells (Figure 2.8D). The lack of clearance suggests tumor-associated macrophage populations within the tumor areas, which are also MDM populations, may be due to suppressed phagocytic activities of these cell populations.

Together, the scRNA-seq and functional data suggested significantly impaired innate immunity in the SKO mouse in the early stage of hepatic response to Myc transformation of hepatocytes. This is one mechanism that accounts for the severe tumor phenotype. These results also provide reasonable explanation for tumor promoting effects of SKO liver observed in previous tumor models (Bard-Chapeau et al., 2011).

2.4 Wide variety of cytokines involved in recruitment of macrophage populations

Because WT and SKO livers differ in the hepatic deletion of Shp2, we next asked which hepatic influences may have caused the difference in macrophage polarization and activity. Shp2 deletion in hepatocytes was previously implicated in metabolic remodeling, including defective bile acid synthesis due to dysregulation of FXR signaling. Shp2 deletion also induces an inflammatory microenvironment with distinct upregulation of the TNFα pathway (Bard-Chapeau et al., 2006; Li et al., 2014a; Liu et al., 2018).

We measured the expression of various cytokines/chemokines involved in recruitment of macrophages at several time points after vector injection (7D) or Myc injection (7D, 10D and 14D) (Figures 2.9A). Difference in macrophage activity did not seem related to CSF1 expression, an important monocyte/macrophage chemokine promoting survival, proliferation, and differentiation (Figure 2.9A). No significant difference was found between WT and SKO livers in the expression of CXCL10, a chemotactic ligand to macrophage-expressed receptor CXCR3, and RxRα, an inhibitor to inflammatory macrophage activity (Figures 2.9A) (Liu et al., 2011; Marra and Tacke,

2014). CCL9, a pro-tumorigenic chemokine secreted by inflammatory macrophages, was lower in SKO liver at all time points (Figure 2.9A). Consistently, the 10D-Myc data showed that CCL9 expression was higher in $CD11b^+$ cDC, Kupffer cell, and MDM populations from WT liver, and was not identified in 10D-Vector data (Figure 2.10A). In contrast, CCL17, a chemokine secreted by non-inflammatory macrophages that promotes tumorigenesis, was higher in SKO liver at all time points (Figure 2.9A). Therefore, CCL9 and CCL17 expression seem to be related to genotypic differences in liver, induced by deletion, or not, of Shp2 in hepatocytes which affect the immune microenvironment.

Immunosuppressive genes PD-L1 and CCL2 were also higher in SKO liver at 10 days and 14 days after Myc transfection, but not in vector-injected control (Figure 2.9A). Expression of these cytokines positively correlates with increasing tumor size and seem to increase in direct response to Myc transfection, as well as suggest a level of T cell suppression may also contribute to tumor-promoting effects in SKO microenvironment, which we have not explored.

We profiled Shp2-deficient hepatocytes for ligand-receptor interactions related to our observed macrophage activity. Distinctively, we did not observe changes in CCL4 and CCL5 expression in association with immune escape as reported previously (Ruiz de Galarreta et al., 2019; Spranger et al., 2015), but detected significantly elevated expression of MIF (macrophage migration inhibitory factor) and Lect2 (leukocyte cell derived chemotaxin 2) in Shp2-deficient hepatocytes at all time points (Table 2.2). Lect2, a hepatokine that modulates macrophages, neutrophils, NK, DC, EC and HSC activities, was identified as a β-catenin target and implicated in liver fibrosis and HCC (Anson et

al., 2012; Ovejero et al., 2004; Xu et al., 2019a). However, Tie1, Lect2's known receptor, is expressed highly in the endothelial cell type at all time points and genotypes except for SKO cells in 10D-Myc data and even lower in 4W-Myc data. This suggests Lect2 may be modulating immune function through Tie1 expression on endothelial cells which may then communicate with immune populations in an indirect manner. To understand the functional hepatokine-macrophage crosstalk requires further extensive study and is discussed further in the Future Directions section.

Together, these data suggest that defects in a variety of innate immune cell functions are likely a major mechanism of immunosuppression in Shp2-deficient liver (Figure 2.10B). Now we add further understanding of unique impaired immune response to tumorigenic stimuli, whereby Myc-transfected oncogenic tumor cells can evade immune clearance by altering macrophage polarization.

Acknowledgements:

Chapter 2 is adapted from material that is in press: Chen, Wendy S.; Liang, Yan; Zong, Min; Liu, Jacey L.; Kaneko, Kota; Hanley, Kaisa L.; Zhang, Kun; Feng, Gen-Sheng. "Single Cell Transcriptomics Reveals Opposing Roles of Shp2 in Myc-driven Liver Tumor Cells and Microenvironment." *Cell Reports*. The dissertation author was a primary investigator and the first author of this material. Single-cell RNA sequencing data was generated by Yan Liang, upon request by dissertation advisor or myself.

Chapter 3:

Unique selection and requirement of Shp2 in Myc tumorigenesis

3.1 Myc-induced tumors are developed from Shp2-positive hepatocytes

Following analysis of NPCs and the microenvironment supporting tumorigenesis, we interrogated intrinsic signaling in hepatocyte and HCC cell populations. In the 4W-Myc tumor-bearing SKO liver, hepatocytes clustered, separately from NPCs, into 5 subpopulations: (1) central vein zone; (2) OxPhos and translation-related; (3) tumor; (4) portal vein zone; and (5) Malat1^{hi} hepatocytes (Figure 3.1A-B). Cluster 1, central vein zone, was characterized by expected elevated expression of central zonation markers *Cyp2e1* and *Glul*, while cluster 4 highly expressed portal zonation markers *Cyp2f2* and *Alb* (Figure 3.1C). Of note, cluster 3 represented Myc^{+} tumor cells featured by high expression of *Afp* (HCC biomarker) and *hMyc* (exogenous Myc) (Figures 3.1A-B). In the integrated WT and SKO 4W-Myc data, Myc^{+} and AFP^{+} cells overlapped in both data sets, indicating similar expression profiles in Myc^{+} tumor cells of both genotypes (Figures 3.2A-B). Remarkably, the tumor cell cluster was absent in the 10D-Myc data, suggesting heterogeneity of Myc-transfected hepatocytes at the pre-neoplastic stage (Figures 3.3A-B). Distinctly, Myc^{+} tumor cells in all tumor nodules in the 4W-Myc data formed a single cluster, distinguished from non-tumor hepatocytes, suggesting clonogenic tumor growth out of heterogeneous Myc-transfected cells (Figures 3.1B, 3.2B, 3.3C).

To define the molecular feature of tumor cells in this model, we utilized MAGIC (van Dijk et al., 2018) for data imputation, which restored sparse single-cell data based on information shared between similar cells. Crucially, this analysis revealed cells with

high exogenous *hMyc* expression (Myc^{hi}) also displayed high *Ptpn11/Shp2* levels, compared to Myc^{low} cells in tumor-bearing SKO livers at 4 weeks (Figure 3.4A). tSNE plot of the 4W-Myc SKO hepatocytes confirmed closely associated expression of *hMyc* and *Ptpn11* in the same cluster of tumor cells (Figure 3.4B). However, the correlation of positive *hMyc* and *Ptpn11* expression was not detected in the 10D-Myc data, when Myc^{+} cells were not well clustered yet (Figure 3.4C), indicating no bias in the efficiency of Myc transfection into Shp2-positive or -negative hepatocytes in the SKO liver. As Shp2 was deleted in around 90% hepatocytes by *Alb-Cre* (Bard-Chapeau et al., 2006), the scRNA-seq data suggests, surprisingly, that the resulting Myc^{+} tumors developed, through a mechanism of forced selection, from the rare $Shp2^{+}$ hepatocytes that escaped from DNA excision in SKO liver (Scheme 3.1).

3.2 Shp2 is required cell-autonomously for Myc-induced HCC

In agreement with the scRNA-seq data, we detected higher Shp2 mRNA and protein levels in tumor than non-tumor tissue and hepatocyte lysates isolated from SKO livers (Figures 3.5A-C), indicating that Myc-induced tumors were indeed derived from Shp2-positive hepatocytes. To define a tumorigenic role of Shp2, we co-injected Myc and Shp2 expression constructs (Myc+Shp2) via HTVi. Similar to Myc alone, co-injection of Shp2 and Myc did not efficiently induce tumors in WT mice (Figures 3.6A-B), suggesting that intrinsic Shp2 over-expression does not have a tumor-promoting effect in WT liver. However, co-transfection of Myc and Shp2 into SKO liver induced faster and more severe tumor growth than Myc alone, with numerous Shp2+Myc+ tumor nodules detected at 3 weeks (Figures 3.6A-C). Tumors driven by Myc or Myc+Shp2 in

SKO livers exhibited high expression of Myc, PCNA and AFP, with higher β-catenin levels detected in Myc-induced tumors (Figure 3.8A). These results identify a supportive role of Shp2 in Myc-driven tumor development and led us to examine the importance of Shp2 in Myc-driven HCC.

Next we injected AAV-TBG-Cre virus to acutely delete Shp2 in hepatocytes and found, when AAV-Cre induced Shp2 deletion 7 days before HTVi, Myc-induced tumor formation was suppressed (Figure 3.7A). Shp2 was deleted in over 90% hepatocytes in the SKO genetic mouse model directed by the *Albumin-Cre* transgene (Bard-Chapeau et al., 2011; Bard-Chapeau et al., 2006; Postic and Magnuson, 2000). Therefore, we replaced the developmental slow-acting Albumin-Cre with the immediate-acting AAV8-Cre for Shp2 deletion. Utilization of AAV-Cre effectively abolished Myc-induced tumor development in the liver (Figure 3.7A). Although Alb-Cre and AAV-Cre showed similarly effective Shp2 deletion in hepatocytes (Figure 3.8B), AAV-Cre induced acute and synchronized gene deletion, as compared to Alb-Cre which mediates progressive gene ablation, highlighting differences in long-term Shp2-deleted hepatic signaling and establishment of a tumor-permissive environment in the liver. There is a significant possibility, based on previous reports, that a rare population of hepatocytes which escape Cre-mediated gene deletion, retaining survival advantages, can selectively assist in progression to HCC (Bisso et al., 2020; Wang et al., 2011; Yamaji et al., 2010).

To further define a cell-autonomous requirement of Shp2, we co-transfected Myc and CMV-Cre into WT and SKO livers (Xu et al., 2019b). This method maintains the Albumin-cre driven gene deletion, but additionally deletes Shp2 in hepatocytes co-transfected with Myc and CMV-Cre, removing the potential of Shp2 expression in Myc-

transfected hepatocytes which escape Albumin-cre mediated gene deletion. Remarkably, selective deletion of Shp2 by addition of CMV-Cre in Myc-transfected cells abrogated HCC development in the previously described tumor-permissive microenvironment of SKO liver (Figure 3.7B) (Scheme 3.1).

HTVi as a technique is inherently biased and transfects more central vein hepatocytes than portal vein hepatocytes. However, $Shp2^{+}$ hepatocytes were detected in 0D-Ctrl data without zonation-based bias (Figures 3.9A-B). Therefore zonation does not select for the transfection of Myc in Shp2+ hepatocytes in SKO liver at 0 to 10 days, but rather Shp2+Myc+ cells develop into tumors by 4 weeks (Figures 3.4A-C). These confounding but intriguing data show the severe tumor phenotype induced by Myc was not only aggravated by a tumor-permissive hepatic microenvironment induced by Shp2 loss in general hepatocyte populations, but also selects for and requires cell-autonomous expression of Shp2.

3.3 Shp2 promotes Myc-induced tumorigenesis by enhancing Ras/Erk signaling

We questioned why Shp2 was specifically required for HCC driven by Myc, which canonically acts downstream of Shp2 in signaling transduction. Previous data showed that pharmaceutical inhibition of Shp2 selectively suppressed proliferation of various cancer cells driven by RTKs (Chen et al., 2016). However, our data here clearly demonstrated a requirement of Shp2 in liver tumorigenesis driven by Myc, a nuclear protein that operates downstream of Shp2 signaling through the MAPK signaling cascade.

To validate a functional requirement of Shp2 supporting Myc signaling, we co-injected a dominant active $NRas^{G12V}$ mutant together with Myc (Ras+Myc) into WT and SKO mice (Figure 3.10A). Similar to Myc alone, co-injection of $NRas^{G12V}$ and Myc drove more severe HCC development in SKO than WT mice (Figures 3.10A, Table 1.1), reinforcing the theory that Shp2 deficiency induces a tumor-promoting environment. Individual introduction of $NRas^{G12V}$ alone causes oncogene-induced senescence of transfected cells around 12 days, with subsequent senescence-induced immune clearance of quiescent transfected cells and lack of tumor development (Kang et al., 2011). Nonetheless, similar to Myc alone, the Ras and Myc model drastically increased tumor burdens in SKO mice as compared to WT mice. However, the average number of tumor nodules increased from 14 by Myc alone to >400 induced by Ras and Myc in SKO liver, when compared by equal amounts of plasmid DNA injected (Figure 3.10B). The larger tumor number aligns with previous HTVi-induced HCC models in correlation with plasmid amount utilized (Liang et al., 2018; Liu et al., 2018). More importantly, unlike the Myc-induced tumors that were Shp2-positive, tumors induced by Ras and Myc were found to be Shp2-negative but retained high p-Erk levels (Figure 3.10C). In addition, carcinogen DEN-induced tumors in SKO liver were also Shp2-negative (Figure 3.10C). These data indicate that the cell-autonomous requirement of Shp2 in Myc-driven tumors could be overridden by an oncogenic Ras mutant, co-transfected with Myc (Scheme 3.1).

Consistent with a documented role of Shp2 in promoting Ras-Erk signaling (Chan and Feng, 2007; Neel et al., 2003), $Shp2^{+}$ tumor tissues exhibited higher Erk levels, relative to the $Shp2^{-}$ non-tumor tissues in SKO livers (Figure 1.4A). One mechanism of

Myc activation is through phosphorylation of Myc at S62 by Erk, to promote Myc stability and activity (Farrell and Sears, 2014; Hayes et al., 2016).

To test the role of Shp2 in promoting Myc signaling through the Ras/Erk pathway, we treated HCC cells with a specific Shp2 inhibitor SHP099 or a Mek inhibitor Trametinib (Figure 3.11A). The stability of Myc protein in proliferating cells is 15-30 minutes, an effective gene mechanism to regulate Myc function (Ciechanover et al., 1991; Salghetti et al., 1999). Indeed, pharmaceutic inhibition of either Shp2 or Mek suppressed p-Erk and p-Myc^{S62} levels in HCC and other cancer cell lines, and could decrease the half-life of Myc protein in these tumor cells (Figures 3.12A-C). Although Shp2 was shown to promote Erk activation *in vitro* many years ago (Feng, 1999; Neel et al., 2003), our study provides *in vivo* evidence demonstrating the significance of Shp2 function in enhancing oncogenic Myc stability through Erk, making Shp2 required for Myc-driven hepatocarcinogenesis. Consistent with the biochemical results *in vitro*, scRNA-seq data analysis showed significantly elevated expression of Myc target genes in Shp2-positive cells in both WT and SKO liver in the 10D-myc data (Figure 3.13A). Only Myc-transfected Shp2^{+} cells at 10D had increased OxPhos and ATP production similar to Myc^{+} tumor cells at 4 weeks (Figure 3.13B). Myc+ Shp2- cells did not show increase in apoptotic markers, suggests indirect clearance methods after being unable to complete neoplastic transformation.

These data indicate Shp2 is necessary and selected for Myc-driven oncogenesis through supporting Myc protein stability through the Ras-Erk signaling pathway (Scheme 3.1).

Acknowledgements:

Chapter 3 is adapted from material that is in press: Chen, Wendy S.; Liang, Yan; Zong, Min; Liu, Jacey L.; Kaneko, Kota; Hanley, Kaisa L.; Zhang, Kun; Feng, Gen-Sheng. “Single Cell Transcriptomics Reveals Opposing Roles of Shp2 in Myc-driven Liver Tumor Cells and Microenvironment.” *Cell Reports*. The dissertation author was a primary investigator and the first author of this material. Single-cell RNA sequencing data was generated by Yan Liang, upon request by dissertation advisor or myself.

Chapter 4:

Requirement of β-catenin in driving Myc-induced tumorigenesis

4.1 Wnt/β-catenin signaling is aberrantly enhanced in Myc$^+$ tumors

The critical role of Shp2 in Ras/Erk/Myc signaling, together with the tumor-promoting environment in SKO liver, illustrated why Myc was sufficient to induce HCC in this mouse line. However, it did not explain why Myc alone had such a robust tumorigenic effect in SKO liver. Consequently, we next analyzed the driving pathways. Unchaperoned pathway enrichment analysis of tumor cells showed upregulation of several signaling and metabolic pathways, especially the Wnt/β-catenin pathway (Materials and Methods) (Figure 4.1A). Wnt pathway targets were highly expressed in the tumor cell cluster, but not genes driven by mTORC or Hippo/YAP signaling pathways, pathways previously strongly associated with Myc-drive HCC models (Figures 4.1B-C) (Bisso et al., 2020; Dolezal et al., 2017; Xu et al., 2019b). Wnt/β-catenin signaling in the liver is essential in hepatobiliary development and zonation. In mature liver, β-catenin controls metabolic zonation around the central vein through direct transcriptional activation of essential liver metabolic processes, including glycolysis, glutamine synthesis, and xenobiotic metabolism. Wnt/β-catenin hyperactivation, through direct mutation and overexpression of β-catenin or inactivation of repressors (i.e. APC), is implicated in a large portion of human liver cancer samples (Cancer Genome Atlas Research Network. Electronic address and Cancer Genome Atlas Research, 2017). β-catenin has also been implicated in binding to Myc promoter and driving Myc expression (Yochum et al., 2008).

Immunostaining verified higher levels of β-catenin expression and glutamine synthetase (GS) in tumor tissues as compared to non-tumor tissues (Figures 4.2A), indicative of upregulated β-catenin transcriptional activity in Myc-induced tumor cells. By analyzing the 0D-ctrl and 10D-Myc data, we also found significantly higher expression of positively-associated Wnt/β-catenin pathway genes in SKO liver and $Shp2^{+}$ hepatocytes, relative to WT (Figures 4.2B-C), suggesting upregulation of both the basal and Myc-induced Wnt/β-catenin signaling in Shp2-deficient liver.

We consequently utilized a recently reported Myc/β-catenin gene signature (Bisso et al., 2020), established in a transgenic mouse HCC model with overexpression of both Myc and β-catenin. Remarkably, the expression of "Myc/β-catenin signature" gene set was enhanced in our tumor cells induced by singular Myc, with marginal expression also detected in the portal vein hepatocytes (Figures 4.3A-B). Modest upregulation of the signature genes was also observed in SKO livers, relative to WT, in the 10D-Myc data (Figure 4.4A-B). Immunoblot analysis of Myc-induced tumors detected higher expression of β-catenin-related genes p-GSK3β and E-cadherin (Figure 1.4A). Biochemical analysis revealed increased β-catenin localization to the nucleus in tumor tissue, compared to non-tumor tissue, further validating increased β-catenin transcriptional activity (Figure 4.5A). Thus, the basal level of Wnt/β-catenin activity was elevated in Shp2-deficient liver, which was boosted by Myc over-expression, resulting tumor gene expression profile similar to the "Myc/β-catenin signature" generated by dual overexpression of Myc and β-catenin in the liver (Bisso et al., 2020). These results suggest β-catenin is not only upregulated but also a co-driving mechanism in Myc tumors.

This finding is particularly interesting because Myc overexpression and *CTNNB1*/β-catenin mutations are frequently detected in different types of cancer, including HCC. Bioinformatics analysis of TCGA and other patient datasets showed that HCC patients with upregulation of both Myc and β-catenin target genes had worse prognosis than those with upregulation of only Myc or β-catenin target genes (Figures 4.6A-B). HCC patients with higher expression or increased copy numbers of *MYC* also had a higher frequency of mutations in *CTNNB1* as well (Figures 4.6A-B). The human HCC data suggest a selective advantage of the two pathways altered concurrently, resulting in more aggressive disease progression. β-catenin was known to bind to and activate the Myc promoter; studies in other cancers suggest that Myc may also induce β-catenin expression via a positive feedback loop (Cho et al., 2013; Cowling et al., 2007). To probe this mechanism, we examined the expression of endogenous c-Myc and did not find a consequent increase of the endogenous Myc expression in exogenous hMyc-overexpressing tumor cells (Figure 4.6C). Thus, our data suggests β-catenin is not acting directly upstream of Myc but rather promotes Myc-driven liver tumorigenesis through other avenues.

4.2 β-catenin transcriptional activity is essential and supports Myc-driven hepatocarcinogenesis

Next we examined the requirement of β-catenin activity in Myc-driven HCC. Co-injection of Myc with a dominant-negative mutant of TCF7l2 (dnTCF), which can inhibit endogenous β-catenin transcriptional activity by preventing β-catenin from binding to transcriptional sites with dnTCF (Figure 4.8A) (Vacik et al., 2011), suppressed Myc-

induced tumor formation in SKO liver (Figures 4.8B-C). This result further supports a notion that β-catenin is required for Myc-dependent HCC, despite being previously placed upstream of Myc in other cancer types. Co-injection of dnTCF with $NRas^{G12V}$+Myc oncogenes did not reduce tumor burdens or tumor cell proliferation (Figures 4.9A-C). Therefore, β-catenin is particularly required for hepato-oncogenesis driven by Myc alone. We then examined changes in tumor initiation with Myc+dnTCF. At day 7, scattered Myc^{hi} cells proliferated in both livers (Figure 4.10A), suggesting that co-transfection with dnTCF did not inhibit initial cell transformation by Myc. However, subsequent growth of Myc^{+} cell nodules was suppressed by dnTCF when examined at day 12 (Figure 4.10A), suggesting that dnTCF abrogated tumor progression rather than initiation.

By breeding $Shp2^{f/f}$ mice with $Ctnnb1^{f/f}$: $Alb\text{-}Cre^{+}$ (BKO) mice, we generated a compound mutant SBKO ($Shp2^{f/f}$:$Ctnnb1^{f/f}$: $Alb\text{-}Cre^{+}$) mouse line with hepatocyte-specific deletion of both Shp2 and β-catenin (Figure 4.11A). The BKO and SBKO mice were born at Mendelian frequency indicating that the new SBKO mice were not impaired during embryonic development. At two months of age, SBKO mice developed healthy hepatic architecture, with no gross anatomical defect (Figures 4.11A-C). Livers showed increased fibrosis even at 2 months of age, similar to SKO genotype (Figure 4.11A). Unlike SKO liver, SBKO liver did not develop spontaneous tumors in older adults (Figure 4.11D). Similar to BKO mice as described previously (Liang et al., 2018; Tan et al., 2006), SBKO mice had smaller liver mass (Figure 4.11B), and exhibited modestly increased cell death, compensatory proliferation, returning β-catenin+

hepatocyte populations, and fibrosis (Figures 4.12A-D). Thus, the SBKO mice inherited pathological features from both SKO and BKO mouse lines.

Next, we used HTVi to transfect Myc into WT, SKO, BKO and SBKO livers and examined the tumor loads. Additional removal of β-catenin from hepatocytes in SKO mice ablated Myc-induced HCC development in SBKO livers (Figures 4.13A-B). Furthermore, Myc injection did not induce tumors in BKO livers with only β-catenin loss in hepatocytes (Figures 4.13A-B); these data further support our initial findings of a requirement of β-catenin for Myc-driven HCC in mice.

To rescue the tumor phenotype, we injected Myc together with an oncogenic truncated β-catenin mutant (ΔN90-β-catenin). Indeed, liver tumors developed in WT, SKO, BKO and SBKO mice 4 weeks following transfection, with more severe tumor phenotypes in the 3 mutants than WT mice (Figures 4.14A-B). The tumors driven by Myc and β-catenin were larger in size and number than that by Myc alone, histopathologically a mixture of HCC and hepatoblastoma (Figures 4.14A-B, Table 1.1). Together, these results clearly demonstrated a functional requirement of β-catenin for hepato-carcinogenesis driven by Myc, which provides an explanation to frequent co-detection of aberrant over-activation of Myc and β-catenin signaling in HCC patients.

Acknowledgements:

Chapter 4 is adapted from material that is in press: Chen, Wendy S.; Liang, Yan; Zong, Min; Liu, Jacey L.; Kaneko, Kota; Hanley, Kaisa L.; Zhang, Kun; Feng, Gen-Sheng. “Single Cell Transcriptomics Reveals Opposing Roles of Shp2 in Myc-driven Liver Tumor Cells and Microenvironment.” *Cell Reports*. The dissertation author was a

primary investigator and the first author of this material. Single-cell RNA sequencing data was generated by Yan Liang, upon request by dissertation advisor or myself.

FIGURES, TABLES, AND SCHEMAS

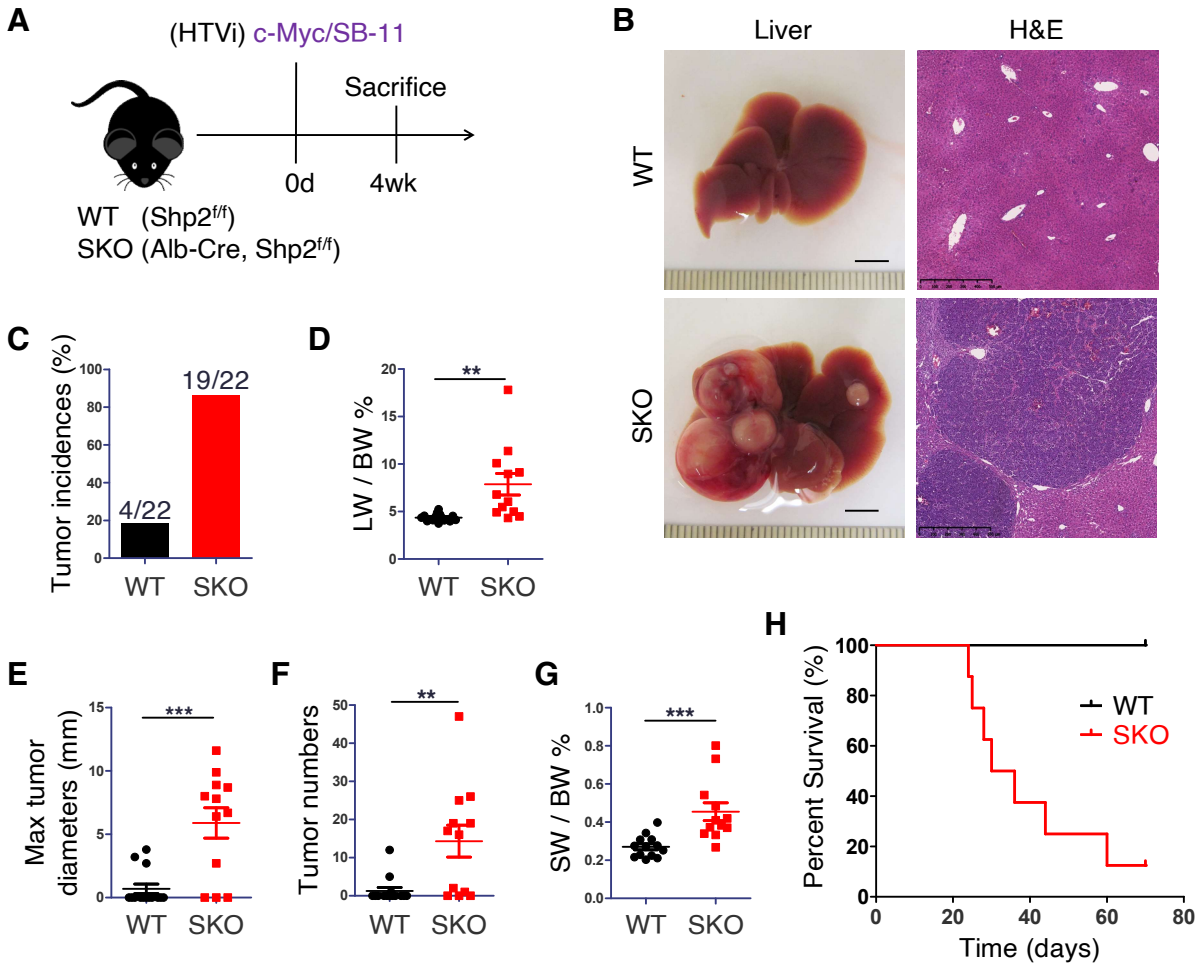

Figure 1.1 Overexpression of Myc drives liver cancer in Shp2-deficient liver

(**A**) Experimental Scheme

(**B**) Representative liver images and H&E staining of liver sections 4 weeks after Myc transfection using Sleeping beauty transposase (SB-11) via HTVi. SKO liver has liver tumors while WT liver does not. Liver scale bar, 0.5 cm. Staining Scale bar, 500 μm.

(**C-G**) Quantified tumor incidences (**C**), liver to body weight ratios (LW/BW) (**D**), maximal tumor diameters (**E**), visible tumor nodule numbers (**F**), and spleen to body weight ratios (SW/BW) (**G**). n = 22. Statistical significance was calculated using students' T-test (**p<0.01; ***p<0.001).

(**H**) Survival curve for Myc-injected WT vs SKO mice (n=8)

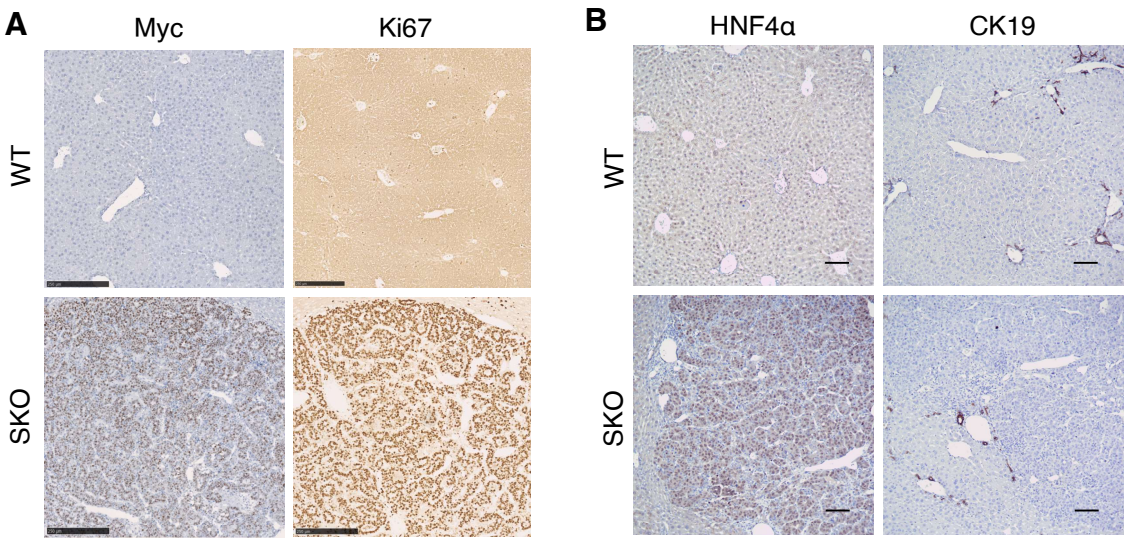

Figure 1.2 Myc drives aggressive hepatocellular carcinoma in Shp2-deficient liver

(**A**) Representative immunostaining of liver sections for Myc and Ki67, 4 wk after Myc transfection, showing highly-proliferative Myc-expressing tumor regions in SKO liver. Scale bar 250 μm.

(**B**) Representative immunostaining of liver sections for HNF4α and CK19, 4 wk after Myc transfection, indicating tumors have hepatocyte, rather than cholangiocyte, identity. Scale bar 50 μm.

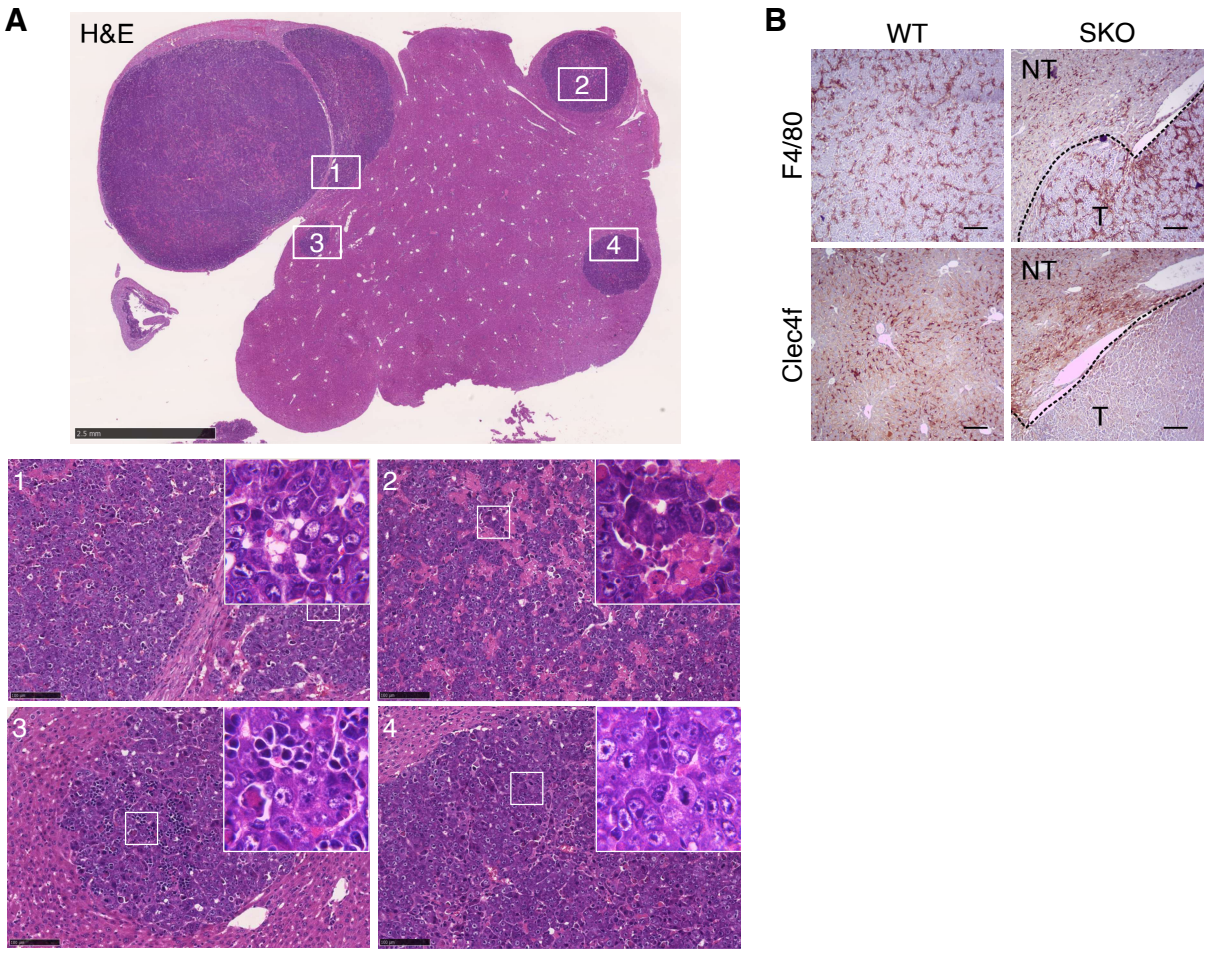

Figure 1.3 Histopathological analysis of Myc-induced HCC

(A) Representative H&E staining of SKO liver 4W post-Myc injection; Trabecular HCC with features detailed in histopathological report (Table 1.1). Top: scale, 2.5 mm; bottom 1-4: scale, 100 µm. Upper Box 4x.

(B) Representative immunostaining of liver sections for F4/80 and Clec4f, 4 wk after Myc transfection, showing macrophage populations in WT and SKO liver. Clec4f+ kupffer cells are excluded from tumor enclosed regions. Scale bar 250 µm.

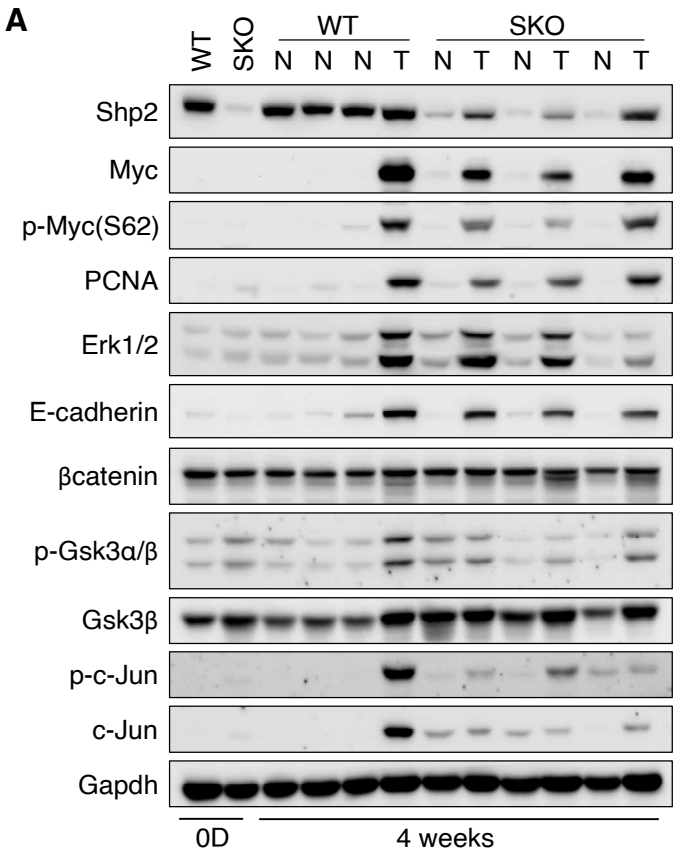

Figure 1.4 Characterization of Myc-induced HCC

(A) Immunoblotting of liver lysates at 0d and 4wk post-HTVi of Myc, using antibodies as indicated. Tumor (T); Non-tumor (NT). Higher levels of Shp2, Myc, p-Myc(S62), PCNA, Erk1/2, E-cadherin, p-β-catenin, β-catenin, p-c-Jun, and c-Jun were detected in T as compared to NT and Ctrl.

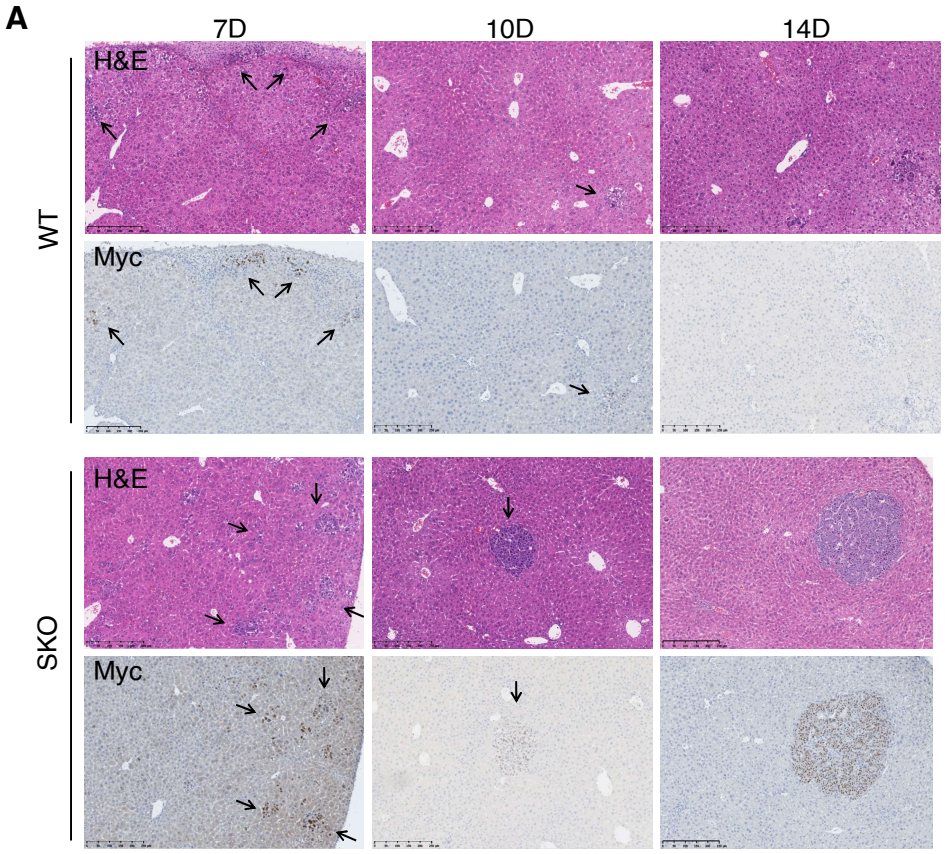

Figure 1.5 Myc-transformed cells are eliminated in WT livers

(**A**) Representative H&E and Myc immunostaining in consecutive sections at 7d, 10d, and 14d after Myc injection. Arrows point to Myc^{+} cell clusters. Scale bar, 250 μm.

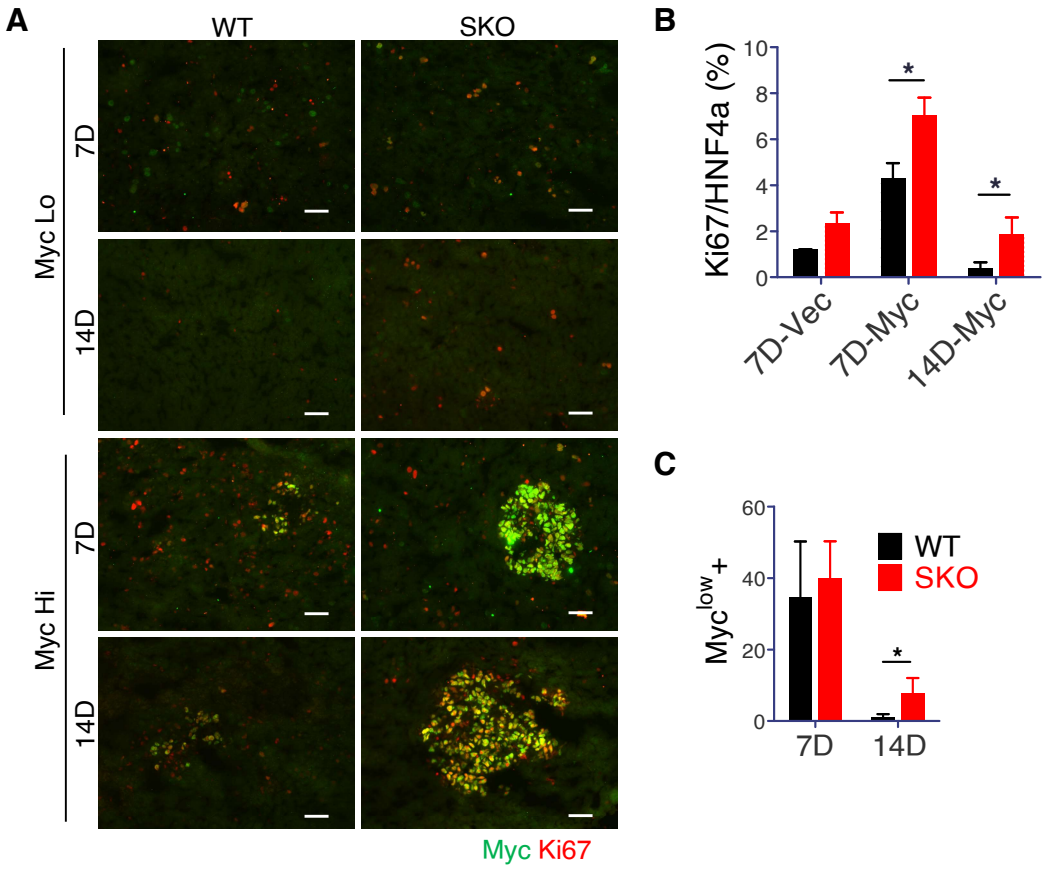

Figure 1.6 Only Myc^{hi}-transfected cells develop into tumors

(**A**) Staining of Myc and Ki67 in WT and SKO livers 7 and 14 days post Myc injection, in Myc^{Lo} and Myc^{Hi} cell colonies. Scale bar, 50 μm.

(**B-C**) Quantified cell numbers of Ki67^{+} per HNF4α^{+} (**B**), Ki67^{+} per Myc^{Lo} (**C**) in WT and SKO livers at 1 and 2 weeks after HTVi.

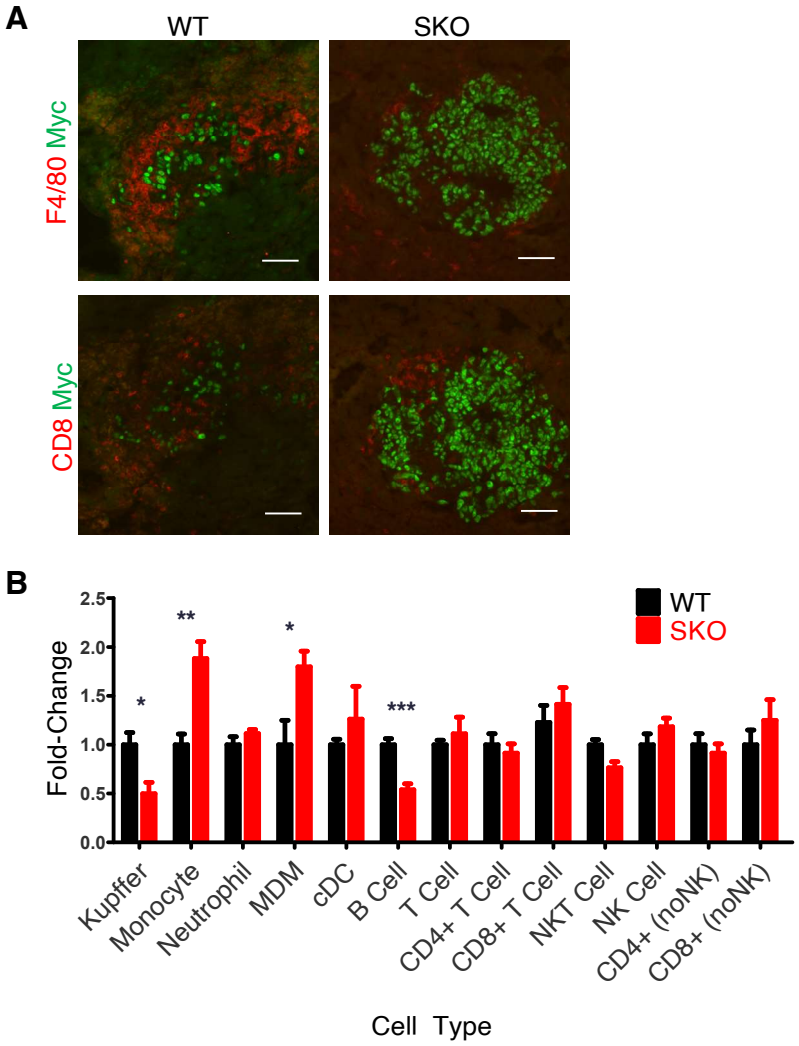

Figure 1.7 Immune population changes in response to Myc-transfected cells

(**A**) Co-staining of Myc with F4/80 (Top), with CD8 (Bottom) in WT and SKO livers at 10d post-Myc transfection. Scale bar, 100 μm.

(**B**) FACS of immune cell populations 12 days after Myc transfection in isolated NPCs of WT and SKO livers: (Initial gate: $CD45^+$ $CD11b^+$) Kupffer cells: $Ly6c^-$ $F4/80^+$; Monocytes: $Ly6c^{Hi}$ $F4/80^-$; Neutrophils: $Ly6c^{Hi}$ $F4/80^-$; monocyte-derived macrophages (MDM): $Ly6c^+$ $F4/80^+$. (Initial gate: $CD45^+$) classical dendritic cells (cDC): $MHCII^+$, $CD11c^+$; B cells: $TCR\beta^-$ $CD19^+$; T cells: $CD19^-$ $TCR\beta^+$. (Gated: $CD45^+$ $TCR\beta^+$) $CD4^+$ and $CD8^+$ T cells; $CD45^+$ NKT ($NK1.1^+$ $TCR\beta^+$) and NK ($NK1.1^+$ $TCR\beta^-$) cells; and $CD45^+$ $TCF\beta^+$ $NK1.1^-$ gated $CD4^+$ and $CD8^+$ T cells. Statistical analysis was done with student's T-test (ns, ** $p < 0.01$, * $p < 0.05$).

Figure 2.1 Single-cell RNA-sequencing of Myc-dependent tumor development

(**A**). Experimental design of scRNA-seq. Single hepatic cells were isolated from WT and SKO livers at day 0 (0D-Ctrl), day 10 (10D-Vector, 10D-Myc), and 4 weeks (4W-Myc). Hepatocytes and NPCs were separated for library preparation and data collection as detailed in Materials and Methods.

(**B-E**). tSNE plots show single cell clusters from integrated scRNA-seq data at 0D-Ctrl (**B**), 10D-Vector (**C**), 10D-Myc (**D**), and 4W-Myc (**E**), after Myc injection. Integrated data sets for each time point include hepatocytes and NPCs in WT and SKO livers, cluster legends on right. Clusters marked with red dots exist only in 4W data.

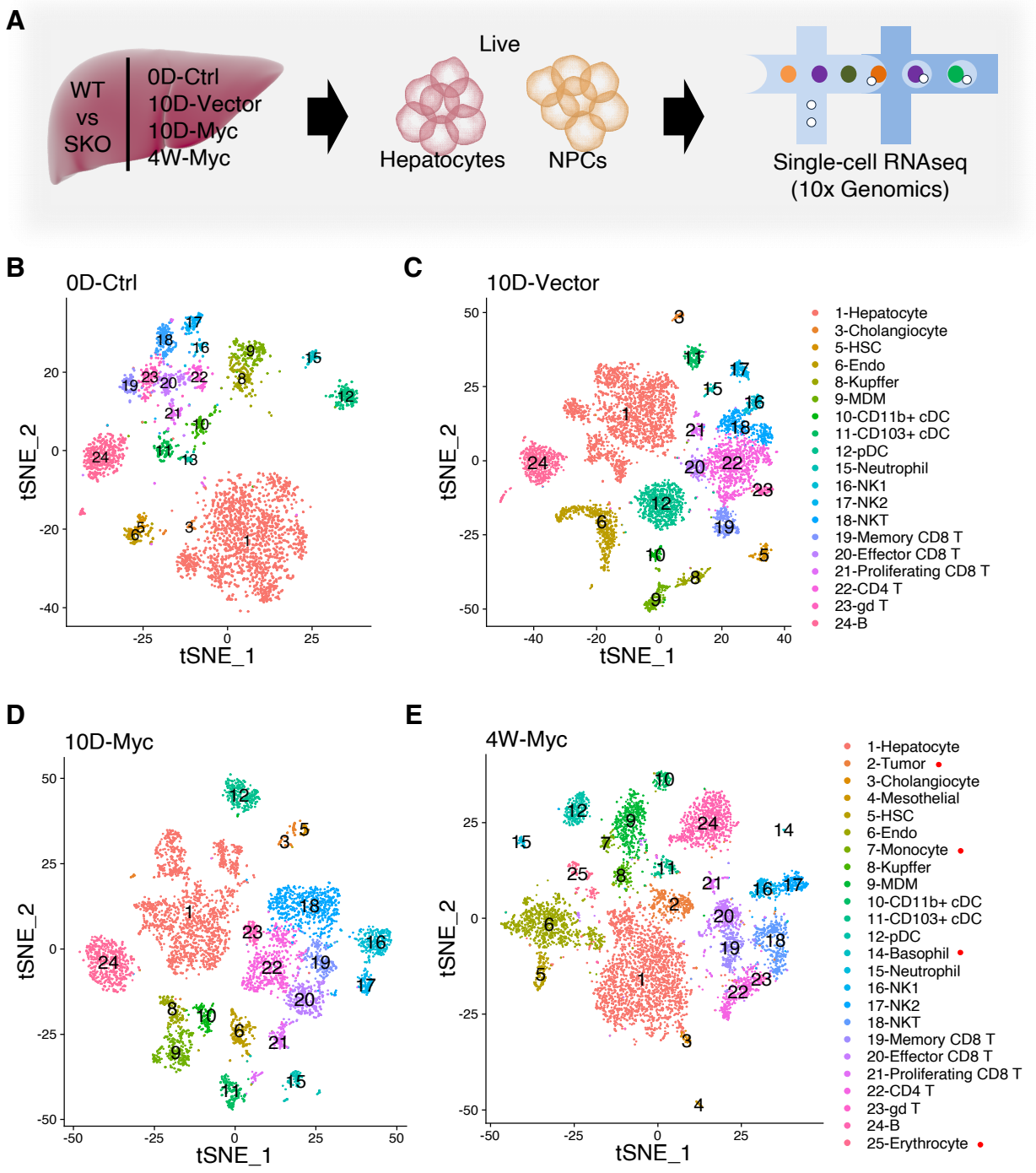
A
WT
vs
SKO
0D-Ctrl
10D-Vector
10D-Myc
4W-Myc
Live
Hepatocytes
NPCs
Single-cell RNAseq
(10x Genomics)
B
0D-Ctrl
C
10D-Vector
D
10D-Myc
E
4W-Myc
tSNE_1
tSNE_2
1-Hepatocyte
2-Tumor
3-Cholangiocyte
4-Mesothelial
5-HSC
6-Endo
7-Monocyte
8-Kupffer
9-MDM
10-CD11b+ cDC
11-CD103+ cDC
12-pDC
14-Basophil
15-Neutrophil
16-NK1
17-NK2
18-NKT
19-Memory CD8 T
20-Effector CD8 T
21-Proliferating CD8 T
22-CD4 T
23-gd T
24-B
25-Erythrocyte

Figure 2.2 Additional plots associated with scRNA-seq data integration.

(**A-D**) Integrated tSNE plots showing clusters of single cells from WT and SKO livers at 0D-Ctrl (**A**), 10D-Vector (**B**), 10D-Myc (**C**), 4W-Myc (**D**). Colored dots label cell types identified in each cluster.

(**E-H**) Important marker genes used for cell type assignment in 0D-Ctrl (**E**), 10D-Vector (**F**), 10D-Myc (**G**), 4W-Myc (**H**) data and their expression levels in said cell type clusters.

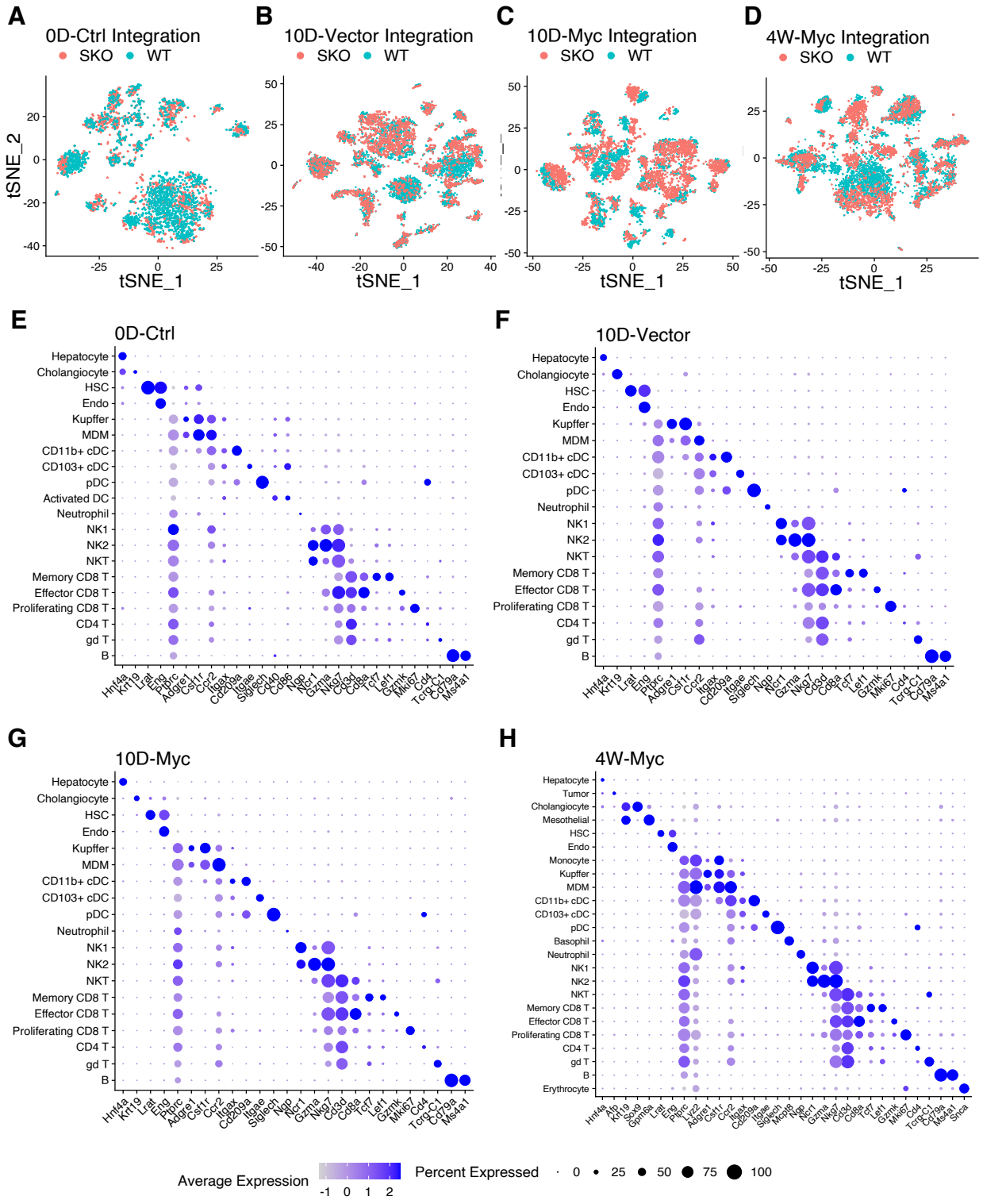
A
0D-Ctrl Integration
SKO WT
tSNE_2
tSNE_1
B
10D-Vector Integration
SKO WT
tSNE_1
C
10D-Myc Integration
SKO WT
tSNE_1
D
4W-Myc Integration
SKO WT
tSNE_1
E
0D-Ctrl
Hepatocyte
Cholangiocyte
HSC
Endo
Kupffer
MDM
CD11b+ cDC
CD103+ cDC
pDC
Activated DC
Neutrophil
NK1
NK2
NKT
Memory CD8 T
Effector CD8 T
Proliferating CD8 T
CD4 T
gd T
B
Hnf4a Krt19 Lrat Eng Ptprc Adgre1 Csf1r Ccr2 Itgax Cd209a Itgae Siglech Cd40 Cd86 Ncp Ncr1 Gzma Nkg7 Cd3d Cd8a Tcf7 Lef1 Gzmk Mki67 Cd4 TcrgC1 Cd79a Ms4a1
F
10D-Vector
Hepatocyte
Cholangiocyte
HSC
Endo
Kupffer
MDM
CD11b+ cDC
CD103+ cDC
pDC
Neutrophil
NK1
NK2
NKT
Memory CD8 T
Effector CD8 T
Proliferating CD8 T
CD4 T
gd T
B
Hnf4a Krt19 Lrat Eng Ptprc Adgre1 Csf1r Ccr2 Itgax Cd209a Itgae Siglech Ncp Ncr1 Gzma Nkg7 Cd8d Cd8a Tcf7 Lef1 Gzmk Mki67 Cd4 TcrgC1 Cd79a Ms4a1
G
10D-Myc
Hepatocyte
Cholangiocyte
HSC
Endo
Kupffer
MDM
CD11b+ cDC
CD103+ cDC
pDC
Neutrophil
NK1
NK2
NKT
Memory CD8 T
Effector CD8 T
Proliferating CD8 T
CD4 T
gd T
B
Hnf4a Krt19 Lrat Eng Ptprc Adgre1 Csf1r Ccr2 Itgax Cd209a Itgae Siglech Ncp Ncr1 Gzma Nkg7 Cd3d Cd8a Tcf7 Lef1 Gzmk Mki67 Cd4 TcrgC1 Cd79a Ms4a1
H
4W-Myc
Hepatocyte
Tumor
Cholangiocyte
Mesothelial
HSC
Endo
Monocyte
Kupffer
MDM
CD11b+ cDC
CD103+ cDC
pDC
Basophil
Neutrophil
NK1
NK2
NKT
Memory CD8 T
Effector CD8 T
Proliferating CD8 T
CD4 T
gd T
B
Erythrocyte
Hnf4a Afp Krt19 Sox9 Epcam6a Lrat Eng Ptprc Lyz2 Adgre1 Csf1r Ccr2 Itgax Cd209a Itgae Siglech Mcpt8 Ncp Ncr1 Gzma Nkg7 Cd3d Cd8a Tcf7 Lef1 Gzmk Mki67 Cd4 TcrgC1 Cd79a Ms4a1 Snca
Average Expression
-1 0 1 2
Percent Expressed
0 25 50 75 100

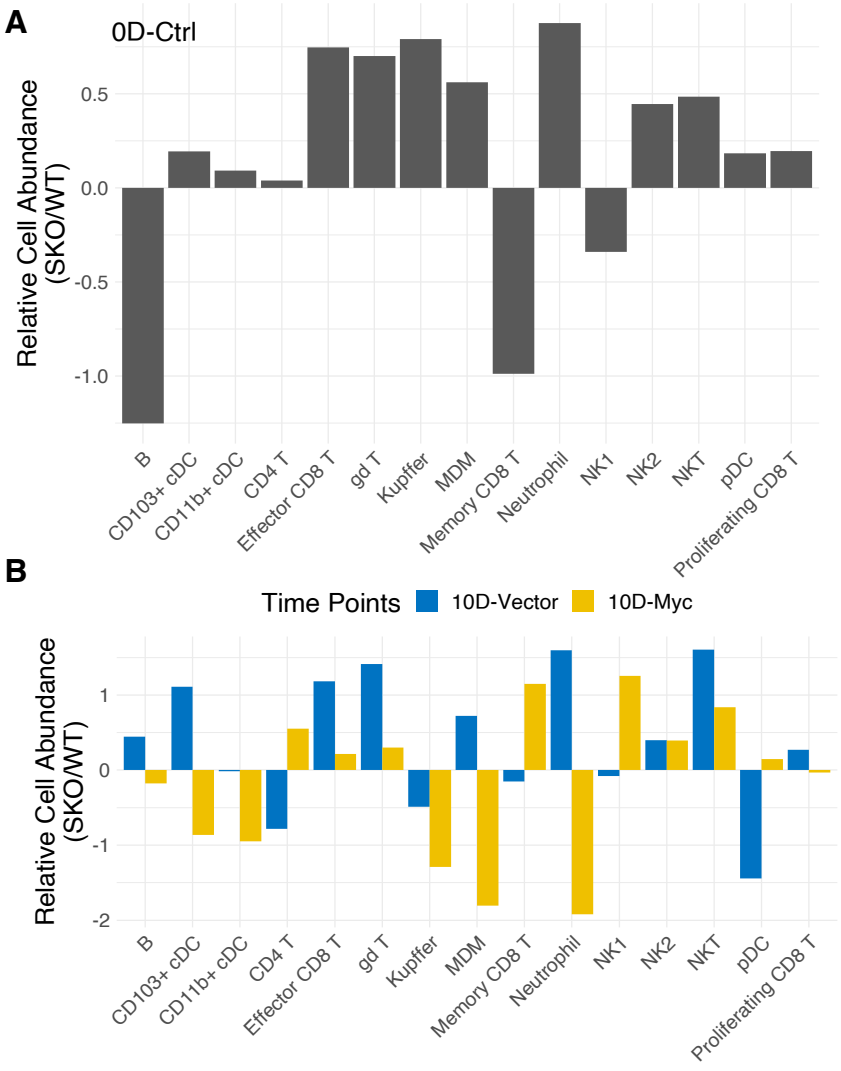

Figure 2.3 Early immune cell populations identified by scRNA-seq analysis
(**A-B**) Comparison of quantified immune cell populations between SKO and WT livers, based on 0D-Ctrl data (**A**), 10D-Vector and 10D-Myc data (**B**). For each cell type, the relative cell abundance was calculated as the log-transformed ratios of SKO vs WT percentages. Positive abundance indicates higher population in SKO.

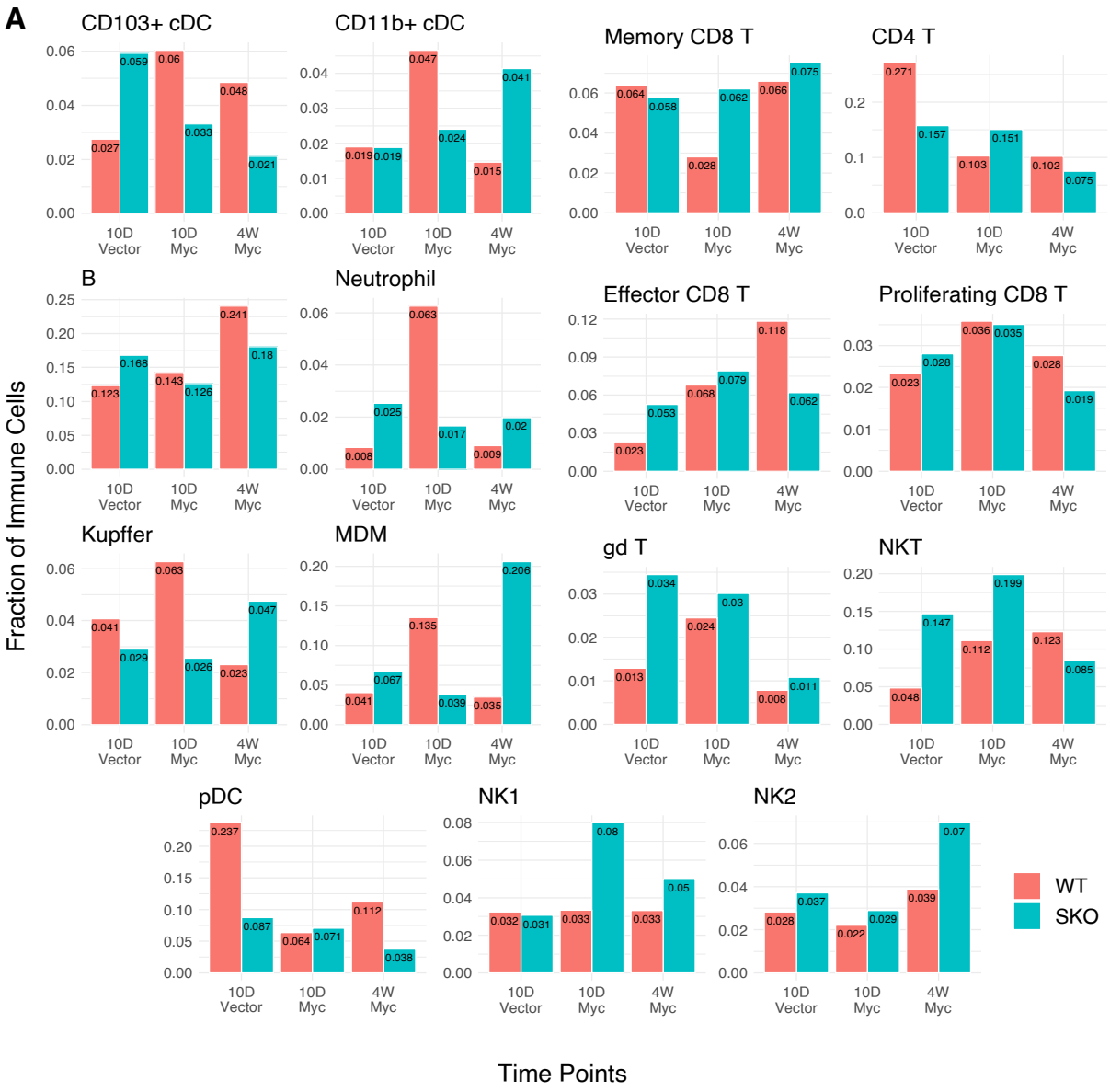

Figure 2.4 scRNA-seq analysis reveals comparative immune population change over time

(**A**) Quantified innate immune cell populations of SKO livers, relative to WT Livers, between 10D-Vector, 10D-Myc, and 4W-Myc data: CD103+ DC, CD11b+ cDC, B, Neutrophil, Kupffer, MDM, memory CD8 T, CD4 T, effector CD8 T, proliferating CD8 T, DN T, NKT, NK1, NK2, and pDC cell populations.

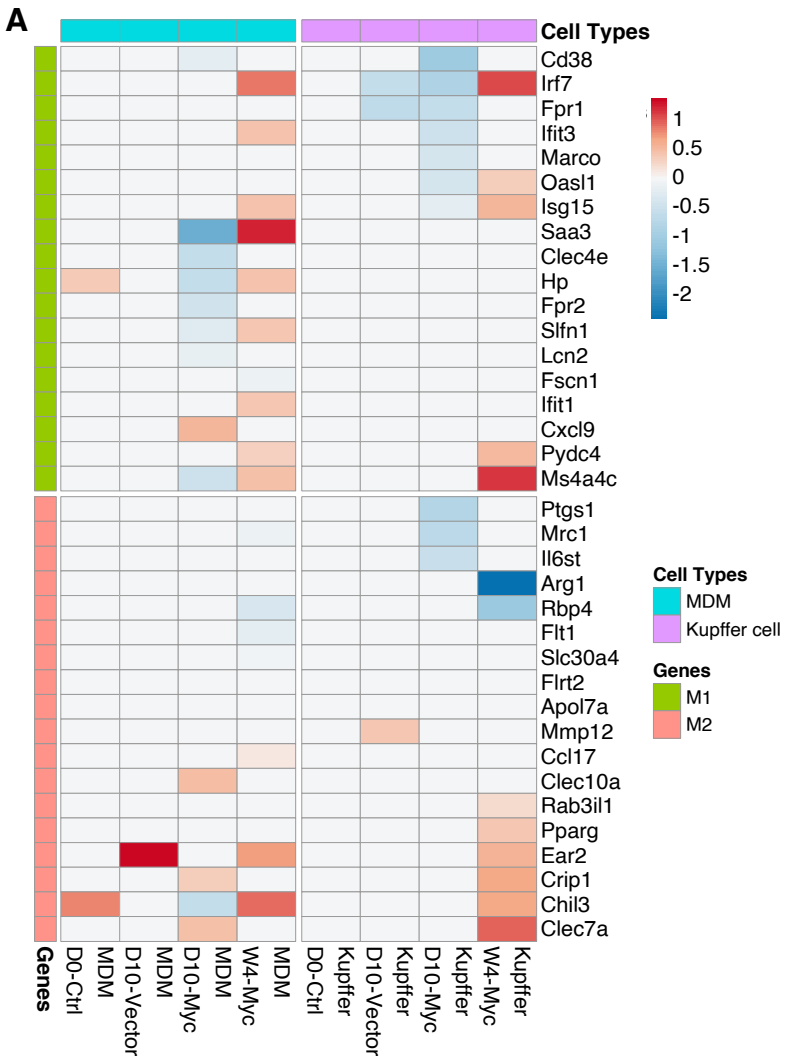

Figure 2.5 Contrasting macrophage polarization uncovered in a permissive TME of SKO liver

(**A**) Differential expression analysis for MDMs (Blue) and Kupffer cells (Red) at all time points. The values in heatmap indicate averaged log2 fold changes in SKO over WT livers, for corresponding cell types at different time points.

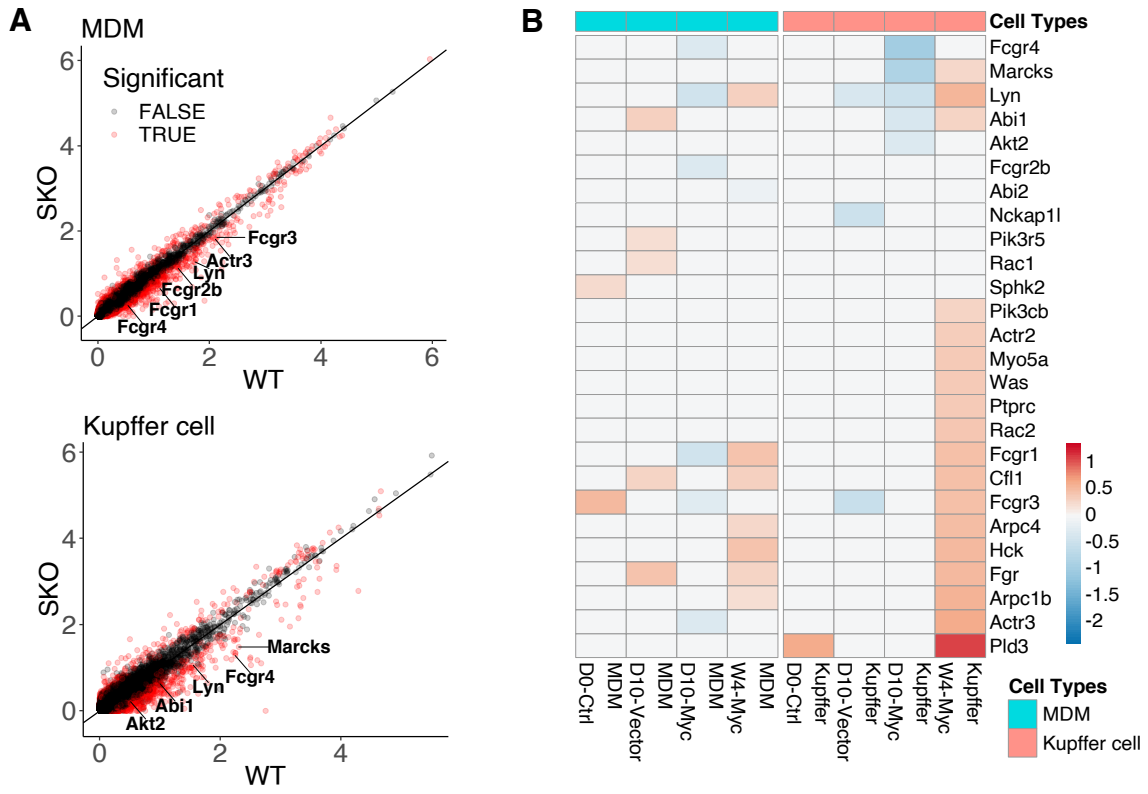

Figure 2.6 Macrophage phagocytosis-related clearance of Myc-transfected cells in WT liver

(**A**) Differential gene expression analysis for MDM (Top) and Kupffer cells (Bottom) in 10D-Myc data. Significantly expressed phagocytosis genes were marked in red; Expression higher in WT than SKO.

(**B**) Differential gene expression analysis for only phagocytosis genes for MDM (Left) and Kupffer cells (Right) in 10D-Myc data. Significantly expressed phagocytosis genes were marked in red, with higher expression in WT than SKO livers.

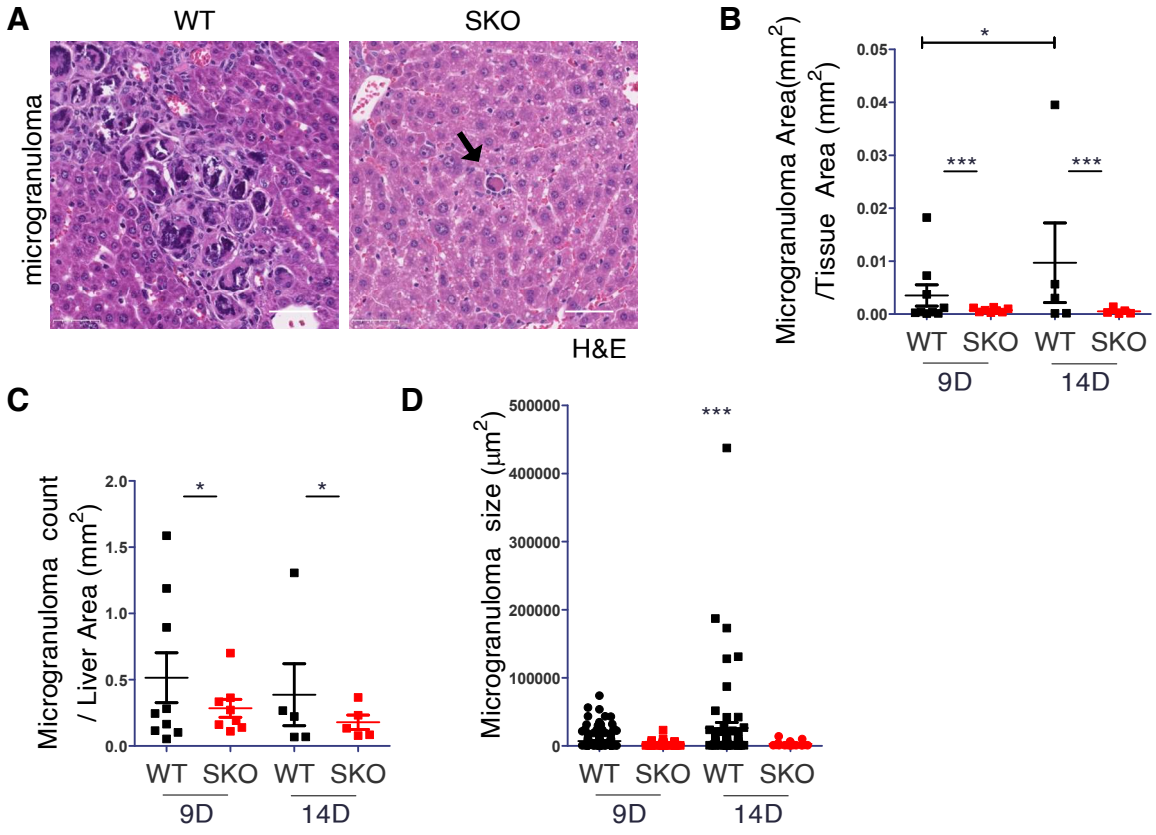

Figure 2.7 Microgranuloma structures reveal macrophage-based clearance of hepatocyte-like colonies

(**A**) Representative H&E of microgranuloma structures in WT and SKO liver at 9d post-Myc transfection. Scale bar, 50 μm.

(**B-D**) Quantified microgranuloma areas per tissue area (**B**), count per tissue area (**C**), and size (**D**) in WT and SKO livers at 9d and 14d. Statistical analysis using student's T-test. (* $p < 0.05$, *** p-value < 0.001).

Figure 2.8 Macrophage depletion doesn't overcome tumor ablation in WT Liver

(**A**) Macrophage depletion experimental scheme

(**B**) Representative liver images of WT and SKO livers after Clodronate Liposome (C.L.) treatment with HTVi Myc injection.

(**C**) Quantification of liver to body weight ratios (LW/BW), visible tumor nodule numbers, and spleen to body weight ratios (SW/BW) (n=3). C.L. did not significantly change tumor burden across both genotypes (n.s.)

(**D**) Immunohistochemistry of F4/80 and CD8 in liver and spleen, showing efficient clearance of macrophage in C.L. injected livers with less efficient clearance in spleens. CD8+ T cell populations were unaffected by C.L. treatment

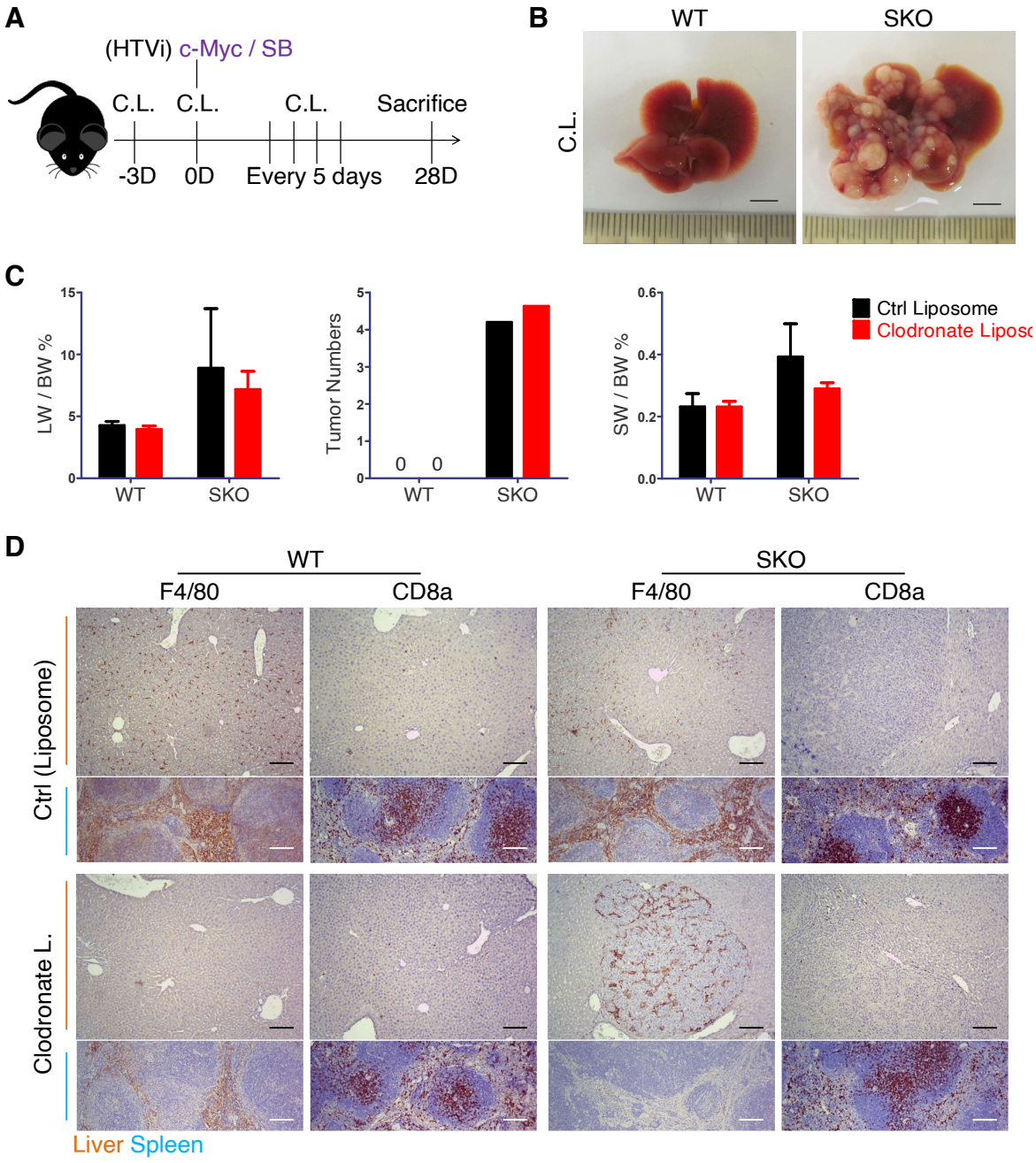
A
(HTVi) c-Myc / SB
C.L.
C.L.
C.L.
Sacrifice
-3D
0D
Every 5 days
28D
B
WT
SKO
C.L.
C
LW / BW %
Tumor Numbers
SW / BW %
WT
SKO
Ctrl Liposome
Clodronate Liposc
D
WT
SKO
F4/80
CD8a
F4/80
CD8a
Ctrl (Liposome)
Clodronate L.
Liver Spleen

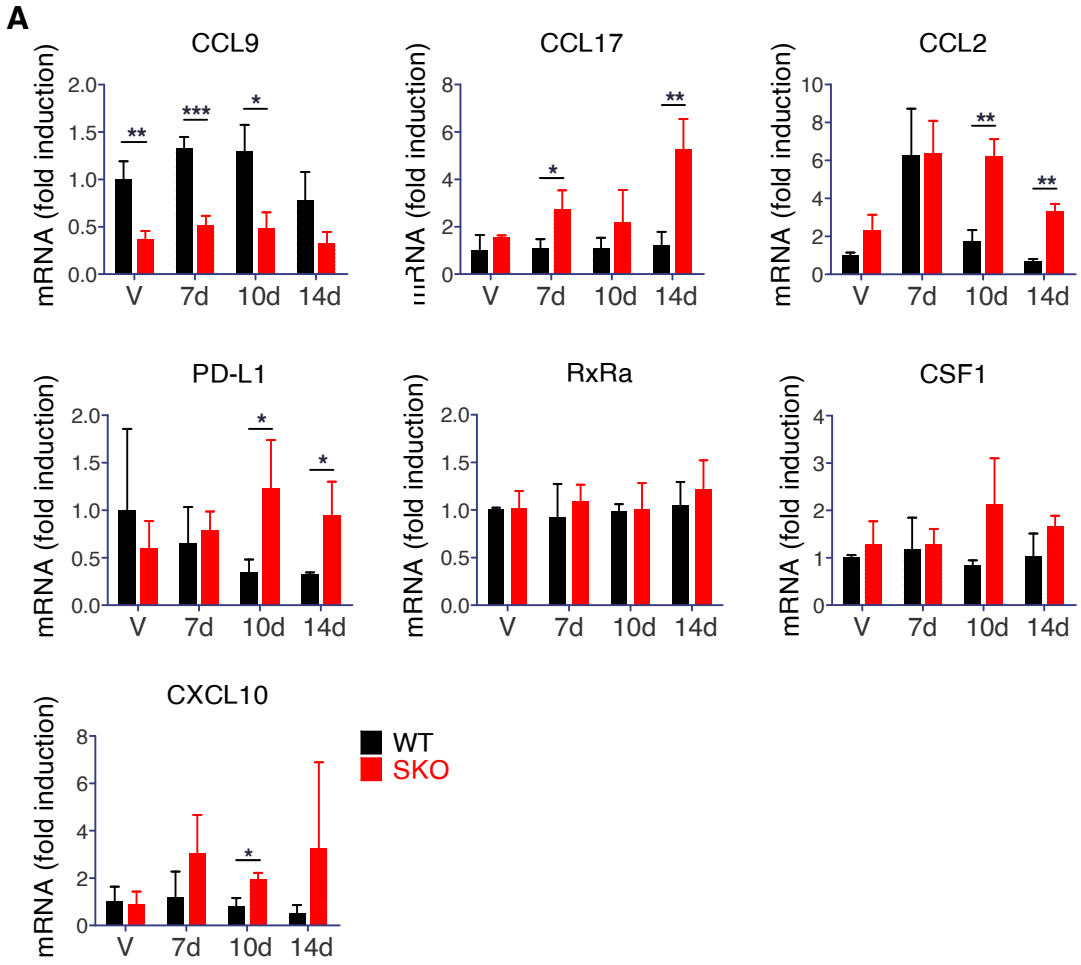

Figure 2.9 Cytokines affected by Shp2-deletion and tumorigenesis to induce permissive TME

(**A**) qRT-PCR analysis of cytokines CCL9, CCL17, CCL2, PD-L1, RxRa, CSF1, and CXCL10 in WT and SKO livers 7d after Vector injection or 7d, 10d, 14d after Myc injection. Statistical analysis used student's T-test. Values are presented as means ± SD. (*** $p < 0.001$, ** $p < 0.01$, * $p < 0.05$).

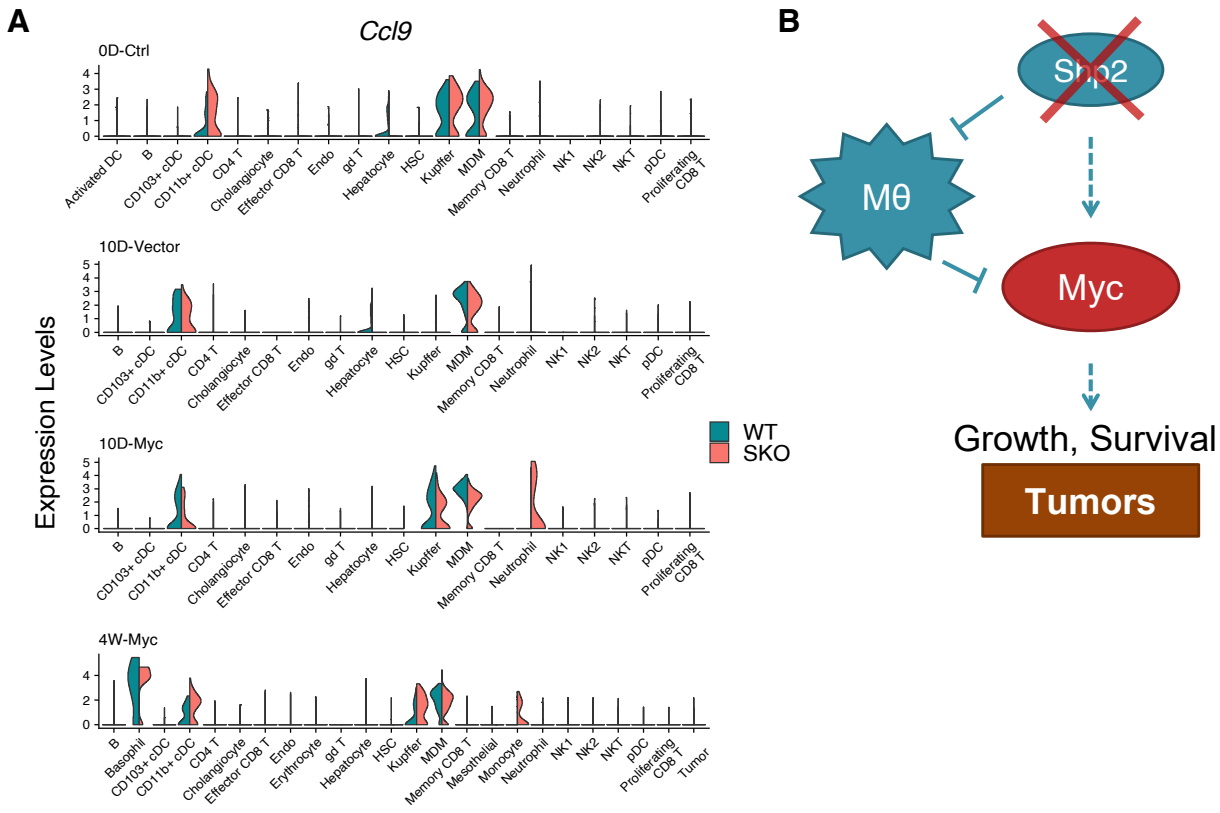

Figure 2.10 Immune induced Ccl9 contributes to tumor-permissive immune microenvironment

(**A**) Violin plots comparing Ccl9 expression between WT and SKO in each cell type as indicated, in 0D-Ctrl, 10D-Vector, 10D-Myc, and 4W-Myc data.

(**B**) Summary of results showing Shp2 ablation generates aberrant macrophages causing tumor permissive microenvironment.

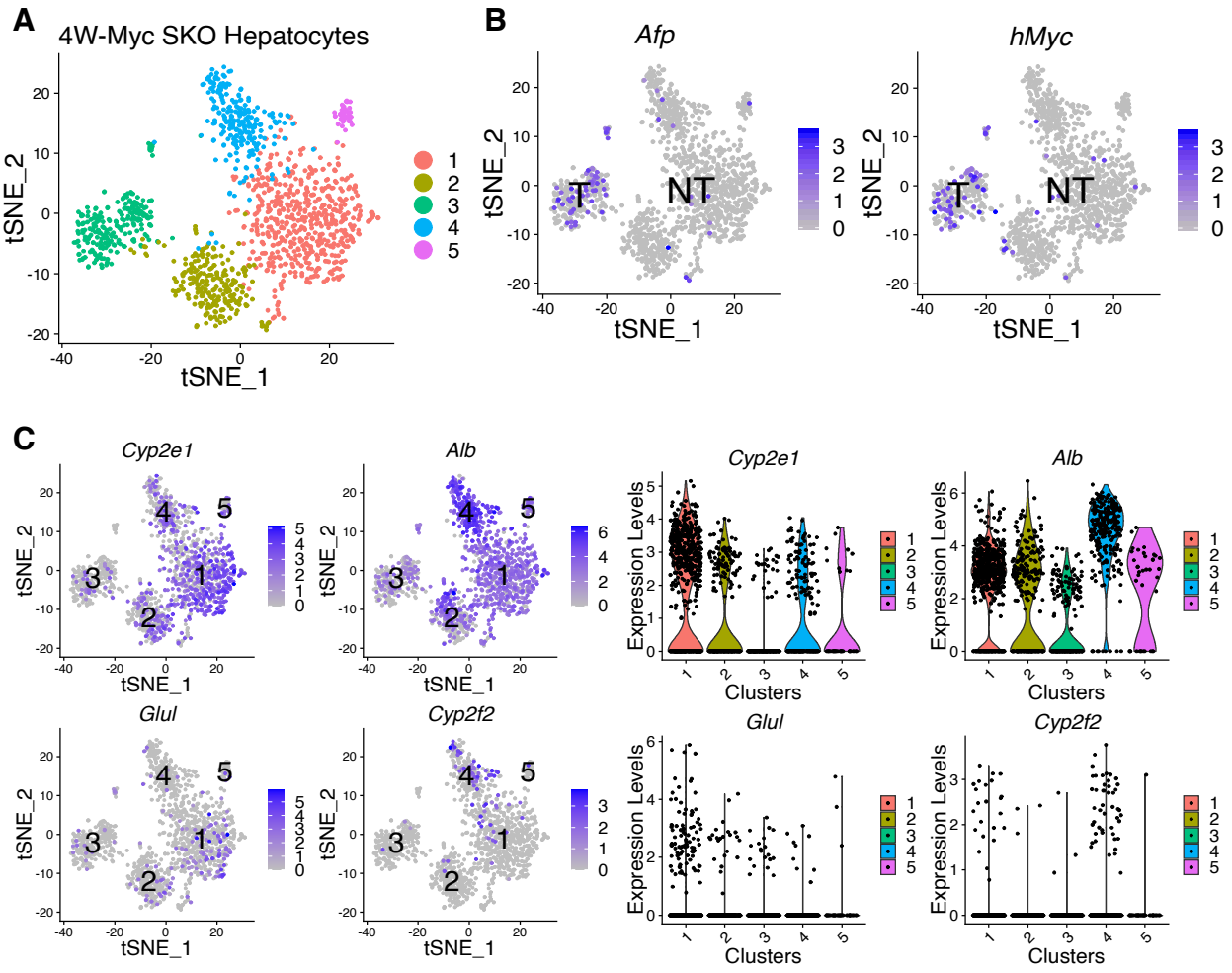

Figure 3.1 Analysis of 4W-Myc SKO scRNA-seq data on hepatocytes and tumor populations

(**A**) tSNE plot shows clustering of hepatocytes in Myc-transfected SKO liver at 4 weeks (4W-Myc SKO). (1) central vein zone; (2) OxPhos & translation-related; (3) tumor; (4) portal vein zone; (5) Malat1^{hi} hepatocytes.

(**B**) tSNE plot of data from 2D where blue dots show higher expression of Afp (α-fetoprotein) and Myc (exogenous Myc) in tumor (cluster 3) than non-tumor cells.

(**C**) 4W-Myc SKO hepatocyte clusters showing tSNE plot (left) and violin plot (right) for expression profiles of known liver zonation markers Cyp2e1, Albumin (Alb), Glutamine synthetase (Glul), and Cyp2f2 in hepatocyte clusters.

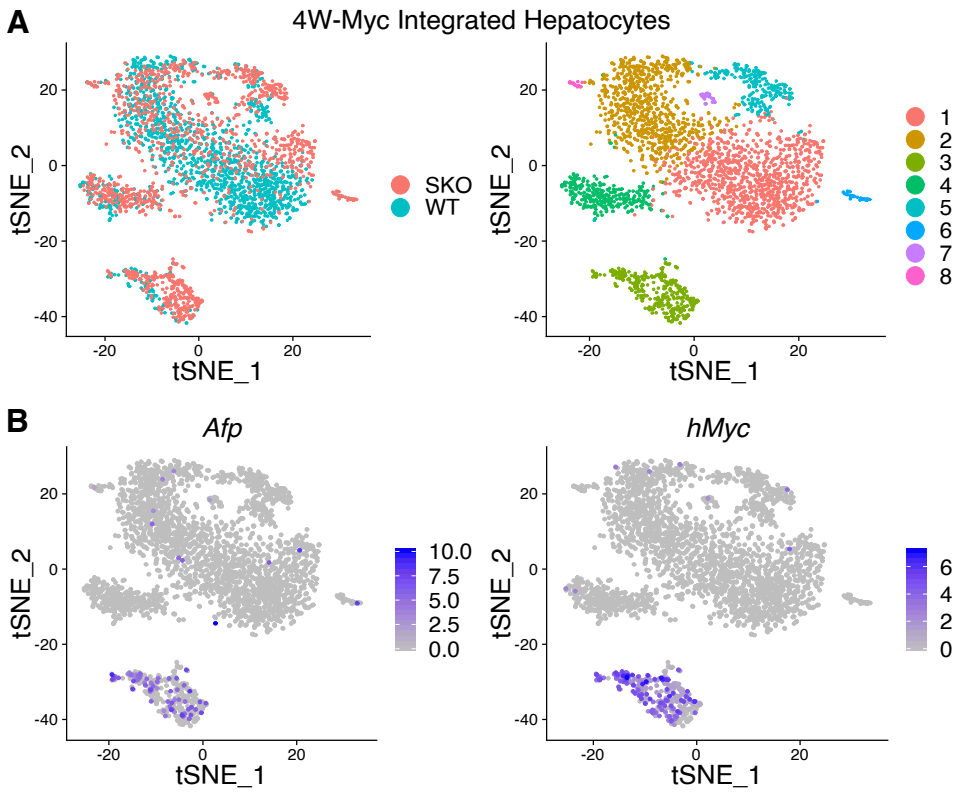

Figure 3.2 Overlap of hMyc^{+} populations in WT and SKO 4W-Myc scRNA-seq data

(**A**) tSNE plot of integrated 4W-Myc hepatocyte data where red and blue dots are WT and SKO (left), and various colors are hepatocyte clustering (right). Clusters include: (1) peri-portal hepatocytes; (2) mid-zone hepatocytes; (3) Tumor cells; (4) OxPhos & translation-related hepatocytes; (5) peri-central hepatocytes; (6) Malat1^{hi} hepatocytes; (7) Usp31^{+} hepatocytes; (8) Cd24a^{+} hepatocytes.

(**B**) AFP and Myc expression profile on tSNE plot of integrated WT and SKO 4W-Myc hepatocyte data showing Afp^{+} (left) and Myc^{+} (right) hepatocytes. Myc^{+} hepatocytes from WT and SKO cluster together, indicating Myc^{+} populations are tumor cells in both of them.

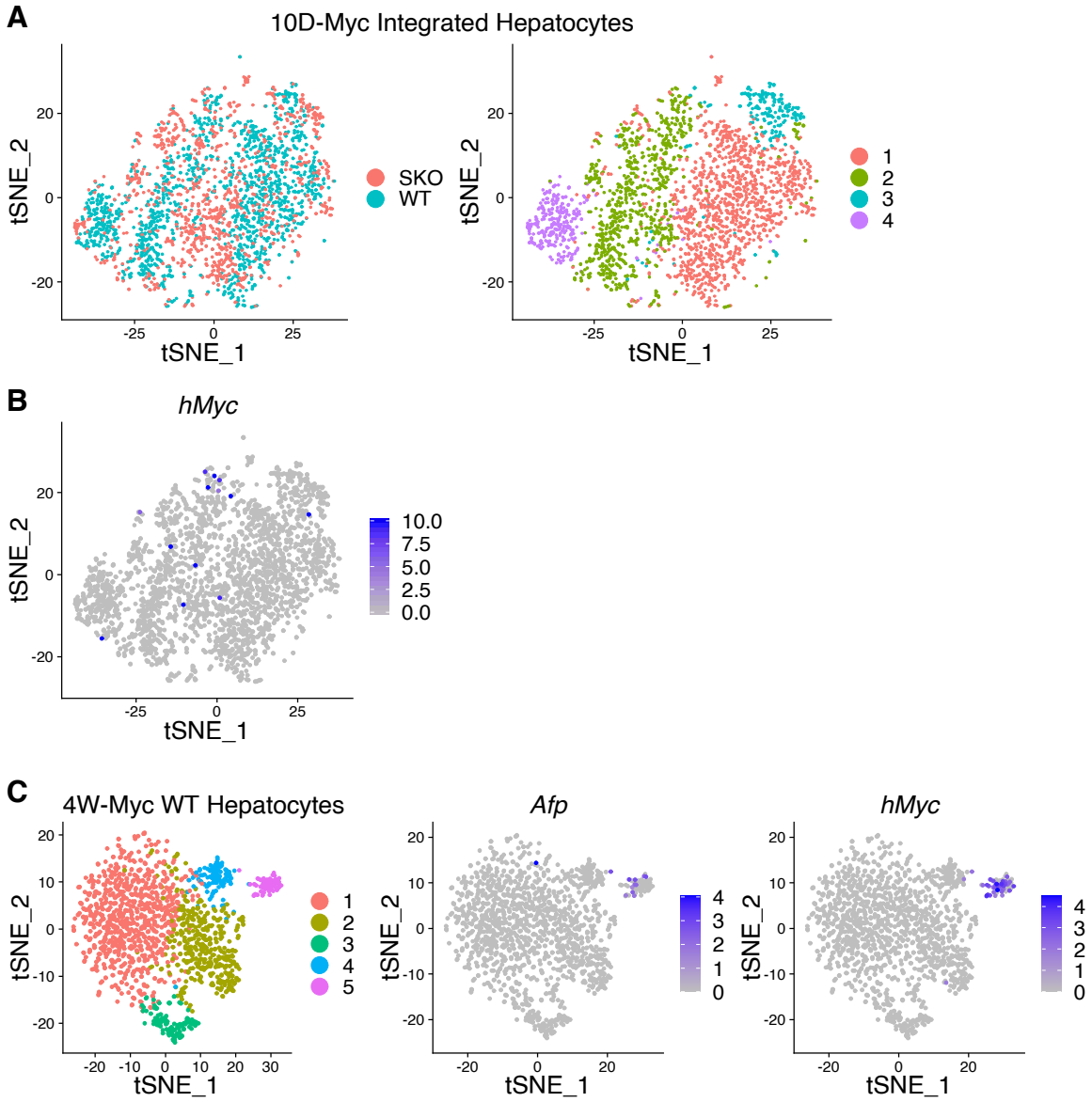

Figure 3.3 Identification of hMyc^{+} populations in scRNA-seq data

(**A**) tSNE plot of integrated WT and SKO 10D-Myc hepatocytes (left), and clusters of hepatocytes (right). Clusters include:: (1) peri-portal hepatocytes; (2) mid-zone hepatocytes; (3) peri-central hepatocytes; (4) Malat1^{hi} hepatocytes.

(**B**) Myc expression profile on tSNE plot of data from 2F, showing that Myc^{+} hepatocytes were scattered among clusters.

(**C**) tSNE plot of hepatocyte clustering from 4W-Myc WT liver showing hepatocyte clustering (left) and expression profiles of AFP and Myc (right). Clusters include: (1) peri-portal hepatocytes; (2) mid-zone hepatocytes; (3) peri-central vein hepatocytes; (4) OxPhos & translation-related hepatocytes; (5) Tumor cells.

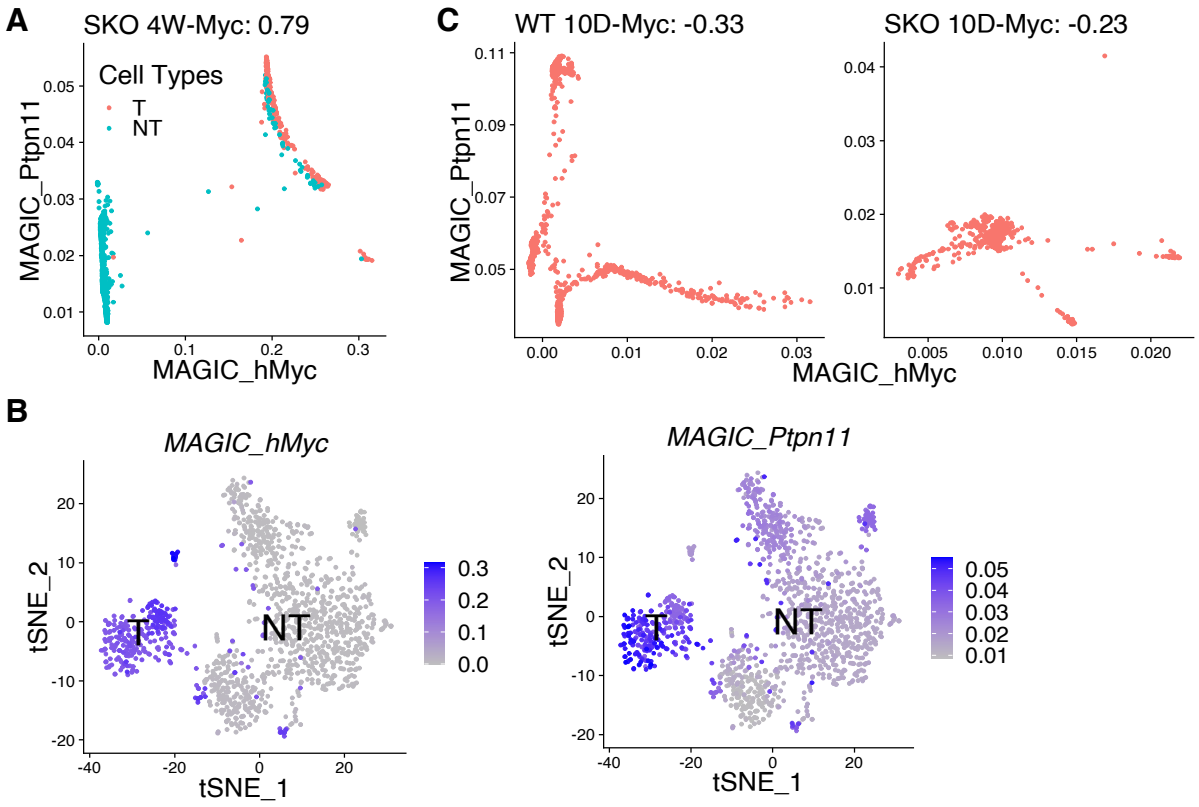

Figure 3.4 Myc-transfected cells select for Shp2+ expression in SKO hepatocytes

(**A**) Post-data imputation by MAGIC of 4W-Myc data, where red dots are tumor and green dots are non-tumor cells, Myc^{+} cells in the 4W-Myc data were largely $Ptpn11/Shp2^{+}$.

(**B**) Corresponding tSNE plots showing Myc or Ptpn11/Shp2 MAGIC-imputed expression profiles in 4W-Myc hepatocyte data, separated by Tumor and Non-tumor. The tumor cell cluster showed high expression of both Myc and Shp2.

(**C**) Post-data imputation by MAGIC of 10D-Myc data; In both WT and SKO data, few Myc^{+} cells were $Shp2^{+}$ at this early time point.

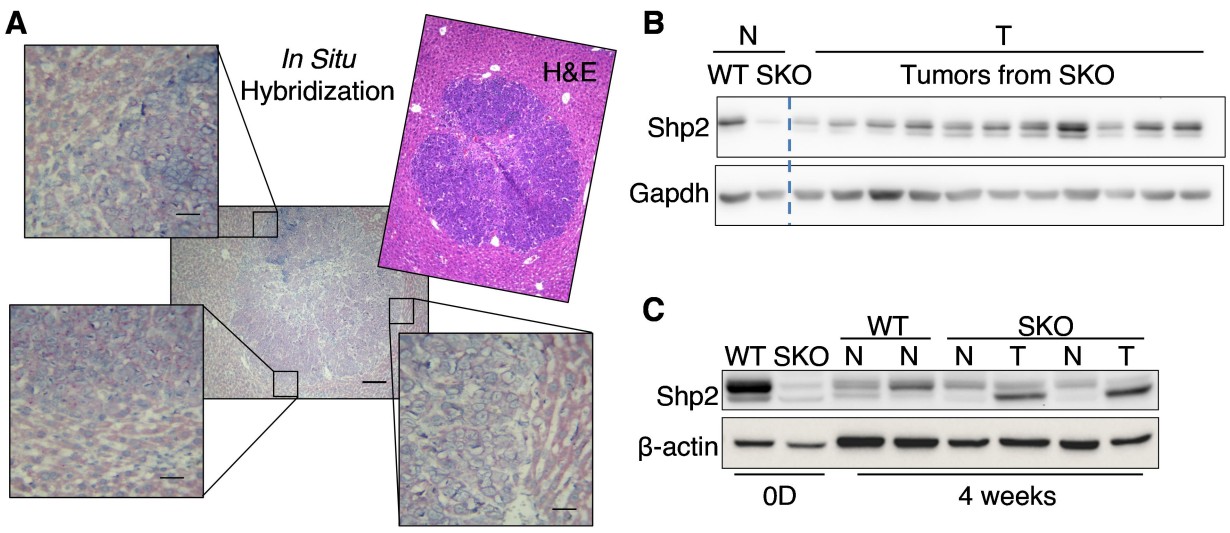

Figure 3.5 Shp2 presence in Myc+ tumors in SKO livers

(**A**) In situ hybridization of Shp2 detecting *Ptpn11/Shp2* mRNA in tumors at 4 weeks post-Myc injection. In pathological comparison to H&E staining in consecutive sections, *Shp2* mRNA levels were high in tumor areas. Scale bar, 50 μm.

(**B**) Immunoblotting of liver lysates from non-tumor (N) and tumor (T) tissues 4 weeks after Myc transfection indicating variable but increased Shp2 expression in tumor tissues.

(**C**) Immunoblotting of isolated hepatocyte lysates from WT and SKO livers at 0 day and 4 weeks after HTVi of Myc.

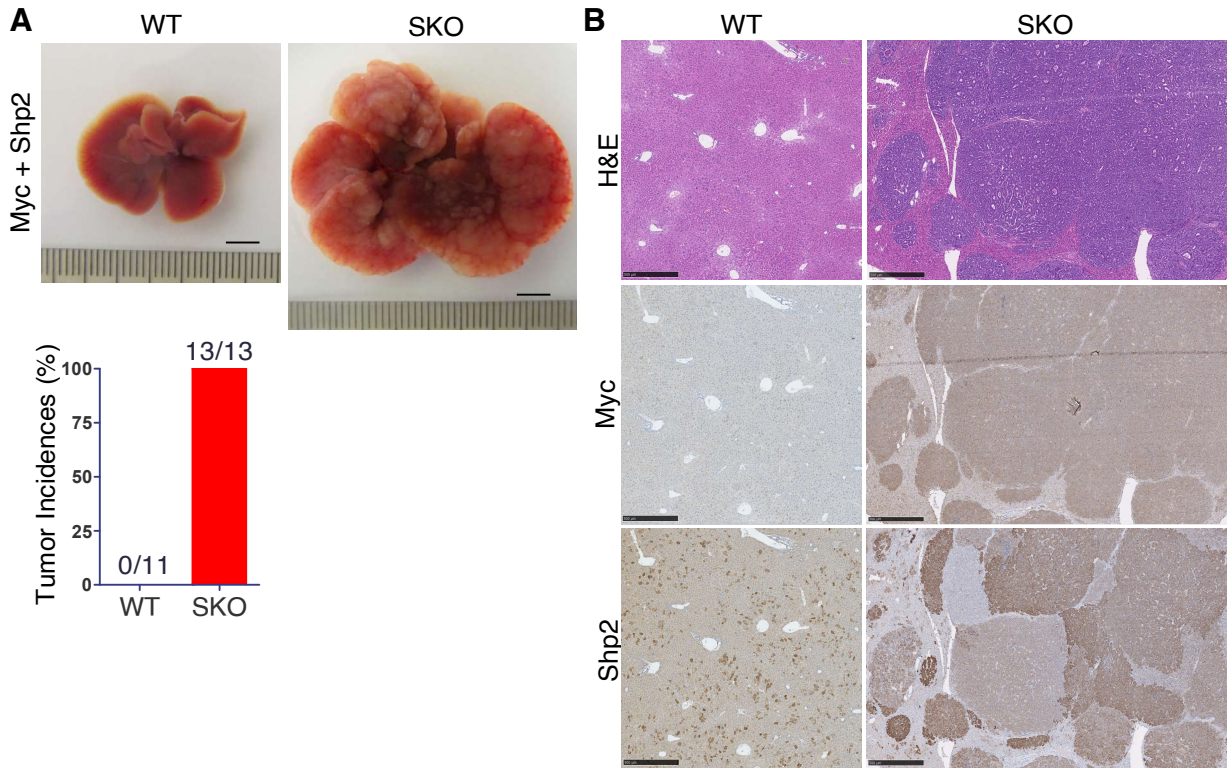

Figure 3.6 Shp2 expression enhances Myc-driven carcinogenesis

(**A**) Representative liver images and quantified tumor incidence rate 3 weeks post-HTVi of Myc and Shp2. n=11-13. Scale bar, 0.5 cm.

(**B**) Representative H&E, and immunostaining for Myc and Shp2 in consecutive sections of SKO livers transfected by Myc+Shp2. Scale bar, 500 μm.

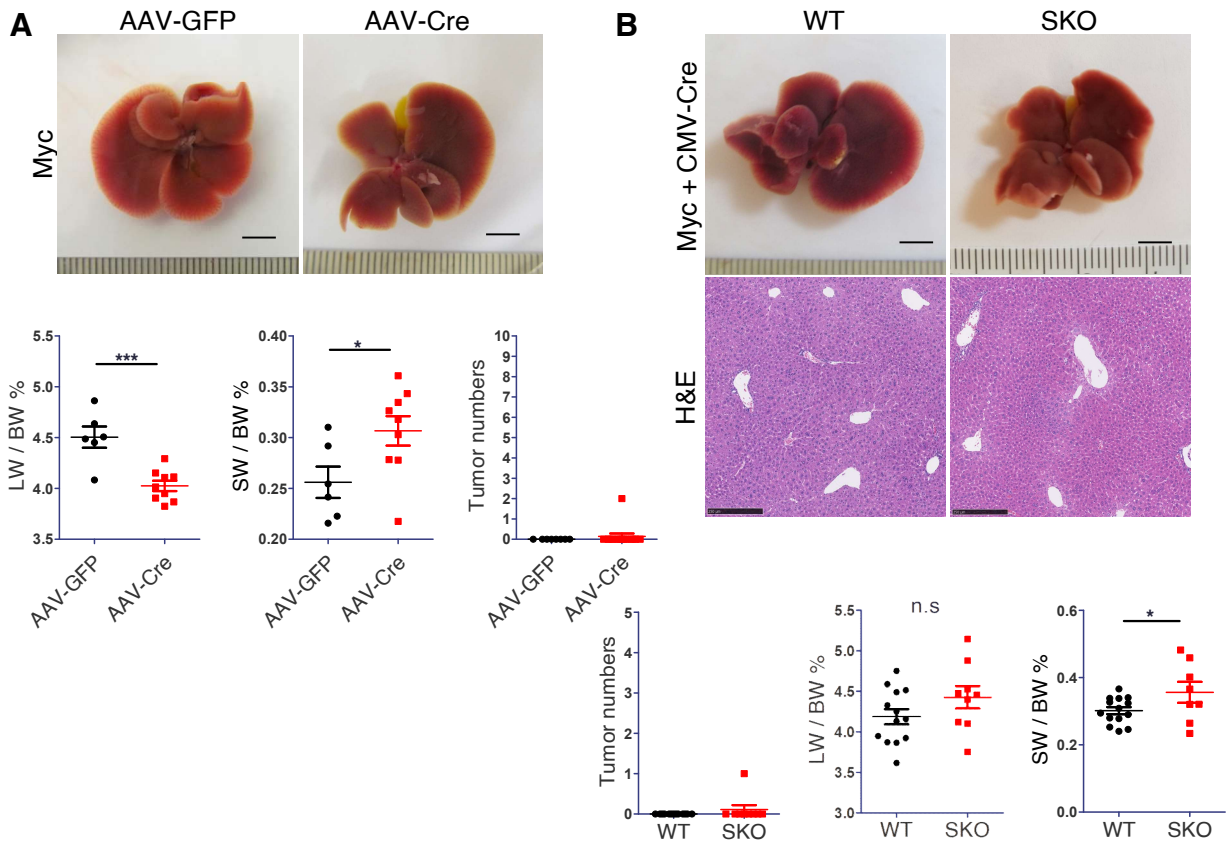

Figure 3.7 Shp2 is required for Myc-driven carcinogenesis

(**A**) WT (Shp2$^{f/f}$) mice were injected with AAV-GFP (n=6) or AAV-Cre (n=9) virus 1wk before Myc transfection via HTVi, and examined at 4wk. Representative liver images (left) and liver to body weight ratios (right). Scale bar, 0.5 cm. Quantification of LW/BW, SW/BW, and tumor numbers of mice at 4 weeks. n=6-10. Students T-test: (* $p < 0.05$, *** p-value < 0.001).

(**B**) Representative liver images and H&E staining of WT and SKO mice 4 weeks after HTVi of Myc and CMV-Cre. Scale bar, 0.5 cm. Quantification of LW/BW, SW/BW, and tumor numbers. n=9-11. Scale bar, 250 μm. Students T-test (* $p < 0.05$).

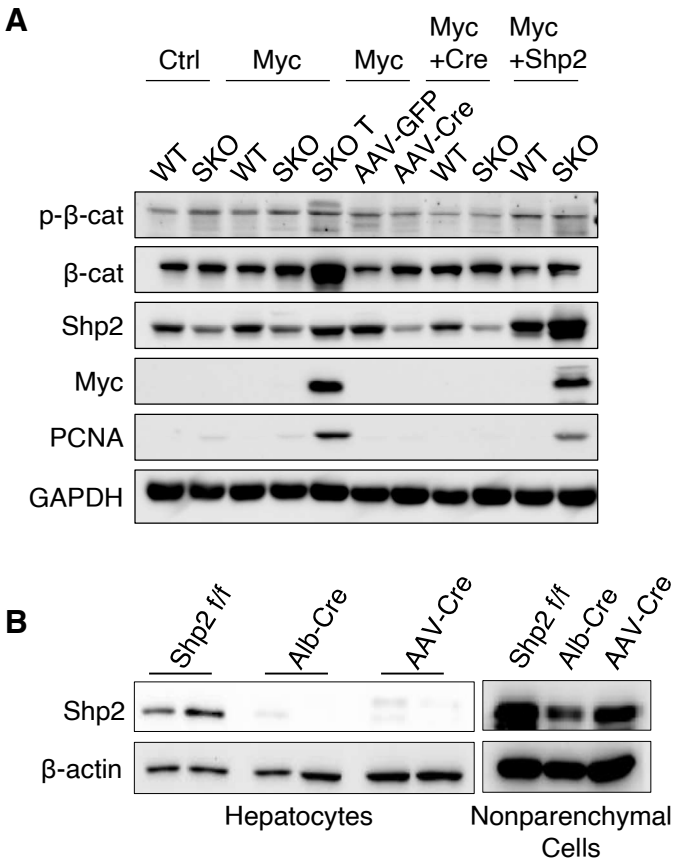

Figure 3.8 Shp2+ hepatocytes assist oncogenic Myc through Erk

(**A**) Immunoblotting of liver, tumor (T) or non-tumor (NT) tissue lysates of WT or SKO mice transfected with Myc, Shp2 with CMV-Cre, or infected with AAV-GFP or AAV-Cre.

(**B**) Shp2 protein level in hepatocyte and non-parenchymal cell lysate from WT Shp2$^{f/f}$, Albumin-cre, and AAV-Cre hepatocyte knock-out murine models at 8 weeks.

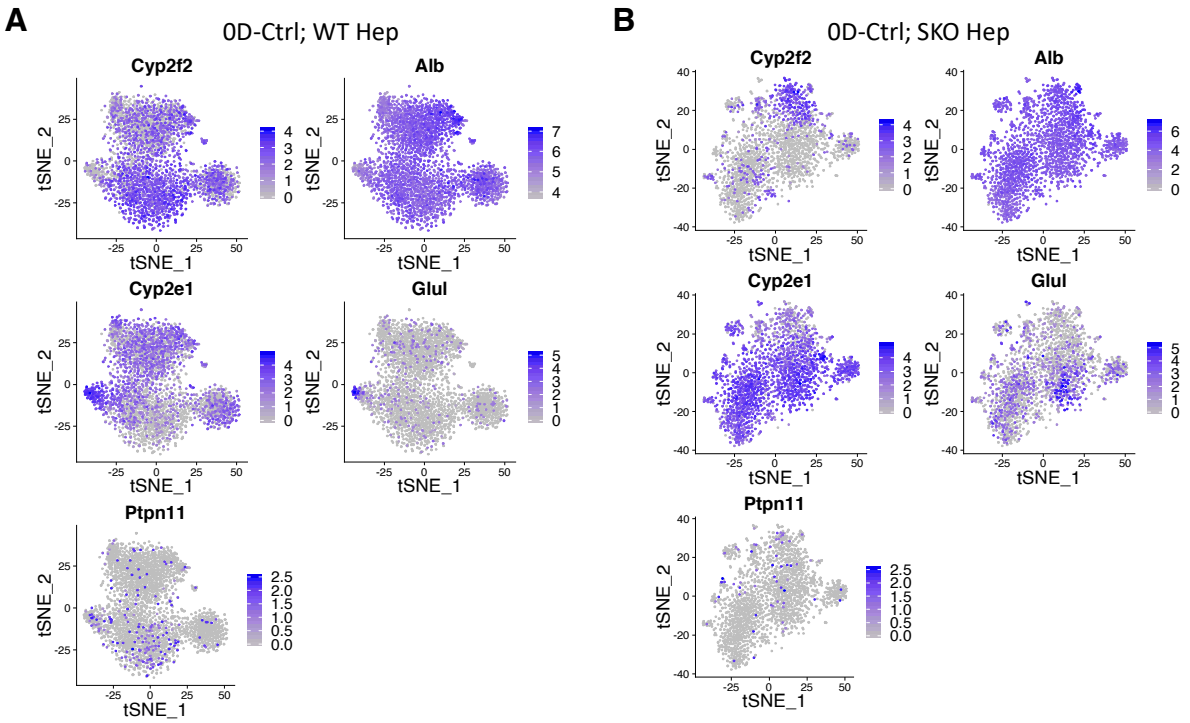

Figure 3.9 Shp2+ hepatocytes that escape deletion are not zonated

(**A-B**) scRNA-seq analysis showing expression of zonation markers and Ptpn11 at 0D-Ctrl timepoint in WT (**A**) and SKO (**B**) hepatocyte data.

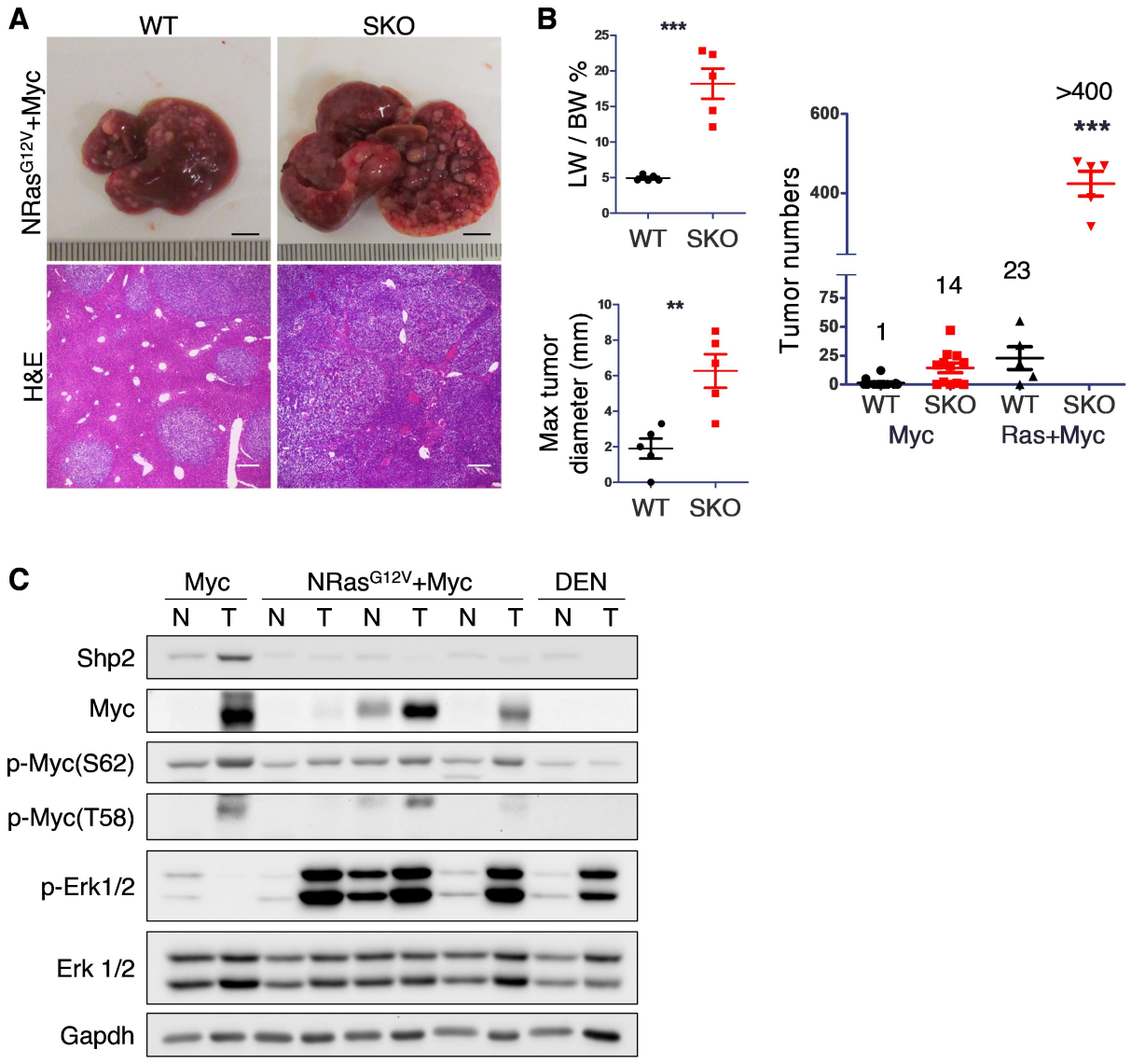

Figure 3.10 Oncogenic Ras bypasses Shp2 requirement in Myc-driven HCC

(**A**) Representative liver and H&E images of WT and SKO liver 4 weeks after HTVi of Ras+Myc (NRas^{G12V} + Myc), n=5. Scale bar, 0.5 cm.

(**B**) (Left) Quantified liver to body weight ratios (LW/BW), maximal tumor diameter of WT and SKO liver 4 weeks after HTVi of Ras+Myc (NRas^{G12V} + cMyc). (Right) Comparison of tumor numbers in WT and SKO livers, 4 weeks after HTVi of Myc alone or Ras+Myc. In SKO liver, Ras+Myc model had dramatically more tumors than Myc model.

(**D**) Immunoblot analysis of liver, tumor (T) or non-tumor (NT) tissue lysates of WT or SKO mice transfected with Myc, Ras+Myc, or tumors induced by diethylnitrosamine (DEN). Statistical significance was calculated using students' T-test (**p<0.01; ***p<0.001). Ras+Myc tumors did not have increased expression of Shp2.

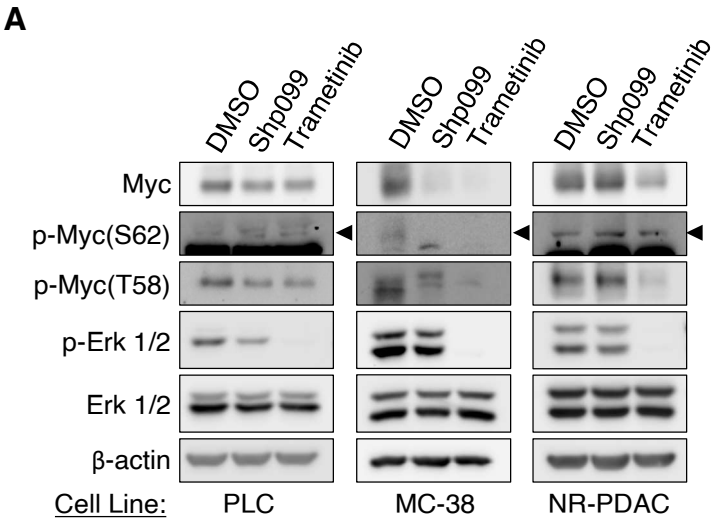

Figure 3.11 Inhibition of Shp2 or Mek causes accelerated Myc degradation

(**A**) Immunoblot analysis of Myc and Erk phosphorylation in PLC, MC38, and NR-PDAC cells treated with Cycloheximide (CHX) (MC38 cells: 50 μg/mL; PLC & NR-PDAC cells: 25 μg/mL), and then DMSO (Ctrl; 16 hr), SHP099 (Shp2 inhibitor), or Trametinib (Mek inhibitor). Cells treated with inhibitor had increased Myc degradation

Figure 3.12 Shp2/MEK inhibition significantly reduces Myc protein stability

(**A-C**) Immunoblot analysis of PLC (**A**), MC38 (**B**), and NR-PDAC (**C**) cell lysates treated with SHP099 (Shp2 inhibitor; 20 μM) for 16 hr or Trametinib (Mek inhibitor; 50 μM) for 4 hr (Bottom), using DMSO as control treatment. Time scale showing Myc protein levels after Cycloheximide (CHX) (MC38 cells: 50 μg/mL; PLC & NR-PDAC cells: 25 μg/mL) treatment. Graph and quantified stats (Right) demonstrating reduced Myc half-life in cells treated with Shp2 and Mek inhibitors.

A

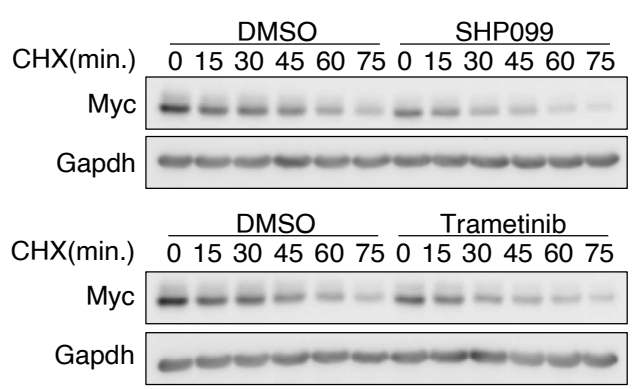

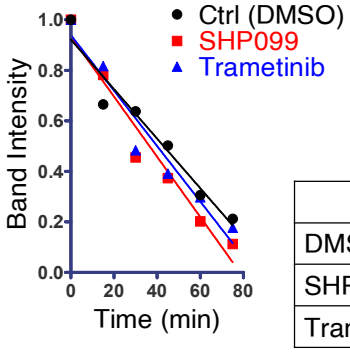

	Myc $t_{1/2}$
DMSO	43.05
SHP099	36.51
Trametinib	39.94

B

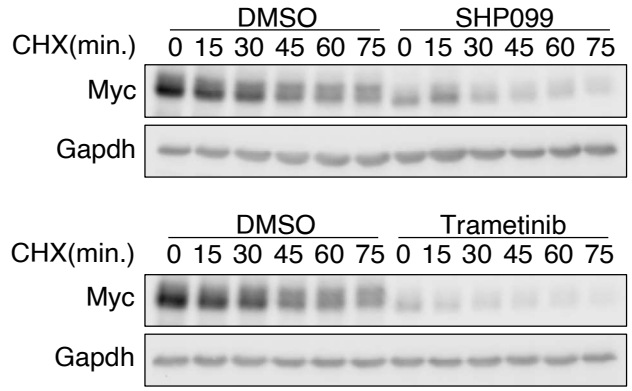

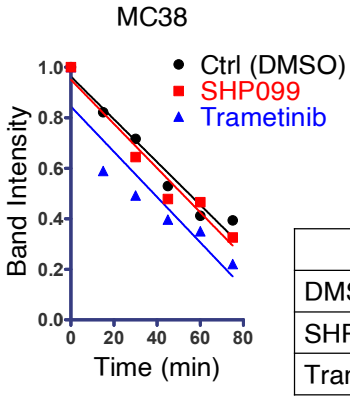

	Myc $t_{1/2}$
DMSO	54.49
SHP099	51.19
Trametinib	38.29

C

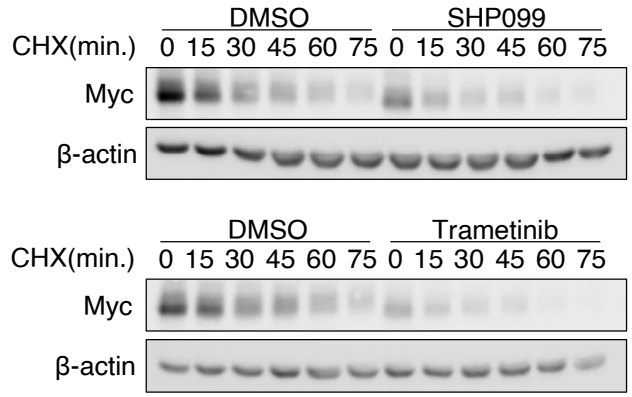

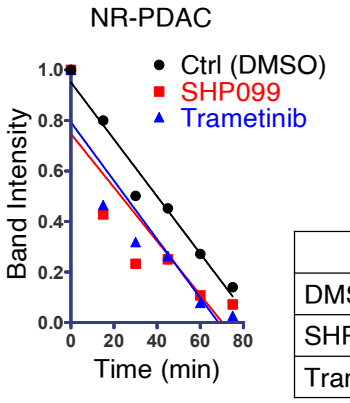

	Myc $t_{1/2}$
DMSO	27.29
SHP099	23.34
Trametinib	25.28

A

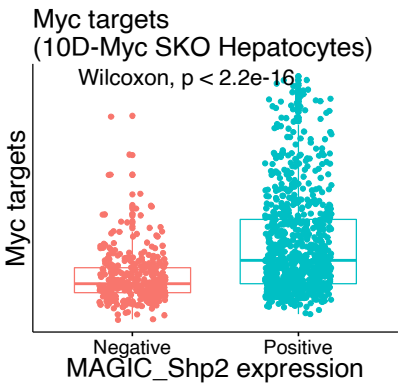

B

Pathways positively regulated in Shp2- Myc+ (vs Shp2- Myc-)	FDR *q* value
REACTOME_THE_CITRIC_ACID_TCA_CYCLE_AND_RESPIRATORY_ELECTRON_TRANSPORT	2.48E-17
REACTOME_RESPIRATORY_ELECTRON_TRANSPORT_ATP_SYNTHESIS_BY_CHEMIOSMOTIC_COUPLING_AND_HEAT_PRODUCTION_BY_UNCOUPLING_PROTEINS	1.79E-16
HALLMARK_OXIDATIVE_PHOSPHORYLATION	2.96E-15
REACTOME_RESPIRATORY_ELECTRON_TRANSPORT	1.88E-14
WP_ELECTRON_TRANSPORT_CHAIN_OXPHOS_SYSTEM_IN_MITOCHONDRIA	3.12E-14
KEGG_PARKINSONS_DISEASE	1.47E-11
KEGG_OXIDATIVE_PHOSPHORYLATION	5.97E-10
WP_NONALCOHOLIC_FATTY_LIVER_DISEASE	3.60E-09
REACTOME_TRANSLATION	3.88E-09

Figure 3.13 GSEA identifies significantly increased metabolism in Myc+ cells

(**A**) Box plots of 10D-Myc SKO data demonstrating hepatocytes with correlated expression levels of MAGIC-imputated Shp2 and Myc target genes. Statistical significance was calculated using Wilcoxon test.

(**B**) Unsupervised pathway enrichment analysis identified top results of Shp2-Myc+ cells, as compared to Shp2-Myc- cells, in SKO liver indicating pathways upregulated in Myc+ tumor cells.

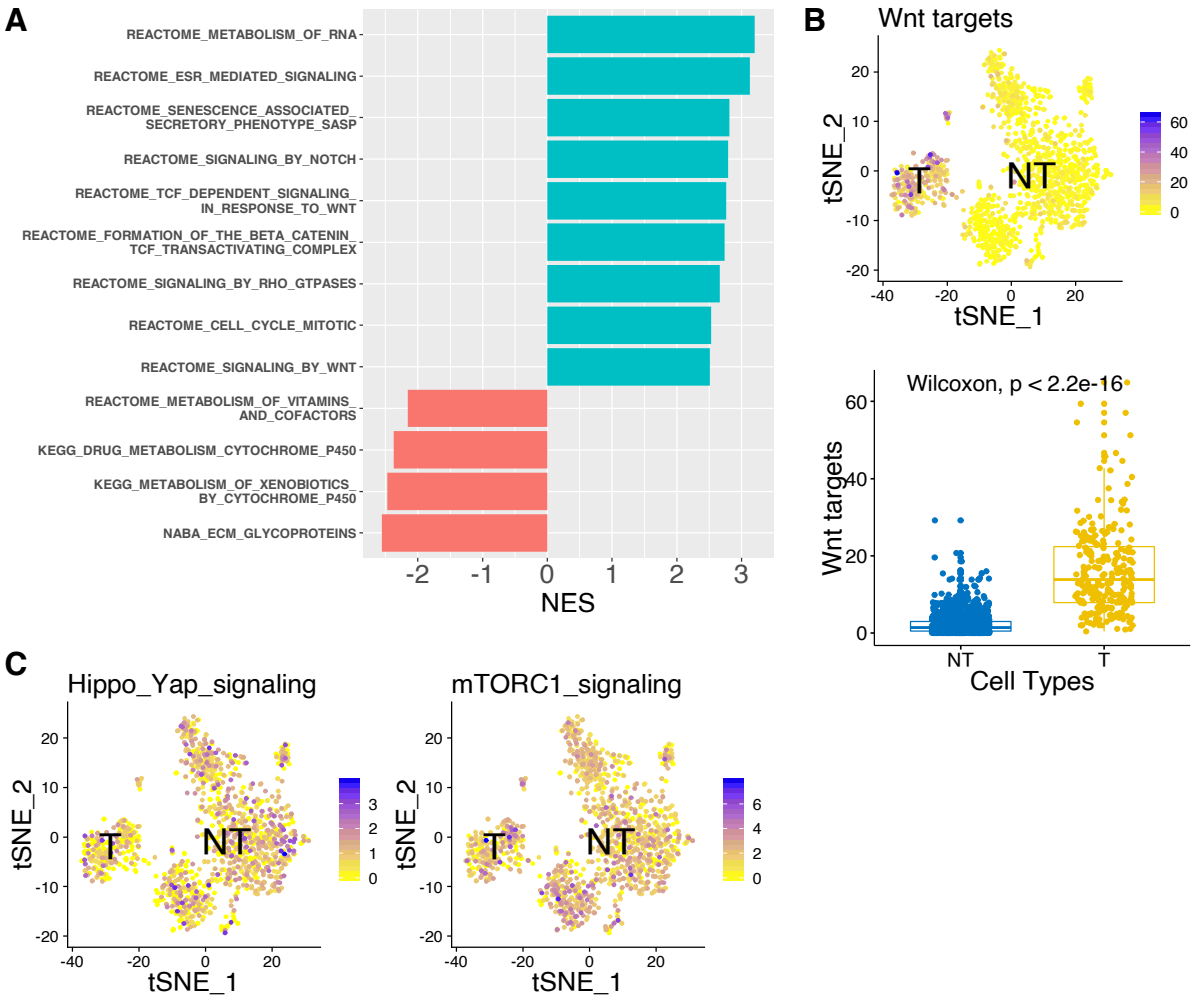

Figure 4.1 Pathway analysis indicates upregulated Wnt/β-catenin signaling in Myc-driven HCC

(**A**) Pathway enrichment analysis with normalized enrichment score (NES) using differentially expressed genes between tumor (T) and non-tumor (NT) cells from 4W-Myc SKO data. Pathway with positive NES was over-represented in tumor cells, and pathway with negative NES was under-represented in tumor cells.

(**B**) tSNE plot and boxplot of scores defined for Wnt target gene sets in 4W-Myc SKO data. Tumor cells show higher expression of Wnt target genes. Statistical significance was calculated using Wilcoxon test.

(**C**) tSNE plot of scores defined for Hippo/YAP and mTORC1 pathway genes in 4W-Myc SKO data. Both pathways are downstream of Myc signaling, but are neither significantly upregulated in tumor cells.

Figure 4.2 Wnt/β-catenin signaling is aberrantly upregulated in Myc-driven HCC

(**A**) Representative staining for β-catenin and glutamine synthetase (GS) in WT and SKO livers, 4 weeks after Myc transfection. Scale bar, 250 μm.

(**B**) Boxplots comparing scores defined for Wnt target genes at 0D-Ctrl (Left) and 10D-Myc (Right) time points. Wnt target gene levels were modestly higher in SKO than WT.

(**C**) Box plots of 10D-Myc WT (Left) and SKO (Right) hepatocytes. Cells with positive Shp2 expression had higher expression of Wnt target genes. Statistical significance was calculated using Wilcoxon test.

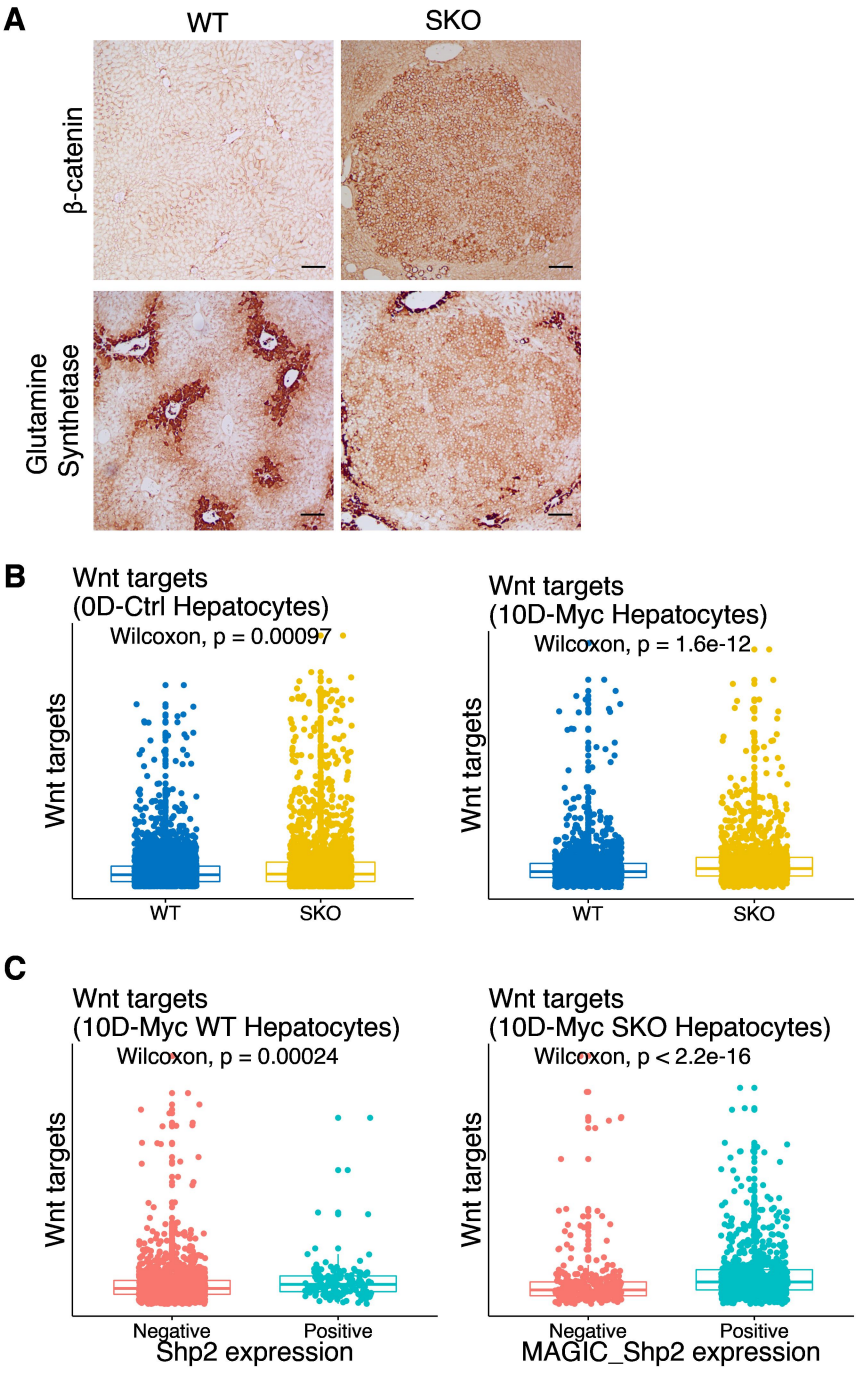
A
WT
SKO
β-catenin
Glutamine Synthetase
B
Wnt targets
(0D-Ctrl Hepatocytes)
Wilcoxon, p = 0.00097
Wnt targets
WT
SKO
Wnt targets
(10D-Myc Hepatocytes)
Wilcoxon, p = 1.6e-12
Wnt targets
WT
SKO
C
Wnt targets
(10D-Myc WT Hepatocytes)
Wilcoxon, p = 0.00024
Wnt targets
Negative
Positive
Shp2 expression
Wnt targets
(10D-Myc SKO Hepatocytes)
Wilcoxon, p < 2.2e-16
Wnt targets
Negative
Positive
MAGIC_Shp2 expression

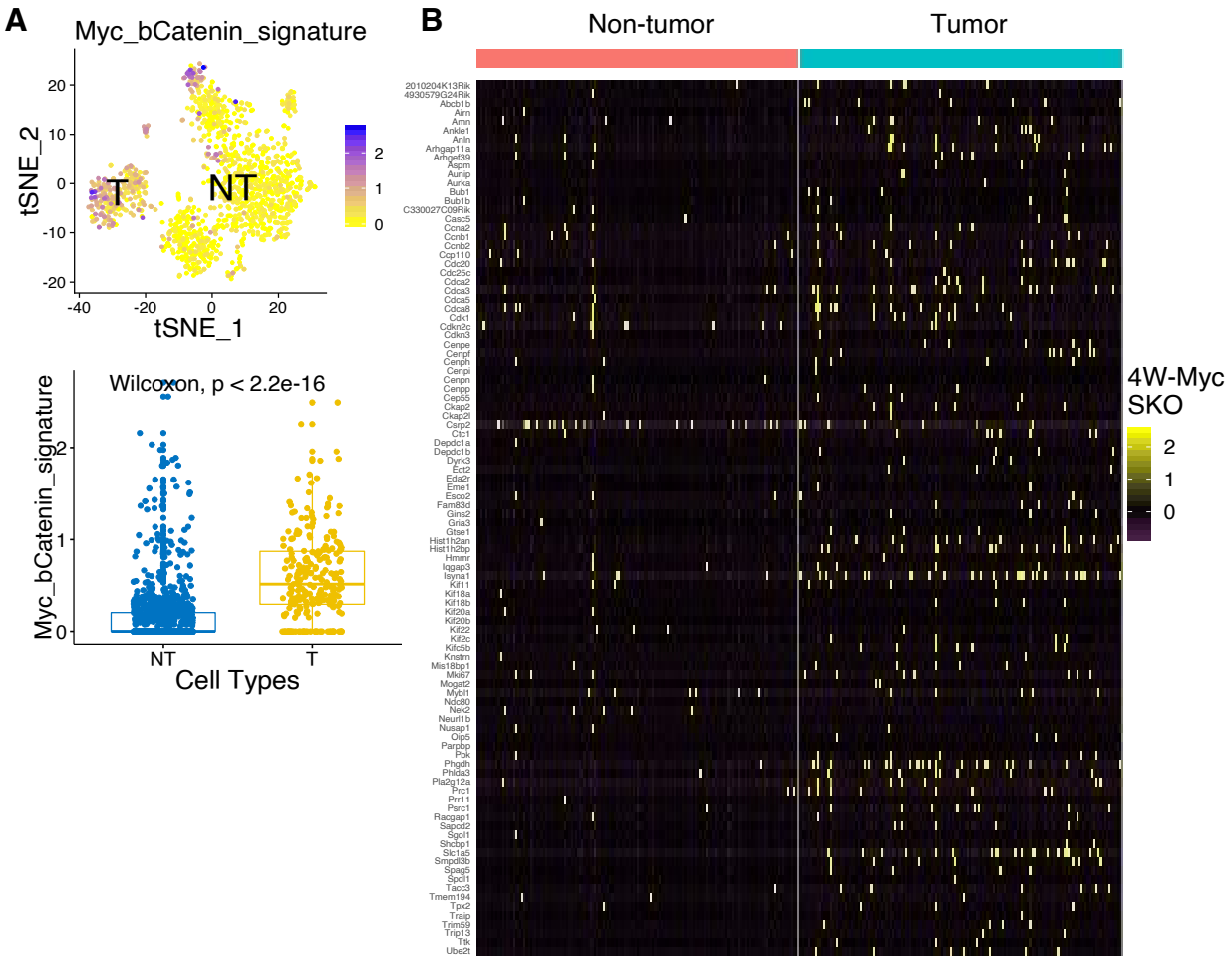

Figure 4.3 Myc/βcatenin signature gene enriched in tumor cluster

(**A**) tSNE and box plot of Myc-bCatenin gene signature from Bisso et al. 2020 in 4W-Myc SKO hepatocyte data showing high expression in tumor cluster. Statistical significance was calculated using Wilcoxon test.

(**B**) Heatmap showing expression profile of genes in “Myc/β-catenin signature” (Bisso et al., 2020), between tumor and non-tumor hepatocytes in 4W-Myc data in SKO liver (**D**), and WT and SKO in 10D-Myc data (**E**). Each column is a single cell, each row is a gene. Statistical significance was calculated using Wilcoxon test.

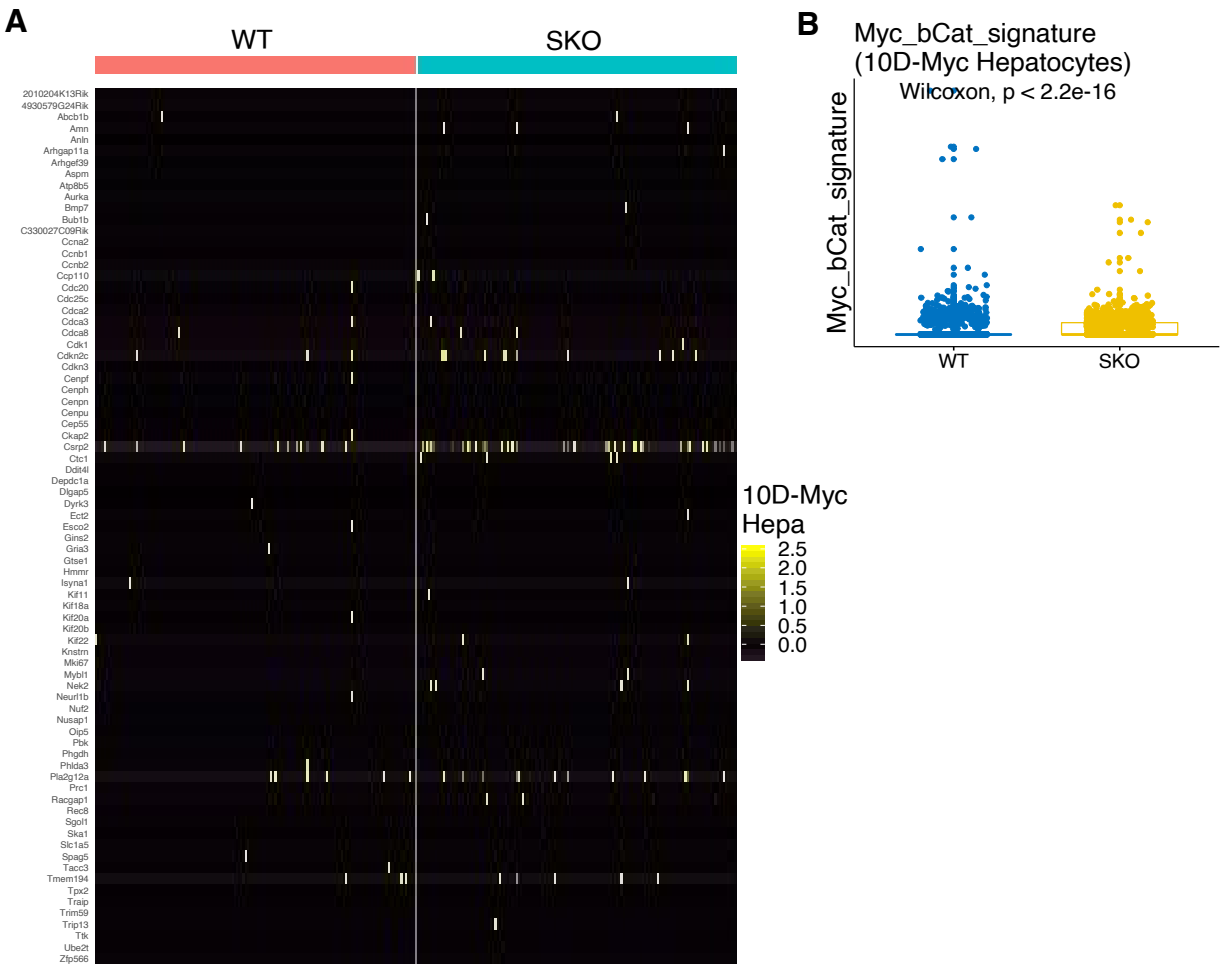

Figure 4.4 Myc/βcatenin signature gene enriched at tumor initiation stage

(**A**) Heatmap showing expression profile of genes in “Myc/β-catenin signature” (Bisso et al., 2020), between WT and SKO in 10D-Myc hepatocyte data. Each column is a single cell, each row is a gene. Statistical significance was calculated using Wilcoxon test.

(**B**) Box plot showing scores defined for the “Myc/β-catenin signature” in 10D-Myc hepatocytes, related to 4W-Myc data in Figure 4.3A.

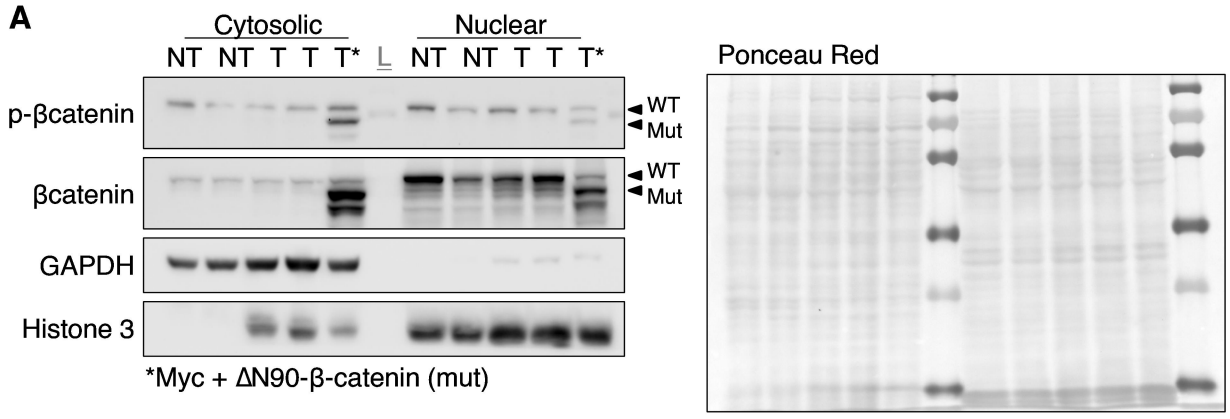

Figure 4.5 Increased nuclear β-catenin suggests increased transcriptional activity (**A**) Immunoblot of tumor and non-tumor lysates 4 weeks after transfection of Myc or Myc+ΔN90-β-catenin (truncated mutant), with cytosolic and nuclear fractions, with Ponceau red as loading control.

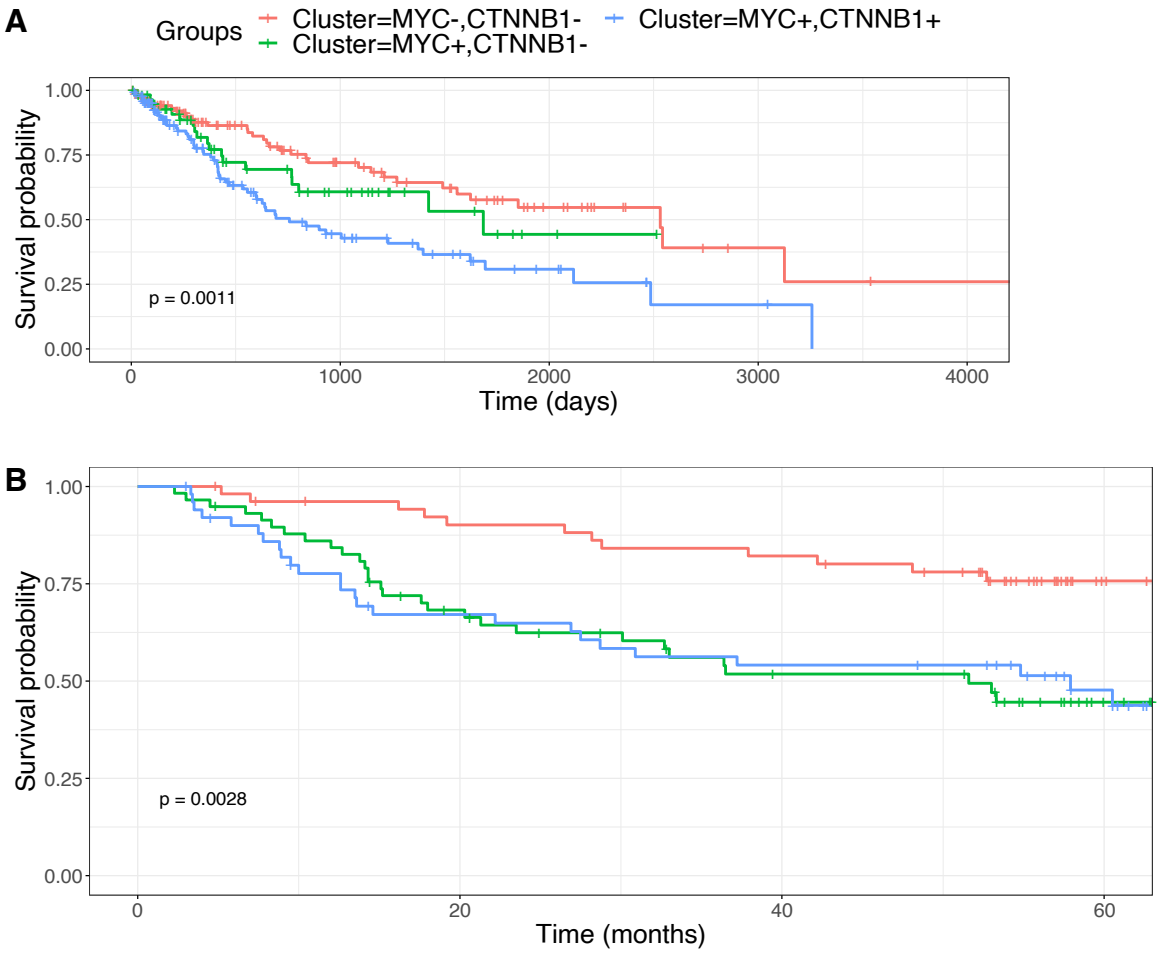

Figure 4.6 Myc and β-catenin overexpression in HCC patients predicts poor survival

(**A-B**) Kaplan-Meier survival analysis of HCC patients with MYC^{-} $CTNNB1^{+}$, MYC^{+} $CTNNB1^{-}$, and MYC^{+} $CTNNB1^{+}$ based on mRNA expression levels in TCGA database (**A**) and GSE14520 dataset (**B**). Patients with $MYC^{+}CTNNB1^{+}$ show significantly worse survival.

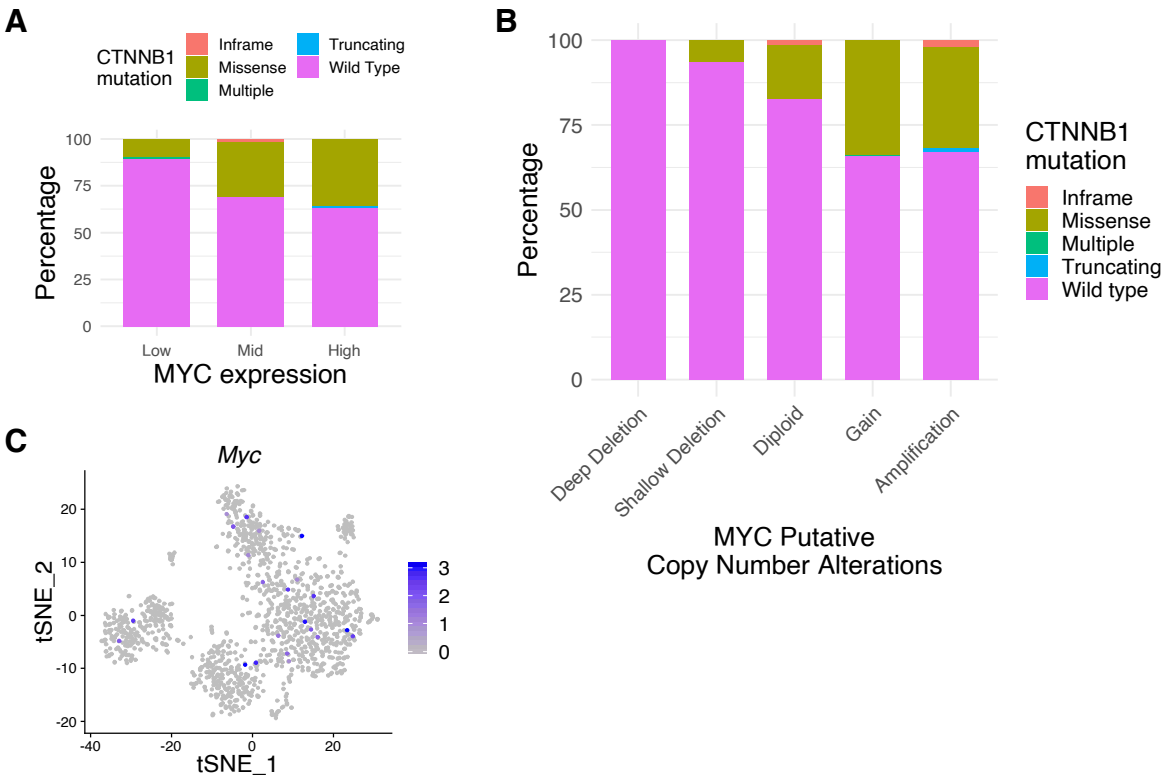

Figure 4.7 Correlated Myc and β-catenin abnormalities in HCC patients

(**A-B**) A total of 371 HCC patients in TCGA data were separated by Myc expression (**A**) or Myc copy number alterations (**B**) into columns and then distinguished by β-catenin mutational profiles within each column. Patients with higher Myc expression or Myc copy number alterations had higher CTNNB1 mutation rates.

(**C**) tSNE plot of endogenous Myc levels in 4W-Myc SKO hepatocyte data, showing lack of correlation between hepatocyte cluster and endogenous Myc expression.

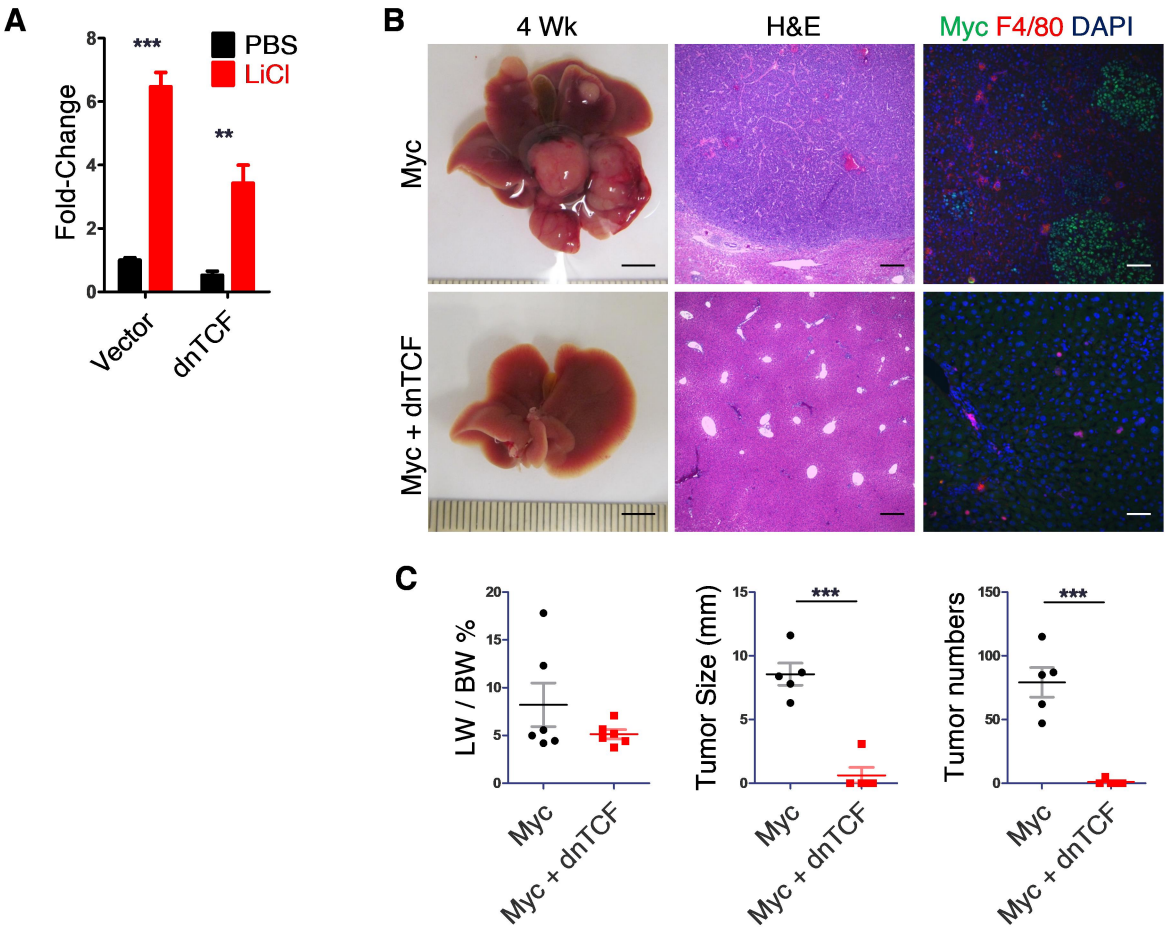

Figure 4.8 β-catenin transcription activity is required for Myc-dependent tumorigenesis

(**A**) 293T cells transfected with Super TopFlash reporter and either Vector backbone or dnTCF plasmid, treated with LiCl (20mM). dnTCF suppressed LiCl induced β-catenin transcriptional activity.

(B) Representative liver images, H&E and immunostaining of Myc and F4/80 for SKO livers 4 weeks after transfection of Myc or Myc+dnTCF. Liver scale bar, 0.5 cm; H&E, 250 μm; Immunostaining, 100 μm.

(**C**) Quantification of liver to body weight ratios, LW/BW, maximal tumor sizes, and tumor numbers in SKO livers (n=6). Statistical analysis used student's T-test. (*** $p < 0.001$).

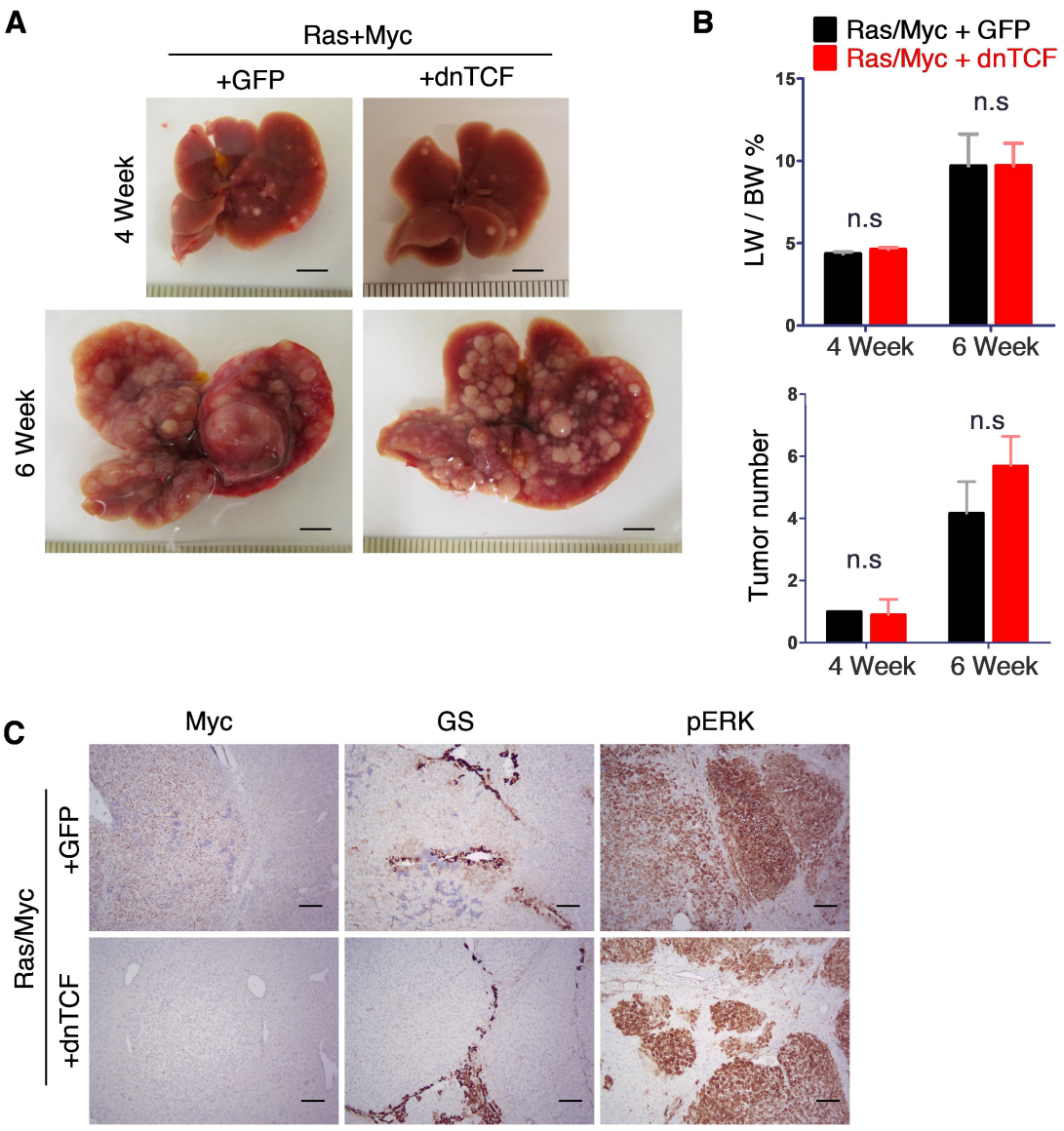

Figure 4.9 Transcriptional repression of β-catenin does not affect Ras/Myc tumor growth

(**A**) Representative images of WT livers at 4 and 6 weeks post-HTVi of Ras/Myc + GFP or Ras/Myc + dnTCF. (4 week, n=4; 6 week, n=10). Scale bar, 0.5 cm.

(**B**) Quantification of liver to body weight ratios (LW/BW) and tumor numbers. Statistical significance calculated by students T-test. Values are presented as means ± SD. (n.s. P>0.05).

(**C**) Representative staining for Myc, GS, and p-Erk in WT livers 6 weeks after HTVi of Ras/Myc + GFP or Ras/Myc + dnTCF. Scale bar, 250 μm.

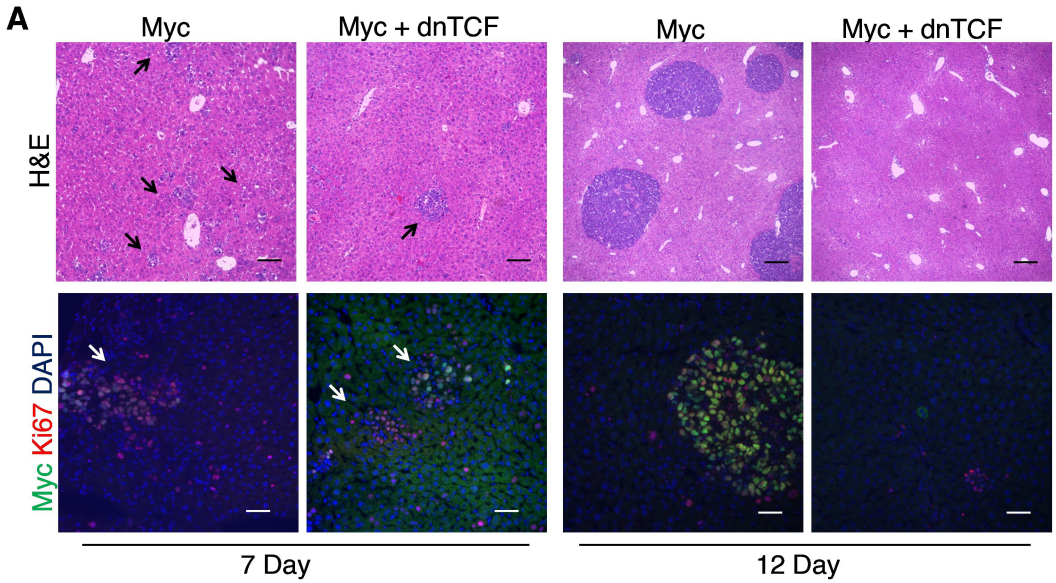

Figure 4.10 Lack of β-catenin interferes with tumor development not initiation
(**A**) Representative H&E (top) and immunostaining of Myc and Ki67 (bottom) in SKO livers 7 and 12 days after HTVi of Myc or Myc + dnTCF. Top Scale bar, 250 μm. Bottom Scale bar, 100 μm.

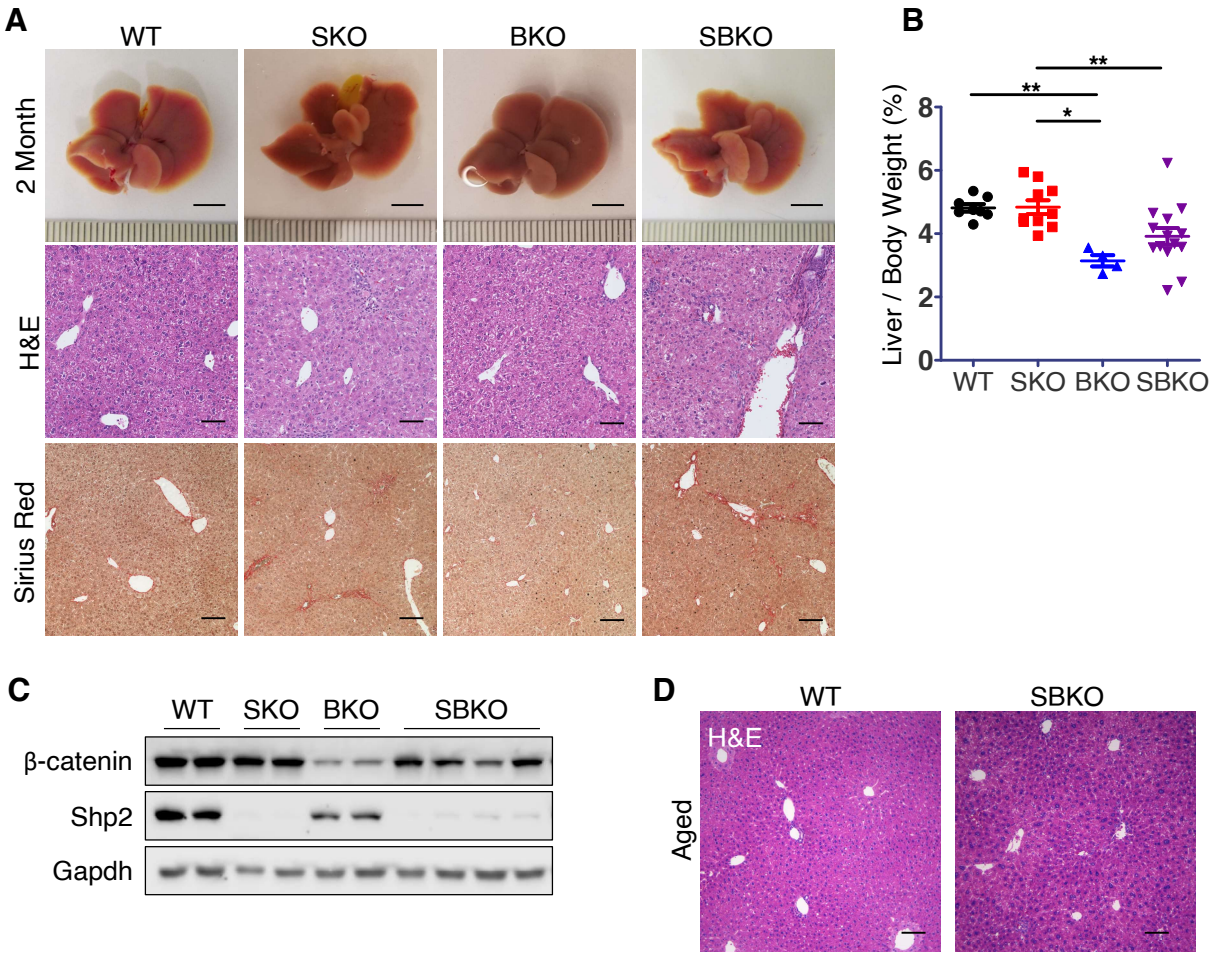

Figure 4.11 Characterization of SBKO liver deficient for Shp2 and β-catenin

(**A**) Representative images of WT, SKO, BKO, and SBKO livers at 2 months, with Liver (top), H&E (middle), and Sirius red staining (bottom). Liver scale bar, 0.5 mm. Staining scale bar, 250 μm.

(**B**) Quantification of liver to body weight ratios, (n=10). Statistical significance calculated by one-sided ANOVA with post-hoc Tukey test. Values are presented as means ± SD. (* $p<0.05$; ** $p<0.01$; *** $p<0.001$).

(**C**) Immunoblot showing Shp2 and β-catenin expression in respective genotypes.

(**D**) H&E staining showing hepatic architecture of 15-month SBKO livers. Scale bar, 250 μm.

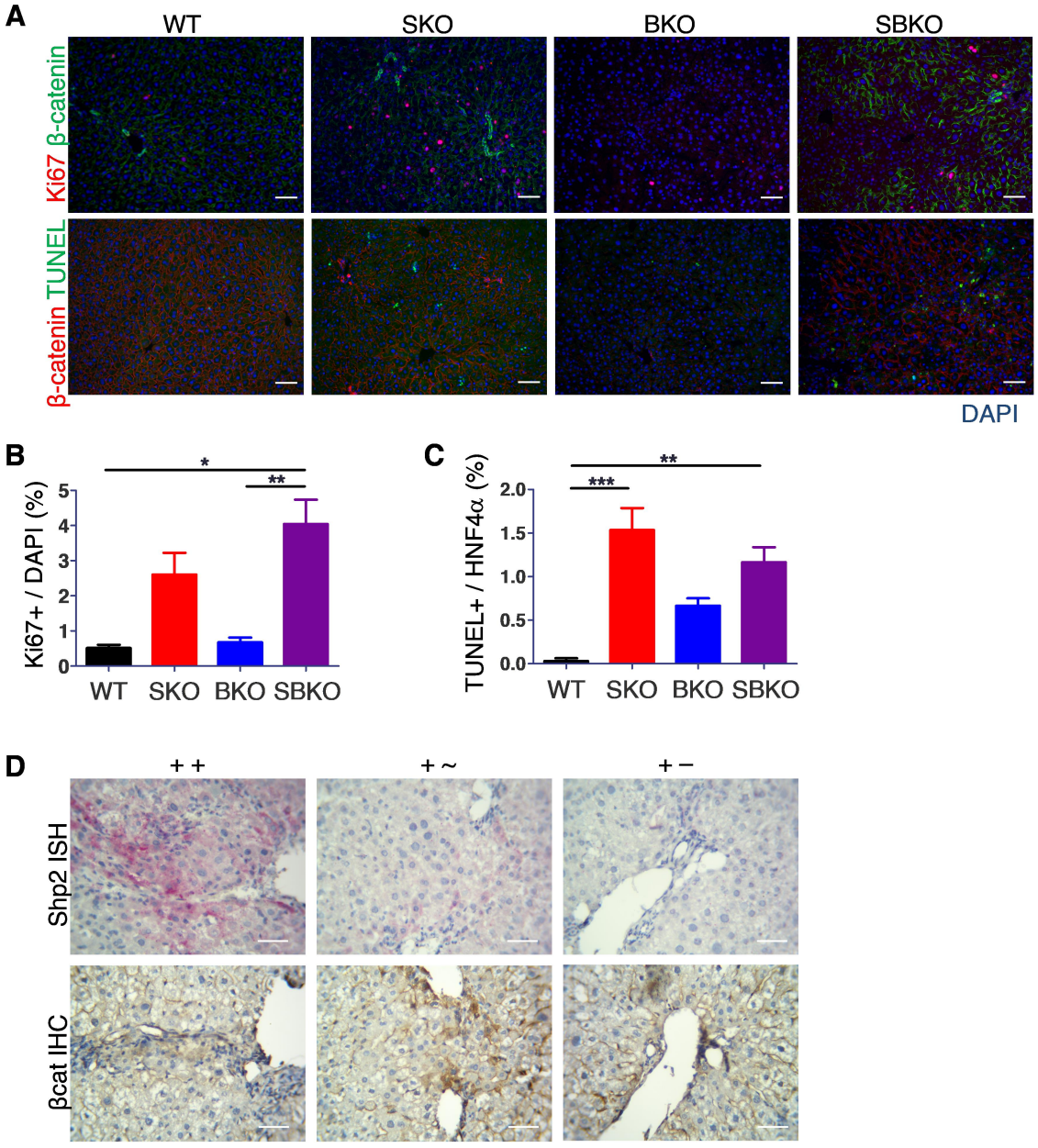

Figure 4.12 SBKO livers have chronic liver damage and regenerative proliferation

(**A-C**) Representative immunostaining of Ki67 and β-catenin (top) and β-catenin and TUNEL (bottom) in respective genotypes, with quantification of Ki67^{+}/DAPI (**B**) and TUNEL^{+}/HNF4α (**C**). n=5, Scale bar, 100 μm. Statistical significance calculated by one-sided ANOVA with post-hoc Tukey test. Values are presented as means ± SD. (* $p<0.05$; ** $p<0.01$; *** $p<0.001$).

(**D**) In situ hybridization of Shp2 and immunostaining of β-catenin in consecutive sections. Scale bar, 50 μm.

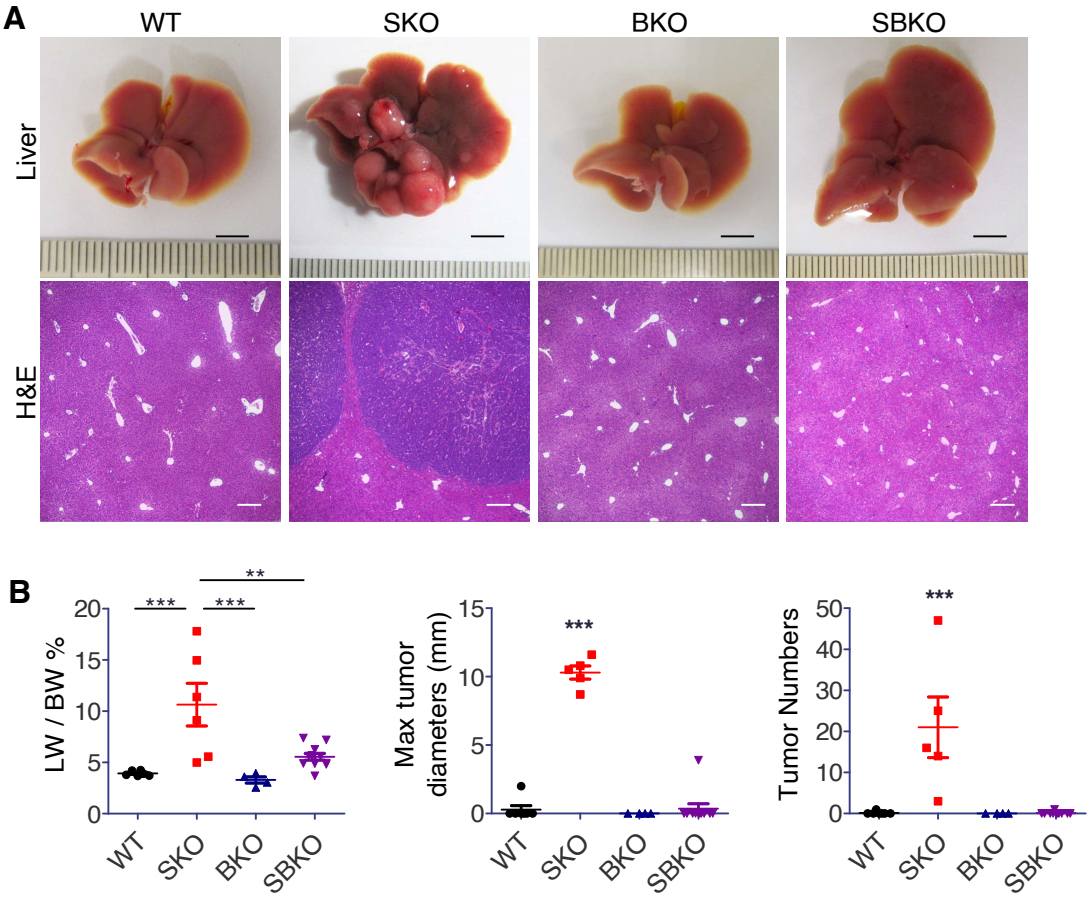

Figure 4.13 Genetic knockout of β-catenin ablates Myc-dependent tumorigenesis independent of Shp2 presence

(**A-B**) Representative liver images (**A**), quantification of liver to body weight ratios, maximal tumor diameters, and tumor numbers (**B**) in WT, SKO, BKO, and SBKO mice 4 weeks after Myc transfection. (n=6-9) Top scale bar, 0.5 mm; bottom scale bar, 250 μm. Statistical analysis used one-sided ANOVA with posttest Tukey. (*** $p < 0.001$, ** $p < 0.01$).

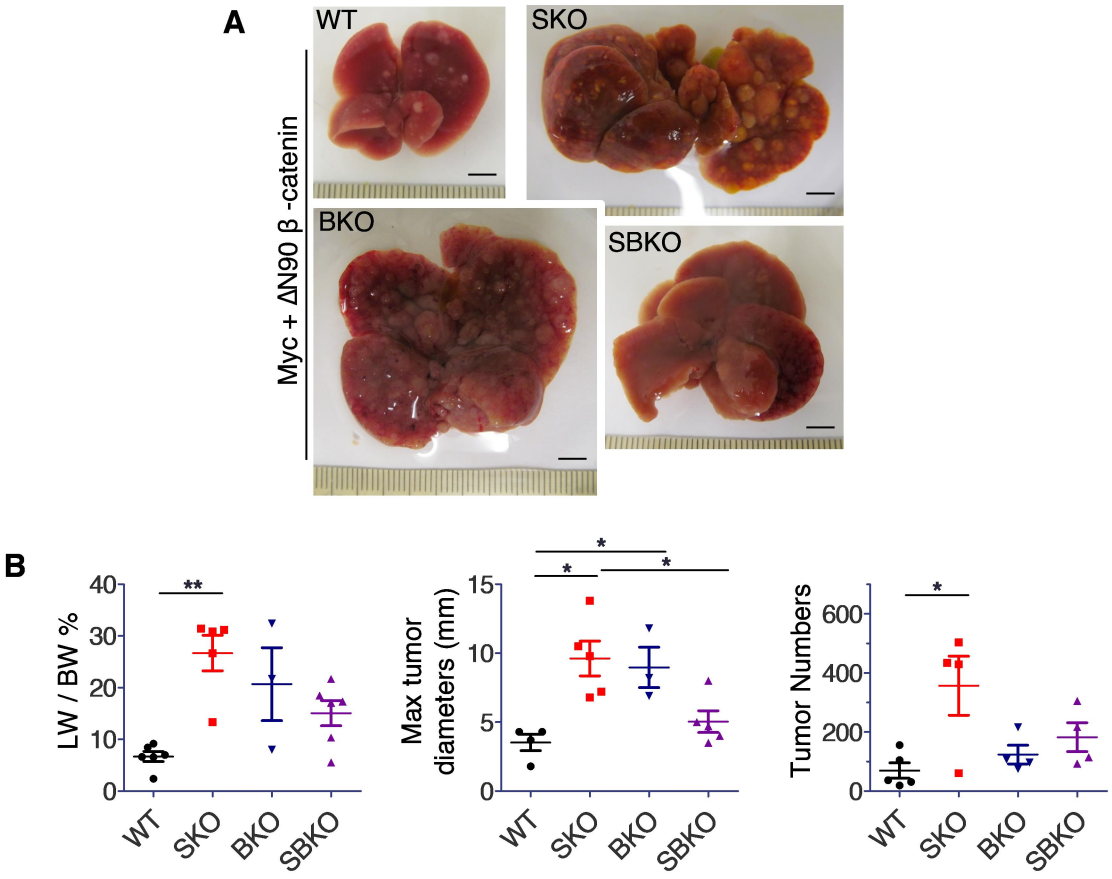

Figure 4.14 Oncogenic β-catenin rescues tumor phenotype in livers deficient for Shp2 and/or β-catenin

(**A-B**) Representative liver images (**A**), quantification of LW/BW ratios, maximal tumor diameters, and tumor numbers (**B**) in WT, SKO, BKO, and SBKO mice 4 weeks after HTVi of Myc/ΔN90-β-catenin (n=4-6). Scale bar, 0.5 mm. Statistical analysis used one-sided ANOVA with post-test Tukey. (** $p < 0.01$, * $p < 0.05$).

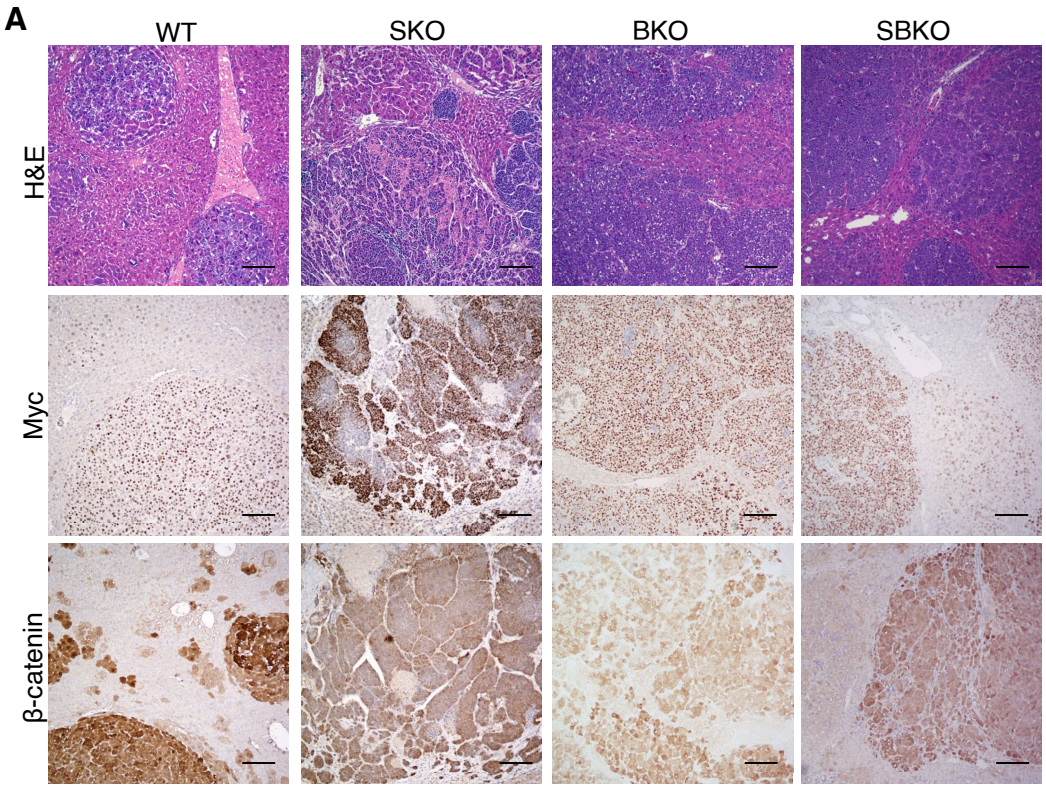

Figure 4.15 β-catenin and Myc induce aggressive liver cancer

(**A**) Representative H&E (Up), immunostaining for Myc (middle) and β-catenin (low) of livers 4 weeks after transfection of Myc and β-catenin in WT, SKO, BKO, and SBKO mice. Scale bar, 250 μm.

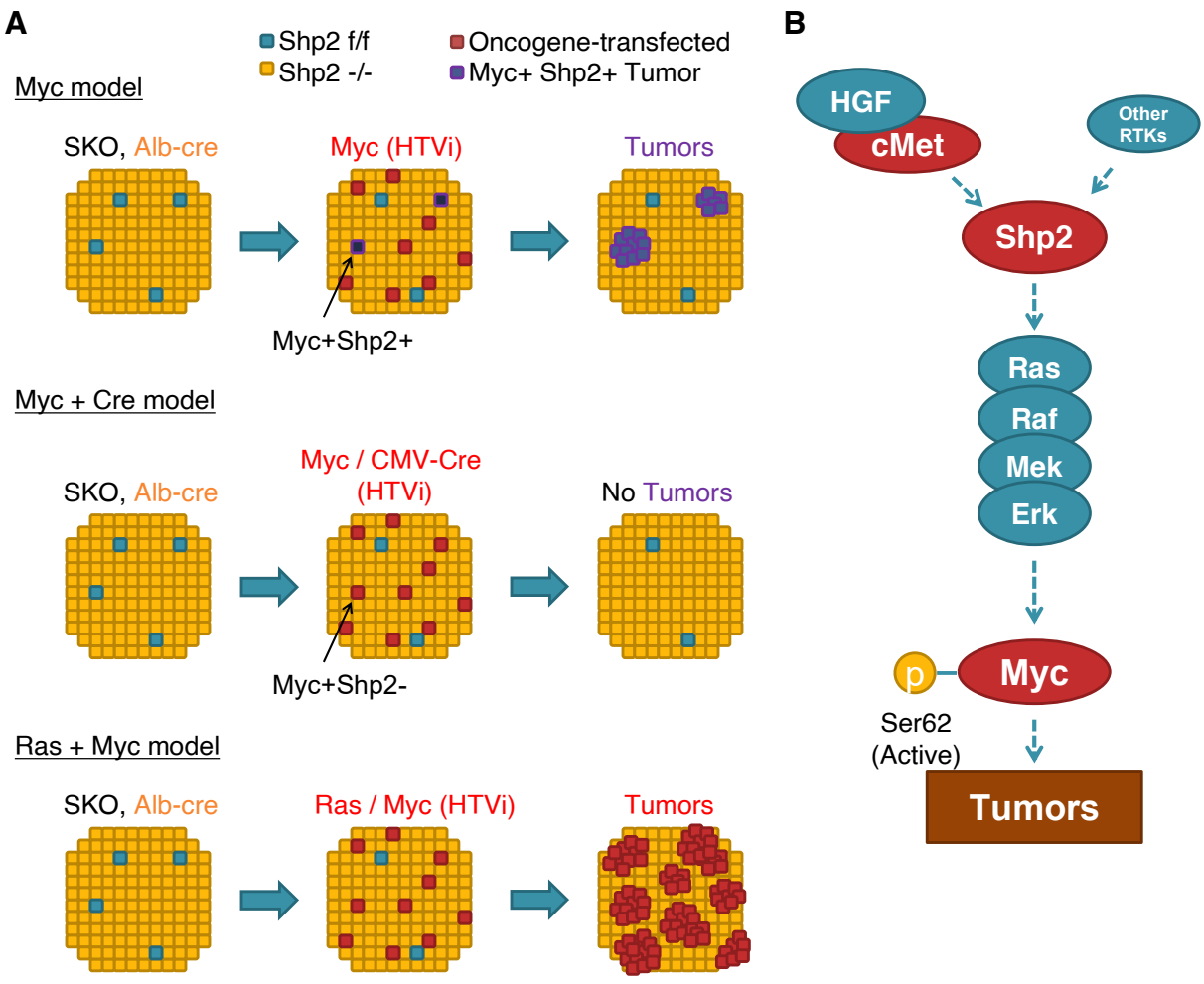

Scheme 3.1: Shp2 selection and requirement in Myc model

(**A**) In SKO (Albumin-Cre, Shp2$^{f/f}$) liver, whereby Albumin-cre drives deletion of Shp2 in most (~95%) hepatocytes, HTVi of oncogenes in various murine models of liver cancer, cause different phenotypes. Myc-transfected cells (red) that happen to be transfected in Shp2+ hepatocytes (blue) end up developing into tumors (purple). Myc and CMV-Cre transfected cells (red), which end up only in Myc+Shp2- cells, do not develop tumors. Ras and Myc transfected cells develop into tumors regardless of transfection into Shp2+ or Shp2- hepatocytes.

(**B**) Intracellular Shp2 works to drive the Ras/Erk pathway to support Myc protein stability (active and stable pMyc^{S62}) and carcinogenesis.

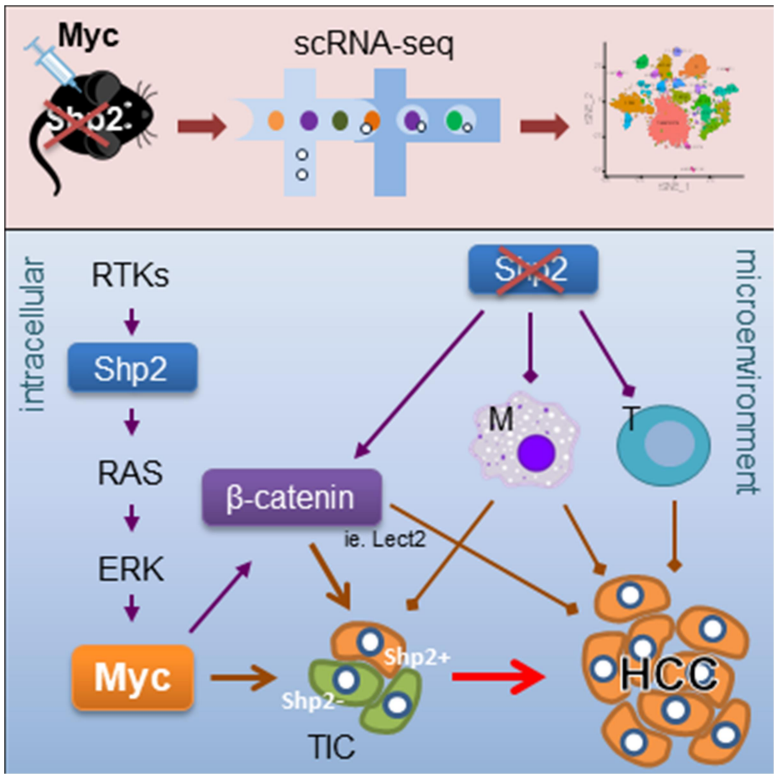

Scheme 5.1. Mechanisms of tumor development of Myc-driven liver cancer
Characterization of Myc-induced HCC in SKO mice, through functional and scRNA-seq analysis, yields variety of mechanisms supporting tumorigenesis. Ablation of Shp2 in hepatocytes alters tumor immune microenvironment and induces tumor permissive macrophage populations. Intracellular expression of Shp2 assists in Ras/Erk signaling transduction to support Myc protein stability. β-catenin transcriptional expression is required for Myc-driven HCC intrinsically but may also play a role in altering TME.

Table 1.1: Tumor Histopathology Analysis

Histopathological results of Hematoxylin and Eosin-stained tissue samples of tumor models in SKO mice. Analysis performed by Dr. Nissi Varki (Professor of Pathology, UCSD)

Sample	Genotype	Tumor model	Tumor Histopathology
SJ1268	SKO	Myc	Trabecular HCC, well-differentiated, hepatoblastoma-like features, high nucleus-to-cytoplasmic ratio, highly aggressive, Inflammatory infiltrates
SM707	SKO	Myc	Trabecular HCC, well-differentiated, hepatoblastoma-like features, high nucleus-to-cytoplasmic ratio, highly aggressive
S446	SKO	Myc	Trabecular HCC, well-differentiated, hepatoblastoma-like features, high nucleus-to-cytoplasmic ratio, highly aggressive
S441	SKO	Myc	Trabecular HCC, well-differentiated, hepatoblastoma-like features, high nucleus-to-cytoplasmic ratio, highly aggressive
S425	SKO	Myc	Trabecular HCC, well-differentiated, hepatoblastoma-like features, high nucleus-to-cytoplasmic ratio, highly aggressive
SM705	WT	Myc	Trabecular HCC, well-differentiated, hepatoblastoma-like features, high nucleus-to-cytoplasmic ratio, highly aggressive
S445	WT	Myc	Trabecular HCC, well-differentiated, hepatoblastoma-like features, high nucleus-to-cytoplasmic ratio, highly aggressive
SM30	SKO	Myc + Shp2	Trabecular HCC and highly malignant poorly differentiated HCC, highly aggressive
SM34	SKO	Myc + Shp2	Trabecular HCC and highly malignant poorly-differentiated HCC, highly aggressive
S535-6	SKO	Ras + Myc	Well-differentiated HCC, Mallory-Denk bodies
S541	SKO	Ras + Myc	Well-differentiated HCC, Mallory-Denk bodies
SB738	SKO	Myc + β-catenin	Hepatoblastoma and well-differentiated HCC
SB739	SKO	Myc + β-catenin	Hepatoblastoma and well-differentiated HCC

Table 2.1: Relevant cell numbers for scRNA-sequencing analysis

			Before filtering	After filtering	Total after filtering
0D-Ctrl	WT	Hep	1290	1232	4610
		NPC	1600	1100	
	SKO	Hep	1023	871	
		NPC	1930	1407	
10D-Vector	WT	Hep	1290	1195	7888
		NPC	3075	3039	
	SKO	Hep	1297	1293	
		NPC	2497	2361	
10D-Myc	WT	Hep	1000	989	6631
		NPC	1985	1951	
	SKO	Hep	905	886	
		NPC	2888	2805	
4W-Myc	WT	Hep	1349	1349	8198
		NPC	2713	2569	
	SKO	Hep	1381	1373	
		NPC	3024	2907	

Table 2.2: Cytokine expression in hepatocytes

Ligands expression between WT and SKO hepatocytes at each time point, using scRNA-seq analysis. Values are presented as log fold-change of the average expression. Positive values indicate higher expression in SKO hepatocytes

	0D-Ctrl		**10D-Vector**	
	avg_logFC (SKO/WT)	**p_adj**	**avg_logFC (SKO/WT)**	**p_adj**
Ccl2	0.0228231090	1.00E+00	-0.0348341890	1.00E+00
Ccl4	0.0230392399	1.00E+00	0.0050715960	1.00E+00
Ccl5	0.0484332990	1.00E+00	-0.0364395020	1.00E+00
Ccl6	0.0440357818	1.58E-01	-0.0049858090	1.00E+00
Ccl7	0.0098169779	1.00E+00	Not Detected	
Ccl9	-0.4318557608	1.22E-32	-0.2689959190	3.35E-11
Ccl25	Not Detected		-0.0209034900	1.00E+00
Ccl27a	Not Detected		-0.0073178150	1.00E+00
Cxcl1	-0.1008580890	4.15E-01	-0.4277598090	1.65E-32
Cxcl2	0.0073602910	1.00E+00	Not Detected	
Cxcl9	0.2861360420	6.60E-16	0.0135539410	1.00E+00
Cxcl10	0.0608337100	2.54E-01	0.0167738800	1.00E+00
Cxcl11	0.0064971040	1.00E+00	-0.0314060290	1.00E+00
Cxcl12	-0.0190080910	1.00E+00	-0.0054141520	1.00E+00
Cxcl13	Not Detected		-0.0004689840	1.00E+00
Cxcl14	-0.0045888470	1.00E+00	-0.0179419980	1.00E+00
Cxcl16	0.0437289610	1.00E+00	0.0180524880	1.00E+00
Lect2	0.429395800	6.54E-21	0.2782983000	5.06E-05
Mif	0.278377906	3.34E-05	0.2496263000	7.64E-06
Nampt	0.310062400	8.71E-10	0.0457770400	1.00E+00
Spp1	0.647512450	5.51E-05	0.1547416200	1.00E+00
Vegfa	-0.046265820	1.00E+00	-0.0462658200	1.00E+00
Aimp1	Not Detected		Not Detected	
	10D-Myc		**4W-Myc**	
	avg_logFC (SKO/WT)	**p_adj**	**avg_logFC (SKO/WT)**	**p_adj**
Ccl2	0.0084754580	1.00E+00	0.0580210650	1.00E+00
Ccl4	-0.0137855930	1.00E+00	-0.0075470760	1.00E+00
Ccl5	-0.0215245270	1.00E+00	0.0672150760	1.00E+00
Ccl6	-0.0131183870	1.00E+00	0.0541973530	1.00E+00
Ccl7	Not Detected		Not Detected	

Table 2.2: Cytokine expression in hepatocytes, Continued
Ligands expression between WT and SKO hepatocytes at each time point, using scRNA-seq analysis. Values are presented as log fold-change of the average expression. Positive values indicate higher expression in SKO hepatocytes

Ccl7	Not Detected		Not Detected	
Ccl9	-0.2937460760	1.04E-01	-0.4399599750	1.99E-01
Ccl25	-0.0255756590	1.00E+00	-0.0198205990	1.00E+00
Ccl27a	0.0038820450	1.00E+00	0.1692218530	2.04E-02
Cxcl1	-0.7388919460	7.68E-24	0.0920983100	3.35E-01
Cxcl2	-0.0266341510	1.00E+00	0.0564091500	1.00E+00
Cxcl9	-0.0699571270	1.00E+00	-0.0243349200	1.00E+00
Cxcl10	-0.0341036060	1.00E+00	0.0750315600	1.00E+00
Cxcl11	-0.0073713550	1.00E+00	-0.0531037500	1.00E+00
Cxcl12	0.1090831720	6.29E-05	-0.4662282600	1.00E+00
Cxcl13	Not Detected		Not Detected	
Cxcl14	-0.0483053900	1.00E+00	0.0220272900	1.00E+00
Cxcl16	0.0247155580	1.00E+00	0.0474723400	1.00E+00
Lect2	0.2974101000	3.01E-16	0.9584413000	4.26E-66
Mif	0.4399941700	1.80E-35	0.9535501200	1.78E-80
Nampt	0.0221337400	7.23E-02	0.1122796000	6.70E-03
Spp1	0.6107580000	1.00E+00	0.6108792000	1.00E+00
Vegfa	0.0099134810	1.06E-01	0.0665659000	1.00E+00
Aimp1	Not Detected		0.1975240600	3.31E-06

CHAPTER 5: DISCUSSION

By combining scRNA-seq with functional and mechanistic analyses, we have elucidated a complex mechanism of Shp2-promoted Ras-Erk-Myc pathway in synergy with a tumor-permissive niche, induced paradoxically by deleting Shp2 and genetic disruption in neighboring cells, which resulted in aggressive Myc-driven hepatocarcinogenesis.

Establish Myc-driven murine HCC model

Uniquely, Myc oncogene alone was sufficient to drive HCC, an oncogene which was previously known to require two oncogenes for efficient liver tumor development in tumor-resistant C57BL/6 mice. We observed tumor development within 4 weeks, which was surprising as many combinations of oncogenes utilizing HTVi required at least 8+ weeks to develop significant tumor burden. Most HTVi models also require co-transfection of dual oncogenic drivers (Ras/Akt, Ras/Myc, c-Met/β-catenin, etc), making our model unique, driven only by Myc overexpression. Our model almost matches the HTVi-induced Myc-driven hepatoblastoma model in FVB/N mice, which develops tumors in 6 weeks. Utilizing this effective and quick HCC model, we were able to elucidate mechanisms of cell-intrinsic and -extrinsic signals that cooperate and intertwine to drive aggressive Myc-driven primary liver cancer development (Scheme 3.1).

Novel protocol for scRNA-sequencing of whole liver cancer model

In this study, we developed a novel protocol of hepatic cell isolation for scRNA-seq that robustly covers all cell types in tumorigenic murine liver. Recent advances in scRNA-seq analysis in murine and human liver have assisted in elucidating developmental and tumor-related analyses at previously unheard of detailed resolutions. (Halpern et al., 2017; Hou et al., 2016; Ma et al., 2019; Xiong et al., 2019; Zhang et al., 2019; Zheng et al., 2017a). The application of this new technology to the liver field was hindered by difficulties in isolating high quality delicate hepatic cells alongside tumor and non-parenchymal populations, in fibrotic or otherwise diseased liver. This is the first report on scRNA-seq analysis of all hepatic cell types in a murine HCC model, including hepatocytes, tumor cells and NPCs, analyzed at several time points. Uniquely, we utilized scRNA-sequencing data with molecular and functional assays to identify and elucidate a complex model of Shp2 gain and loss in driving and promoting HCC, respectively.

Proto-oncogene Shp2 ablation generates tumor-permissive microenvironment

Shp2 deficiency in the liver triggered an immunosuppressive environment reflected in significantly impaired capacity to eliminate Myc-transformed hepatocytes at the early pre-malignant stage. Monocyte-derived macrophage and Kupffer cell populations were altered in SKO liver, specifically in response to Myc-transformed tumor cells and Shp2-ablated hepatocytes, with shift towards M2 polarization and reduction in phagocytic activity. These innate immune cells, along with decreased

populations of dendritic cells and neutrophils, assisted in creating an immuno-suppressive environment partially due to the increase in chemokines such as CCL9. These observations are in agreement with a recently published study which indicated upregulation of β-catenin in tumor cells, which was noted in our model, can induce dysregulation of dendritic cell antigen-presentation as a mechanism to immunosuppression (Ruiz de Galarreta et al., 2019; Spranger et al., 2015). However, in contrast to the previous studies identifying key chemokines CCL4 and CCL5 (Dolezal et al., 2017; Ruiz de Galarreta et al., 2019; Spranger et al., 2015), our results suggest functions of Lect2, CCL2, CCL9, CCL17 and MIF in suppressing various innate immune cell functions and blocking tumor initiation. Specifically, observations of monocyte and macrophage chemotaxis in specific response to Myc-overexpression, is likely coupled with down-regulation of multiple immune recognition components induced by genetically altered hepatocytes (Dolezal et al., 2017).

Our observation of upregulated PD-L1 expression may also assist in generating immunosuppressive environment by interfering with T cell recognition of these tumors. This may also contribute to the lack of apparent difference in T cell populations in WT and SKO liver at tumor initiation. Our previous studies uncovered Shp2's role in FGFR4 and FXR signaling to control of bile acids (BA) synthesis (Li et al., 2014a). Ablating Shp2 caused a cholestasis phenotype with dramatically increased BA levels in the liver which is known to suppress immune cell functions (Li et al., 2014a) and altered metabolite levels significantly direct immune dysfunction. Further mechanistic analysis is required to elucidate potential immunosuppressive tumor environment induced by hepatocyte genetic manipulation.

Proto-oncogene Shp2 essential for oncogenic Myc stability

Shp2-positive cells were selected for in the growth of Myc-induced tumors, as identified in scRNA-seq analysis and supported through *in vivo* knock-out and overexpression models. A number of recent reports showed that chemical inhibition of Shp2 had growth-inhibitory effect synergistic with other inhibitors of Ras-Erk signaling in a variety of cancer cell lines (Ahmed et al., 2019; Dardaei et al., 2018; Fedele et al., 2018; Mainardi et al., 2018; Ruess et al., 2018; Wong et al., 2018), making Shp2 an attractive drug target. However, Shp2 has been found to have paradoxically tumor-promoting and -inhibiting effects in liver and other solid tumors (Bard-Chapeau et al., 2011; Liu et al., 2018; Luo et al., 2016; Yang et al., 2013), raising concerns about specific use of Shp2 inhibitors in oncology treatment.

Following previous data revealing its essential role in oncogenic signaling initiated by RTK, this study has elucidated an indispensable Shp2 function in promoting Erk signaling and Myc stability for Myc-driven HCC development. Single cell transcriptomics showed clearly that Myc-induced tumors only developed from the rare Shp2-positive cells in Shp2-deficient liver through forced selection, though Myc transfection was unbiased to Shp2-deletion status in hepatocytes. Ours and other studies suggest hepatocytes that escape Cre-mediated gene deletion of proto-oncogenes have survival advantages and selectively progress to HCC (Bisso et al., 2020; Wang et al., 2011; Yamaji et al., 2010). Of note, HCC development driven by $NRas^{G12V}$ and Myc did not require Shp2, with the resulting tumors being Shp2-negative. Thus, in contrast to a classical view in epistasis analysis, we demonstrated that over-

expression of Myc did not compensate for the essential role of Shp2 that acts upstream of Myc in cell signaling. This study provides solid evidence for a stringent requirement of an intact Ras-Erk pathway in Myc-driven carcinogenesis in vivo, despite a body of literature on Ras-Erk-Myc signaling in cancer cells (Farrell and Sears, 2014; Hayes et al., 2016; Vaseva et al., 2018).

Aberrant upregulation of Wnt/β-catenin signaling promotes Myc-driven HCC

A curious mechanism underlying this dramatic HCC phenotype is the dramatically upregulated Wnt/β-catenin signaling in Myc-induced tumorigenesis. Shp2 deficiency in the liver contributed by aberrantly elevated β-catenin signaling. The basal Wnt/β-catenin signaling level was upregulated in Shp2-deficient liver, which was further augmented by Myc overexpression (Scheme 5.1). Myc^{+} tumors in SKO liver were featured by elevated expression of a "Myc/β-catenin signature" gene set, which were characterized in tumors driven by both Myc and β-catenin (Bisso et al., 2020).

Although the cooperativity of Myc and β-catenin has been interrogated in a variety of cell types and tumors, their epistatic relationship in hepatocytes or hepato-oncogenesis has been brought into question. In contrast to previous data, positioning Myc downstream of β-catenin (Sansom et al., 2007; Wong et al., 2015), our intriguing data reveal an unconventional role of oncogenic Myc acting on β-catenin in liver cancer; the exact molecular mechanism requires further extensive study. Although the underlying mechanism remains to be deciphered, the data presented here suggest both cell-intrinsic and -extrinsic mechanisms for upregulation of Wnt/β-catenin signaling in this Myc-induced liver tumor model. It is possible that the expression of β-catenin and its

critical downstream target molecules (s) is regulated directly by Myc in hepatocytes, but we do not rule out another possibility that Myc and β-catenin work in mutually enhancing parallel pathways.

Other studies also hint at cooperative effects of Myc and β-catenin in HCC and colorectal cancer, further supporting our theory, though the mechanism of signaling crosstalk have not been explored (Bisso et al., 2020; Hao et al., 2019). Myc can also activate LEF1, a binding partner to β-catenin, in colon cancer cells without APC, thus driving retention of nuclear β-catenin leading to activation of Wnt/β-catenin pathway in Myc-expressing cells (Hao et al., 2019). Co-transfection of a dominant-negative form of transcriptional partner TCF7l4 suppressed tumor development induced by Myc, and Myc failed to induce HCC in mice with β-catenin deleted in hepatocytes. Furthermore, additional β-catenin removal even abrogated Myc-driven tumorigenesis in SKO mice, which was rescued by co-transfection of Myc and β-catenin.

Though not fully explored, we also observed effect of upregulated β-catenin activity effect on immune populations. Although the critical role of oncogenic β-catenin in induction of immunosuppression unveiled in this study is in agreement with previous reports (Ruiz de Galarreta et al., 2019; Spranger et al., 2015), conflicting data exist with regard to the underlying mechanisms. In contrast to the claimed roles of CCL4 and CCL5 (Ruiz de Galarreta et al., 2019; Spranger et al., 2015), our results suggest functions of several hepatokines in suppressing various innate immune populations and blocking tumor initiation. In particular, Lect2 is a β-catenin target gene product that has been implicated in liver fibrosis and HCC (Anson et al., 2012; Ovejero et al., 2004; Xu et al., 2019a). This hepatokine was shown to modulate activities of HSCs and infiltrated

inflammatory and immune cells, including macrophages, neutrophils, NK, DC, and EC in the liver, although the underlying mechanisms are under explored (Meex and Watt, 2017). Upregulated PD-L1 expression, potentially related to β-catenin expression, may also induce immune escape during tumor progression driven by cooperative activities of Myc and β-catenin (Ruiz de Galarreta et al., 2019). Further mechanistic analysis is required to elucidate the immunosuppressive tumor environment induced by aberrant β-catenin signaling in Shp2-deficient liver.

Thus, β-catenin is essential for Myc-dependent tumorigenesis even in a tumor-conducive environment in the SKO liver. Collectively, these data support an unconventional role of Myc acting upstream of β-catenin in liver cancer. Importantly, both Myc amplification and *CTNNB1* mutations have been detected simultaneously in many HCC samples. In particular, over 50% of hepatoblastoma cases were found to have Myc overexpression and also mutations in *CTNNB1* (Zheng et al., 2017b). Elucidating the underlying mechanisms will guide design of more effective therapy for this cohort of HCC patients, who showed poor prognosis and survival.

Significance in challenges to precision medicine and targeting Myc-driven cancers

A combination of the high frequency of Myc presence in liver and other organ cancers, as well as the oncogene addiction phenomena frequent in Myc-driven tumors, means Myc is a vital therapeutic target (Abou-Elella et al., 1996; Jain et al., 2002). Due to ubiquitous Myc expression across normal and abnormal tissues, clinical toxicity is a serious complication and consideration in therapeutic inhibition of Myc. The results in

this study, as well as other studies, suggest Myc-driven tumors in the liver are vulnerable to inhibition of downstream supporting genes and therefore provide additional more-druggable therapeutic targets. Just as Shp2 inhibitors have proven efficacious in treating MAPK- or RTK-driven solid cancers, similar alternative-therapeutics for indirect suppression of Myc may prove highly efficacious treatments. Further studies utilizing Shp2, MEK, or β-catenin inhibitor on Myc-dependent cancer may prove fruitful for targeting human cancers with Myc-dependency. These pathway dependencies may be limiting in various ways: Organ-specific or cancer specific. Furthermore, use of Shp2 inhibitor in combination with Myc inhibitor may allow for synergistic therapeutic effects, allowing for smaller doses of each inhibitor in combination, and reduction in clinical toxicity.

Curiously, ours and others HCC models involving overexpression of Myc, whether alone or with overexpression of additional oncogenes, have similar histopathological characteristics which may result from necessary growth patterns. Myc-driven HCC models, utilizing overexpression of Myc with concurrent overexpression of another proto-oncogene (ie. Myc/Mcl1, Myc/Ras, Myc/Akt HTVi models), develop HCC with basophilic hepatocytes arranged in trabecular pattern and pseudoglandular structures (Bisso et al., 2020; Jia et al., 2020; Xu et al., 2019b). HCC models driven partially by β-catenin also have histopathologically similar tumors, but Myc and β-catenin driven model resemble Myc-driven HCC, indicating the aggressive control Myc has over tumor appearance and likely reflected in pathway regulation (Molina-Sanchez et al., 2020). Studying the relation of Myc-driven liver cancer histopathology and gene expression patterns may reveal similar growth characteristics and gene expressions of

cancers from several origins. Similar tumors imply neoplastic transformation is dictated primarily by Myc transcriptional activity, even in the presence of other oncogenic driving influences. Machine learning can be utilized to correlate histopathological results of patient biopsies driver genes and pathway vulnerabilities, thus bypassing costly sequencing analyses. Therefore, the opportunity exists for pathological identification of biopsies to directly lead to precision in selecting for effective targeted therapeutics.

This study clarifies conflicting data on Shp2 in cancer and suggests a potential of targeting Shp2 in treatment of Myc-dependent HCCs, in addition to inhibition of tumors driven by RTKs (Chen et al., 2016). However, inhibiting Shp2 also led to markedly elevated Wnt/β-catenin signaling and a tumor-promoting TME. This mosaic mechanism of liver tumorigenesis presents a new challenge to the idea of precision medicine in cancer therapy. The intertwined cell-intrinsic and -extrinsic mechanisms disclosed here may also explain the rapid and aggressive growth of relapsed tumors from residual tumor cells which survived the targeted treatment of primary tumors. Therapeutics identified only through in vitro or xenograft screens of clonal tumor cells are unlikely to accurately predict the effects of oncogene suppression. Rather, understanding and incorporating the role of the host immune system in addition to the mechanism by which oncogene inactivation induces tumor regression would significantly contribute to the development of cancer therapeutics. Specific targeting of cell-intrinsic oncogenic pathways must be combined with simultaneous correction of the secondary immunosuppressive tumor environment to achieve efficacious and lasting therapeutic effect.

FUTURE DIRECTIONS

Genetic deletion in hepatocytes affects liver immune microenvironment's response to tumor initiation

In this study, we show Shp2-ablated hepatocytes and Myc-transfected hepatocytes causes M2 macrophage polarization and impaired phagocytosis. Several weeks later, tumors mature alongside the same Shp2-ablated hepatocytes and Myc-driven HCC. However, macrophage polarization is significantly different, predominantly skewed to inflammatory M1 identity & expression of phagocytic genes is higher in SKO than WT liver. Therefore a future direction to investigate is how hepatocytes and HCC tumor cells direct transient macrophage identity and function within the tumor microenvironment.

First we need to decipher the direct vs indirect contributors to macrophage activity. If macrophage activity and polarization can be directly altered by co-culture or conditioned media from primary SKO hepatocytes, this suggests a direct ligand-receptor relationship. We can then utilize time-dependent cytokine secretion and perform multiplex ELIZA on tumor cell-derived conditioned media to identify key effector hepatocyte-secreted ligands. Preliminary data in hepatocyte-ligand and macrophage-receptor relationships in the Myc model have been generated using scRNA-sequencing data (Figures 5.2, 5.3). Utilizing this data will allow us to preliminarily verify upregulation of complementary receptors of the identified hepatocyte-ligands identified *in vitro*.

Our Myc model also produced an increase in neutrophils and classic dendritic cells, which may indirectly signal macrophages through secretion of chemokines such

as CCL5 (Ruiz de Galarreta et al., 2019). To identify the importance of indirect signaling through other immune populations, further analysis is needed on the effect of dendritic and neutrophil chemokine secretion in the Myc model at 10 day and 4 weeks, in addition to transitory culture of treated neutrophil or dendritic cells with hepatocytes and macrophages to identify influence on macrophage polarization and activity.

Previously we noted that metabolic dysregulation in SKO hepatocytes caused TNF4a regulated inflammation in the liver, as identified by bulk RNA-sequencing data (Liu et al., 2018). Some immune changes are likely in response to altered hepatocyte metabolic function, such as in response to aberrant buildup of metabolites, elevated oxidative stress, or physical changes in liver pathophysiology due to increased fibrosis causing toxic side-effects or differential cytokine release. Therefore, one aspect of investigation should be on metabolite imbalance influencing immune microenvironment. Specifically to address excess bile acid secretion directly causes what types of cytokine/chemokine release and subsequent changes in immune behavior.

Finally, we would like to identify the importance of host immunity in this Myc model and its persistence in other oncogene-driven HCC models. The immune tumor microenvironment is established partially in specific response to gene expression changes induced by oncogenic driver Myc, as seen in our cytokine data (Figures 2.9A, 2.10A-B). Previously, studies show elevated β-catenin expression in hepatocytes can escape anti-PD-L1 treatment by aberrantly altering dendritic cells through CCL5 signaling (Ruiz de Galarreta et al., 2019). Therefore we want to examine how, under the umbrella of tumor permissiveness, different oncogenic drivers may change chemokine

secretion. We will perform multiplex ELIZA and compare tumor cell-derived conditioned media from several HCC mouse models driven by various oncogenes.

Here we provided clear evidence that deletion of proto-oncogene Shp2 in hepatocytes strongly influences the immune tumor microenvironment in response to Myc+ cells during tumor initiation. In the field of precision medicine it is essential to identify potential factors weighing on response to immunotherapy treatments. Gene ablations can induce non-fatal metabolic changes in hepatocytes, like Shp2 ablation, which may not be identified under current standard of patient selection. Tumor-associated macrophages support HCC by secreting various cytokines to enhance cancer metastasis, and maintain cell dedifferentiation. Less is known on the influence of hepatic signaling on macrophage function in the tumor microenvironment. This project outlines how hepatocytes utilize chemokine release to activate and direct macrophage phagocytosis during the tumor during initiation stage. Therapeutic advances would benefit from targeted therapeutics that both directly inhibit tumor survival, but also prime the immune microenvironment to immunotherapy. Significance of this study is to investigate a future utilizing the innate immune system and macrophage phagocytosis in cancer immunotherapy.

Liver-specific mechanisms of β-catenin and oncogenic Myc signaling crosstalk

Previous studies show β-catenin deficiency, but not Myc ablation, suppresses phenotype induced by APC loss in liver (Reed et al., 2008). This differs from prior results in the intestines, whereby either Myc or β-catenin loss restores functionality from APC loss (Sansom et al., 2007). These early results suggest Myc expression in the

mature adult hepatocytes is not primarily regulated by β-catenin activity. Our recent study shows β-catenin is essential for Myc-dependent tumorigenesis, even in a tumor-permissive microenvironment generated by SKO liver. Collectively, these data support an unconventional role of Myc acting on β-catenin in liver cancer and liver-specific roles of Myc and β-catenin signaling in parallel.

First, we wish to examine the relationship of oncogenic Myc and β-catenin in liver cancer. Other β-catenin studies also hint at organ-specific signaling differences in β-catenin and Myc crosstalk. In breast cancer, overexpression of Myc was shown to inhibit Dkk1 expression, thus indirectly activating Wnt/β-catenin expression and causing a positive feedback loop through β-catenin-driven Myc expression (Cowling et al., 2007). Due to the exogenous nature of our oncogenic Myc, the positive feedback loop would drive endogenous Myc expression, which was not upregulated in our tumor model (Figure 4.7C). In a Myc+β-catenin+ model of murine HCC, tumors select for expression of YAP or TAZ, suggesting synergistic signaling may work through the Hippo/YAP pathway (Bisso et al., 2020). Our data indicates the Myc-induced tumor cells did not have selective upregulation of Hippo/YAP pathway (Figure 4.1C). Myc can also activate LEF1, binding partner to β-catenin, in colon cancer cells without APC, thus driving retention of β-catenin nucleus leading to activation of Wnt pathway in Myc-expressing cells (Hao et al., 2019). In our model, we specifically noted increase in nuclear β-catenin and β-catenin transcriptional activity, which agrees with the above studies.

To test the nature of Myc and β-catenin crosstalk in HCC and basal liver, we will utilize Myc-dependent HCC cell lines and select for lines with sensitivity to β-catenin inhibition. Next we will test the predicted intermediate signaling factors, such as LEF1

and DKK1 by CRISPR knockout *in vitro*. Other potential targets can be extracted from scRNA-sequencing data, from overlap of known β-catenin transcriptional targets and the signaling network of upregulated genes in Myc-driven tumor cells. Finally, we will validate the model by HTVi injection of Myc and CRISPR gRNA of likely target genes to confirm blockade of β-catenin function and tumor growth in supporting oncogenic Myc in tumor development.

Another issue to address is clarification of the relationship of β-catenin and Myc in normal liver, specifically whether β-catenin directly drives Myc transcriptional activity in any capacity. We will use Co-IP to examine the dynamics of β-catenin binding to Myc promoter in primary hepatocytes and HCC cells, using intestinal cells as positive control.

Though not fully explored, we also observed effect of upregulated β-catenin activity effect on immune populations. In Myc + dnTCF model, Myc+ tumor cells were able to initially expand at 7 days, but were then cleared from the SKO liver at 12 days. This phenotype mimics the tumor clearance phenotype noted of Myc+ cells in WT liver. Ours and other studies suggest an important role of oncogenic β-catenin in inducing immunosuppression mechanisms (Ruiz de Galarreta et al., 2019; Spranger et al., 2015). β-catenin activation can lead to defective recruitment of dendritic cells and antigen-specific T cells, with crucial expression of CCL5, allowing for resistance to anti-PD-1 therapies (Ruiz de Galarreta 2019). β-catenin activation may be implicated in potential immune escape mechanisms important in patient selection for liver cancer immunotherapies.

However, our model does not show similar increase in CCL4 or CCL5, therefore other cytokine signals are at play. In our screen for involved cytokines, using

hepatocyte-ligand and macrophage-receptor interactions, we can narrow down on ligands with known relationships to β-catenin, or are correlatively changed with β-catenin signaling. One ligand we have identified already is Lect2. Lect2 (Leukocyte cell-drived chemotaxin 2) is a direct target gene of β-catenin in HCC liver and implicated as a potential HCC biomarker, whereby higher Lect2 serum levels correlates with better survival from HCC and severe liver injury (Slowik and Apte, 2017; Xu et al., 2019a). Lect2 can activate macrophages under inflammatory conditions and Tie2, the putative receptor for Lect2, is expressed in various immune populations, including macrophages (Slowik and Apte, 2017). Therefore we suspect upregulation of β-catenin activity, in combination with Myc, causes increased chemokine release that influences myeloid populations.

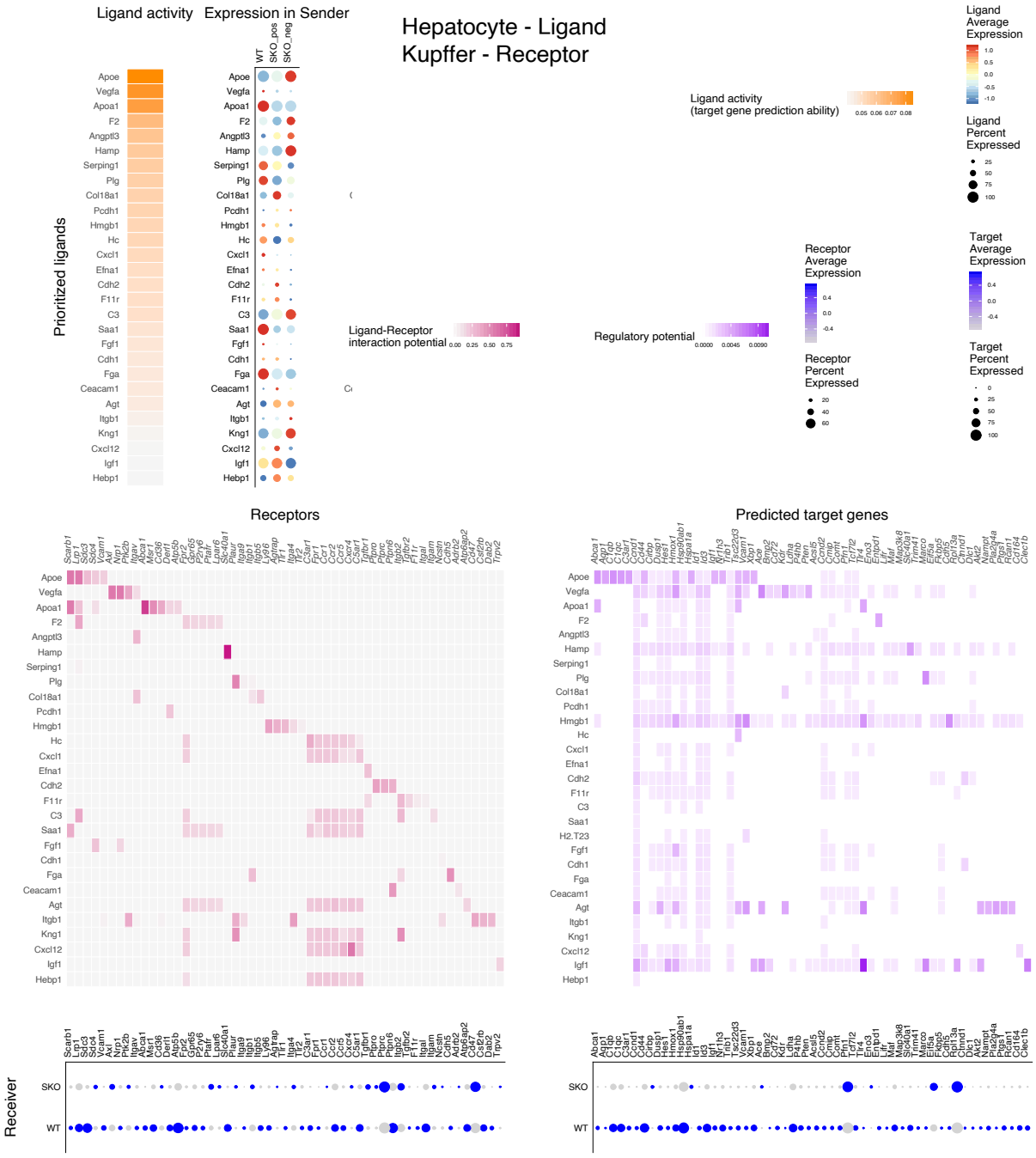

Figure 5.1: Ligand-receptor interactions between hepatocytes and Kupffer cells

(**A**) Target ligand expression level and percentage of cells expressed in hepatocytes in WT, SKO Shp2+, and SKO Shp2- in 10D-Myc hepatocyte data (Top). Receptor interaction potential in Kupffer cells (Left, magenta) and regulatory potential (Right, purple) with expression level and percentage of cells expressed in Kupffer cells (receiver cell).

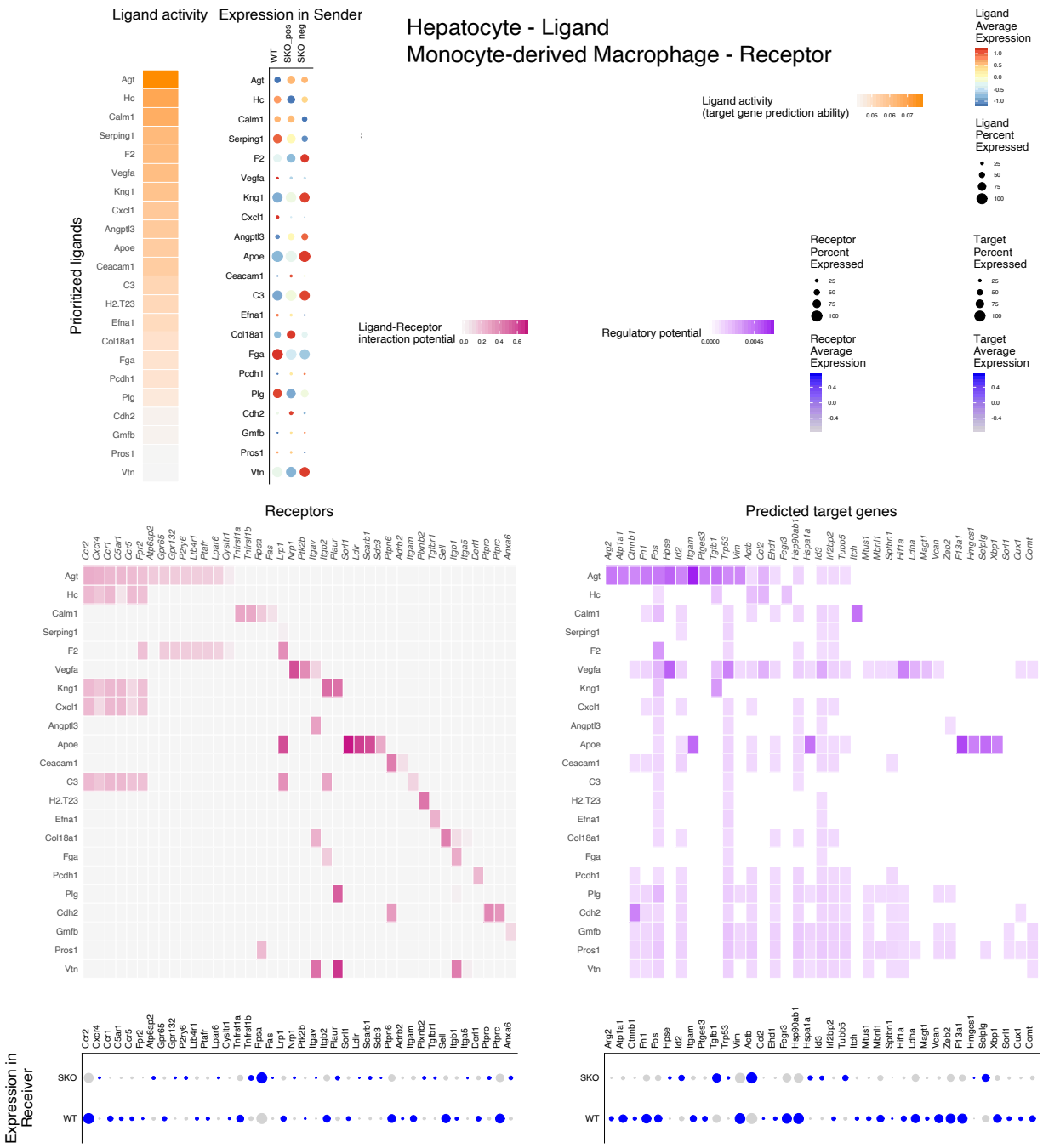

Figure 5.2: Ligand-receptor interactions between hepatocytes and Monocyte-derived macrophages

(**A**) Target ligand expression level and percentage of cells expressed in hepatocytes in WT, SKO Shp2+, and SKO Shp2- in 10D-Myc hepatocyte data (Top). Receptor interaction potential in monocyte-derived macrophage cells (Left, magenta) and regulatory potential (Right, purple) with expression level and percentage of cells expressed in monocyte-derived macrophage cells (receiver cell).

REFERENCES

Abou-Elella, A., Gramlich, T., Fritsch, C., and Gansler, T. (1996). c-myc amplification in hepatocellular carcinoma predicts unfavorable prognosis. Mod Pathol *9*, 95-98.

Ahmed, T.A., Adamopoulos, C., Karoulia, Z., Wu, X., Sachidanandam, R., Aaronson, S.A., and Poulikakos, P.I. (2019). SHP2 Drives Adaptive Resistance to ERK Signaling Inhibition in Molecularly Defined Subsets of ERK-Dependent Tumors. Cell Rep *26*, 65-78 e65.

Anson, M., Crain-Denoyelle, A.M., Baud, V., Chereau, F., Gougelet, A., Terris, B., Yamagoe, S., Colnot, S., Viguier, M., Perret, C., and Couty, J.P. (2012). Oncogenic beta-catenin triggers an inflammatory response that determines the aggressiveness of hepatocellular carcinoma in mice. J Clin Invest *122*, 586-599.

Bard-Chapeau, E.A., Li, S., Ding, J., Zhang, S.S., Zhu, H.H., Princen, F., Fang, D.D., Han, T., Bailly-Maitre, B., Poli, V., Varki, N.M., Wang, H., and Feng, G.S. (2011). Ptpn11/Shp2 acts as a tumor suppressor in hepatocellular carcinogenesis. Cancer Cell *19*, 629-639.

Bard-Chapeau, E.A., Yuan, J., Droin, N., Long, S., Zhang, E.E., Nguyen, T.V., and Feng, G.S. (2006). Concerted functions of Gab1 and Shp2 in liver regeneration and hepatoprotection. Mol Cell Biol *26*, 4664-4674.

Beer, S., Komatsubara, K., Bellovin, D.I., Kurobe, M., Sylvester, K., and Felsher, D.W. (2008). Hepatotoxin-induced changes in the adult murine liver promote MYC-induced tumorigenesis. PLoS One *3*, e2493.

Bisso, A., Filipuzzi, M., Gamarra Figueroa, G.P., Brumana, G., Biagioni, F., Doni, M., Ceccotti, G., Tanaskovic, N., Morelli, M.J., Pendino, V., Chiacchiera, F., Pasini, D., Olivero, D., Campaner, S., Sabo, A., and Amati, B. (2020). Cooperation between MYC and beta-catenin in liver tumorigenesis requires Yap/Taz. Hepatology.

Bray, F., Ferlay, J., Soerjomataram, I., Siegel, R.L., Torre, L.A., and Jemal, A. (2018). Global cancer statistics 2018: GLOBOCAN estimates of incidence and mortality worldwide for 36 cancers in 185 countries. CA Cancer J Clin *68*, 394-424.

Browaeys, R., Saelens, W., and Saeys, Y. (2020). NicheNet: modeling intercellular communication by linking ligands to target genes. Nat Methods *17*, 159-162.

Burke, Z.D., Reed, K.R., Phesse, T.J., Sansom, O.J., Clarke, A.R., and Tosh, D. (2009). Liver zonation occurs through a beta-catenin-dependent, c-Myc-independent mechanism. Gastroenterology *136*, 2316-2324 e2311-2313.

Cairo, S., Armengol, C., De Reynies, A., Wei, Y., Thomas, E., Renard, C.A., Goga, A., Balakrishnan, A., Semeraro, M., Gresh, L., Pontoglio, M., Strick-Marchand, H., Levillayer, F., Nouet, Y., Rickman, D., Gauthier, F., Branchereau, S., Brugieres, L., Laithier, V., Bouvier, R., Boman, F., Basso, G., Michiels, J.F., Hofman, P., Arbez-Gindre, F., Jouan, H., Rousselet-Chapeau, M.C., Berrebi, D., Marcellin, L., Plenat, F., Zachar, D., Joubert, M., Selves, J., Pasquier, D., Bioulac-Sage, P., Grotzer, M., Childs, M., Fabre, M., and Buendia, M.A. (2008). Hepatic stem-like phenotype and interplay of Wnt/beta-catenin and Myc signaling in aggressive childhood liver cancer. Cancer Cell *14*, 471-484.

Calvisi, D.F., Factor, V.M., Loi, R., and Thorgeirsson, S.S. (2001). Activation of beta-catenin during hepatocarcinogenesis in transgenic mouse models: relationship to phenotype and tumor grade. Cancer Res *61*, 2085-2091.

Cancer Genome Atlas Research Network. Electronic address, w.b.e., and Cancer Genome Atlas Research, N. (2017). Comprehensive and Integrative Genomic Characterization of Hepatocellular Carcinoma. Cell *169*, 1327-1341 e1323.

Carroll, P.A., Diolaiti, D., McFerrin, L., Gu, H., Djukovic, D., Du, J., Cheng, P.F., Anderson, S., Ulrich, M., Hurley, J.B., Raftery, D., Ayer, D.E., and Eisenman, R.N. (2015). Deregulated Myc requires MondoA/Mlx for metabolic reprogramming and tumorigenesis. Cancer Cell *27*, 271-285.

Chan, R.J., and Feng, G.S. (2007). PTPN11 is the first identified proto-oncogene that encodes a tyrosine phosphatase. Blood *109*, 862-867.

Chen, B., Garmire, L., Calvisi, D.F., Chua, M.S., Kelley, R.K., and Chen, X. (2020). Harnessing big 'omics' data and AI for drug discovery in hepatocellular carcinoma. Nat Rev Gastroenterol Hepatol *17*, 238-251.

Chen, X., and Calvisi, D.F. (2014). Hydrodynamic transfection for generation of novel mouse models for liver cancer research. Am J Pathol *184*, 912-923.

Chen, Y.N., LaMarche, M.J., Chan, H.M., Fekkes, P., Garcia-Fortanet, J., Acker, M.G., Antonakos, B., Chen, C.H., Chen, Z., Cooke, V.G., Dobson, J.R., Deng, Z., Fei, F., Firestone, B., Fodor, M., Fridrich, C., Gao, H., Grunenfelder, D., Hao, H.X., Jacob, J., Ho, S., Hsiao, K., Kang, Z.B., Karki, R., Kato, M., Larrow, J., La Bonte, L.R., Lenoir, F., Liu, G., Liu, S., Majumdar, D., Meyer, M.J., Palermo, M., Perez, L., Pu, M., Price, E., Quinn, C., Shakya, S., Shultz, M.D., Slisz, J., Venkatesan, K., Wang, P., Warmuth, M., Williams, S., Yang, G., Yuan, J., Zhang, J.H., Zhu, P., Ramsey, T., Keen, N.J., Sellers, W.R., Stams, T., and Fortin, P.D. (2016). Allosteric inhibition of SHP2 phosphatase inhibits cancers driven by receptor tyrosine kinases. Nature *535*, 148-152.

Cho, J.H., Dimri, M., and Dimri, G.P. (2013). A positive feedback loop regulates the expression of polycomb group protein BMI1 via WNT signaling pathway. J Biol Chem *288*, 3406-3418.

Choi, P.S., van Riggelen, J., Gentles, A.J., Bachireddy, P., Rakhra, K., Adam, S.J., Plevritis, S.K., and Felsher, D.W. (2011). Lymphomas that recur after MYC suppression continue to exhibit oncogene addiction. Proc Natl Acad Sci U S A *108*, 17432-17437.

Ciechanover, A., DiGiuseppe, J.A., Schwartz, A.L., and Brodeur, G.M. (1991). Degradation of MYCN oncoprotein by the ubiquitin system. Prog Clin Biol Res *366*, 37-43.

Cowling, V.H., D'Cruz, C.M., Chodosh, L.A., and Cole, M.D. (2007). c-Myc transforms human mammary epithelial cells through repression of the Wnt inhibitors DKK1 and SFRP1. Mol Cell Biol *27*, 5135-5146.

Dang, C.V. (2012). MYC on the path to cancer. Cell *149*, 22-35.

Dang, C.V. (2013). MYC, metabolism, cell growth, and tumorigenesis. Cold Spring Harb Perspect Med *3*.

Dardaei, L., Wang, H.Q., Singh, M., Fordjour, P., Shaw, K.X., Yoda, S., Kerr, G., Yu, K., Liang, J., Cao, Y., Chen, Y., Lawrence, M.S., Langenbucher, A., Gainor, J.F., Friboulet, L., Dagogo-Jack, I., Myers, D.T., Labrot, E., Ruddy, D., Parks, M., Lee, D., DiCecca, R.H., Moody, S., Hao, H., Mohseni, M., LaMarche, M., Williams, J., Hoffmaster, K., Caponigro, G., Shaw, A.T., Hata, A.N., Benes, C.H., Li, F., and Engelman, J.A. (2018). SHP2 inhibition restores sensitivity in ALK-rearranged non-small-cell lung cancer resistant to ALK inhibitors. Nat Med *24*, 512-517.

Das, M., Garlick, D.S., Greiner, D.L., and Davis, R.J. (2011). The role of JNK in the development of hepatocellular carcinoma. Genes Dev *25*, 634-645.

Dauch, D., Rudalska, R., Cossa, G., Nault, J.C., Kang, T.W., Wuestefeld, T., Hohmeyer, A., Imbeaud, S., Yevsa, T., Hoenicke, L., Pantsar, T., Bozko, P., Malek, N.P., Longerich, T., Laufer, S., Poso, A., Zucman-Rossi, J., Eilers, M., and Zender, L. (2016a). A MYC-aurora kinase A protein complex represents an actionable drug target in p53-altered liver cancer. Nat Med *22*, 744-753.

Dauch, D., Rudalska, R., Cossa, G., Nault, J.C., Kang, T.W., Wuestefeld, T., Hohmeyer, A., Imbeaud, S., Yevsa, T., Hoenicke, L., Pantsar, T., Bozko, P., Malek, N.P., Longerich, T., Laufer, S., Poso, A., Zucman-Rossi, J., Eilers, M., and Zender, L. (2016b). A MYC-aurora kinase A protein complex represents an actionable drug target in p53-altered liver cancer. Nat Med.

Digilio, M.C., Conti, E., Sarkozy, A., Mingarelli, R., Dottorini, T., Marino, B., Pizzuti, A., and Dallapiccola, B. (2002). Grouping of multiple-lentigines/LEOPARD and Noonan syndromes on the PTPN11 gene. Am J Hum Genet *71*, 389-394.

Dolezal, J.M., Wang, H., Kulkarni, S., Jackson, L., Lu, J., Ranganathan, S., Goetzman, E.S., Bharathi, S.S., Beezhold, K., Byersdorfer, C.A., and Prochownik, E.V. (2017). Sequential adaptive changes in a c-Myc-driven model of hepatocellular carcinoma. J Biol Chem *292*, 10068-10086.

El-Serag, H.B. (2011). Hepatocellular carcinoma. N Engl J Med *365*, 1118-1127.

Farrell, A.S., and Sears, R.C. (2014). MYC degradation. Cold Spring Harb Perspect Med *4*.

Fedele, C., Ran, H., Diskin, B., Wei, W., Jen, J., Geer, M.J., Araki, K., Ozerdem, U., Simeone, D.M., Miller, G., Neel, B.G., and Tang, K.H. (2018). SHP2 Inhibition Prevents Adaptive Resistance to MEK Inhibitors in Multiple Cancer Models. Cancer Discov *8*, 1237-1249.

Felsher, D.W., and Bishop, J.M. (1999). Transient excess of MYC activity can elicit genomic instability and tumorigenesis. Proc Natl Acad Sci U S A *96*, 3940-3944.

Feng, G.S. (1999). Shp-2 tyrosine phosphatase: Signaling one cell or many. Exp Cell Res *253*, 47-54.

Feng, G.S. (2012). Conflicting roles of molecules in hepatocarcinogenesis: paradigm or paradox. Cancer Cell *21*, 150-154.

Feng, G.S., and Pawson, T. (1994). Phosphotyrosine phosphatases with SH2 domains: regulators of signal transduction. Trends Genet *10*, 54-58.

Finn, R.S., Qin, S., Ikeda, M., Galle, P.R., Ducreux, M., Kim, T.Y., Kudo, M., Breder, V., Merle, P., Kaseb, A.O., Li, D., Verret, W., Xu, D.Z., Hernandez, S., Liu, J., Huang, C., Mulla, S., Wang, Y., Lim, H.Y., Zhu, A.X., Cheng, A.L., and Investigators, I.M. (2020). Atezolizumab plus Bevacizumab in Unresectable Hepatocellular Carcinoma. N Engl J Med *382*, 1894-1905.

Forner, A., Reig, M.E., de Lope, C.R., and Bruix, J. (2010). Current strategy for staging and treatment: the BCLC update and future prospects. Semin Liver Dis *30*, 61-74.

Gabay, M., Li, Y., and Felsher, D.W. (2014). MYC activation is a hallmark of cancer initiation and maintenance. Cold Spring Harb Perspect Med *4*.

Gao, P., Tchernyshyov, I., Chang, T.C., Lee, Y.S., Kita, K., Ochi, T., Zeller, K.I., De Marzo, A.M., Van Eyk, J.E., Mendell, J.T., and Dang, C.V. (2009). c-Myc suppression of miR-23a/b enhances mitochondrial glutaminase expression and glutamine metabolism. Nature *458*, 762-U100.

Gomez-Roman, N., Grandori, C., Eisenman, R.N., and White, R.J. (2003). Direct activation of RNA polymerase III transcription by c-Myc. Nature *421*, 290-294.

Grandori, C., Wu, K.J., Fernandez, P., Ngouenet, C., Grim, J., Clurman, B.E., Moser, M.J., Oshima, J., Russell, D.W., Swisshelm, K., Frank, S., Amati, B., Dalla-Favera, R., and Monnat, R.J., Jr. (2003). Werner syndrome protein limits MYC-induced cellular senescence. Genes Dev *17*, 1569-1574.

Halpern, K.B., Shenhav, R., Matcovitch-Natan, O., Toth, B., Lemze, D., Golan, M., Massasa, E.E., Baydatch, S., Landen, S., Moor, A.E., Brandis, A., Giladi, A., Avihail, A.S., David, E., Amit, I., and Itzkovitz, S. (2017). Single-cell spatial reconstruction reveals global division of labour in the mammalian liver. Nature *542*, 352-356.

Han, T., Xiang, D.M., Sun, W., Liu, N., Sun, H.L., Wen, W., Shen, W.F., Wang, R.Y., Chen, C., Wang, X., Cheng, Z., Li, H.Y., Wu, M.C., Cong, W.M., Feng, G.S., Ding, J., and Wang, H.Y. (2015). PTPN11/Shp2 overexpression enhances liver cancer progression and predicts poor prognosis of patients. J Hepatol *63*, 651-660.

Hanafusa, H., Torii, S., Yasunaga, T., Matsumoto, K., and Nishida, E. (2004). Shp2, an SH2-containing protein-tyrosine phosphatase, positively regulates receptor tyrosine kinase signaling by dephosphorylating and inactivating the inhibitor Sprouty. J Biol Chem *279*, 22992-22995.

Hao, Y.H., Lafita-Navarro, M.C., Zacharias, L., Borenstein-Auerbach, N., Kim, M., Barnes, S., Kim, J., Shay, J., DeBerardinis, R.J., and Conacci-Sorrell, M. (2019). Induction of LEF1 by MYC activates the WNT pathway and maintains cell proliferation. Cell Commun Signal *17*, 129.

Hayes, T.K., Neel, N.F., Hu, C., Gautam, P., Chenard, M., Long, B., Aziz, M., Kassner, M., Bryant, K.L., Pierobon, M., Marayati, R., Kher, S., George, S.D., Xu, M., Wang-Gillam, A., Samatar, A.A., Maitra, A., Wennerberg, K., Petricoin, E.F., 3rd, Yin, H.H., Nelkin, B., Cox, A.D., Yeh, J.J., and Der, C.J. (2016). Long-Term ERK Inhibition in KRAS-Mutant Pancreatic Cancer Is Associated with MYC Degradation and Senescence-like Growth Suppression. Cancer Cell *29*, 75-89.

Heindryckx, F., Colle, I., and Van Vlierberghe, H. (2009). Experimental mouse models for hepatocellular carcinoma research. Int J Exp Pathol *90*, 367-386.

Hoffman, B., and Liebermann, D.A. (2008). Apoptotic signaling by c-MYC. Oncogene *27*, 6462-6472.

Hou, Y., Guo, H., Cao, C., Li, X., Hu, B., Zhu, P., Wu, X., Wen, L., Tang, F., Huang, Y., and Peng, J. (2016). Single-cell triple omics sequencing reveals genetic, epigenetic, and transcriptomic heterogeneity in hepatocellular carcinomas. Cell Res *26*, 304-319.

Huang, A., Yang, X.R., Chung, W.Y., Dennison, A.R., and Zhou, J. (2020). Targeted therapy for hepatocellular carcinoma. Signal Transduct Target Ther *5*, 146.

Huang, Y., Ge, W., Zhou, J., Gao, B., Qian, X., and Wang, W. (2021). The Role of Tumor Associated Macrophages in Hepatocellular Carcinoma. J Cancer *12*, 1284-1294.

Jain, M., Arvanitis, C., Chu, K., Dewey, W., Leonhardt, E., Trinh, M., Sundberg, C.D., Bishop, J.M., and Felsher, D.W. (2002). Sustained loss of a neoplastic phenotype by brief inactivation of MYC. Science *297*, 102-104.

Jia, J., Che, L., Cigliano, A., Wang, X., Peitta, G., Tao, J., Zhong, S., Ribback, S., Evert, M., Chen, X., and Calvisi, D.F. (2020). Pivotal Role of Fatty Acid Synthase in c-MYC Driven Hepatocarcinogenesis. Int J Mol Sci *21*.

Kang, T.W., Yevsa, T., Woller, N., Hoenicke, L., Wuestefeld, T., Dauch, D., Hohmeyer, A., Gereke, M., Rudalska, R., Potapova, A., Iken, M., Vucur, M., Weiss, S., Heikenwalder, M., Khan, S., Gil, J., Bruder, D., Manns, M., Schirmacher, P., Tacke, F., Ott, M., Luedde, T., Longerich, T., Kubicka, S., and Zender, L. (2011). Senescence surveillance of pre-malignant hepatocytes limits liver cancer development. Nature *479*, 547-551.

Kerr, D.L., Haderk, F., and Bivona, T.G. (2021). Allosteric SHP2 inhibitors in cancer: Targeting the intersection of RAS, resistance, and the immune microenvironment. Curr Opin Chem Biol *62*, 1-12.

Kim, Y., Sills, R.C., and Houle, C.D. (2005). Overview of the molecular biology of hepatocellular neoplasms and hepatoblastomas of the mouse liver. Toxicol Pathol *33*, 175-180.

Klocke, R., Bartels, T., Jennings, G., Brand, K., Halter, R., Strauss, M., and Paul, D. (2001). Lack of p53 accelerates hepatocarcinogenesis in transgenic mice constitutively overexpressing c-myc in the liver. FASEB J *15*, 1404-1406.

LaMarche, M.J., Acker, M., Argintaru, A., Bauer, D., Boisclair, J., Chan, H., Chen, C.H., Chen, Y.N., Chen, Z., Deng, Z., Dore, M., Dunstan, D., Fan, J., Fekkes, P., Firestone, B., Fodor, M., Garcia-Fortanet, J., Fortin, P.D., Fridrich, C., Giraldes, J., Glick, M.,

Grunenfelder, D., Hao, H.X., Hentemann, M., Ho, S., Jouk, A., Kang, Z.B., Karki, R., Kato, M., Keen, N., Koenig, R., LaBonte, L.R., Larrow, J., Liu, G., Liu, S., Majumdar, D., Mathieu, S., Meyer, M.J., Mohseni, M., Ntaganda, R., Palermo, M., Perez, L., Pu, M., Ramsey, T., Reilly, J., Sarver, P., Sellers, W.R., Sendzik, M., Shultz, M.D., Slisz, J., Slocum, K., Smith, T., Spence, S., Stams, T., Straub, C., Tamez, V., Jr., Toure, B.B., Towler, C., Wang, P., Wang, H., Williams, S.L., Yang, F., Yu, B., Zhang, J.H., and Zhu, S. (2020). Identification of TNO155, an Allosteric SHP2 Inhibitor for the Treatment of Cancer. J Med Chem *63*, 13578-13594.

Lawton, T. (2020). Liver Cancer Insight Report: Current Therapies, Drug Pipeline and Outlook.

Li, S., Hsu, D.D., Li, B., Luo, X., Alderson, N., Qiao, L., Ma, L., Zhu, H.H., He, Z., Suino-Powell, K., Ji, K., Li, J., Shao, J., Xu, H.E., Li, T., and Feng, G.S. (2014a). Cytoplasmic tyrosine phosphatase Shp2 coordinates hepatic regulation of bile acid and FGF15/19 signaling to repress bile acid synthesis. Cell Metab *20*, 320-332.

Li, S., Hsu, D.D., Wang, H., and Feng, G.S. (2012). Dual faces of SH2-containing protein-tyrosine phosphatase Shp2/PTPN11 in tumorigenesis. Front Med *6*, 275-279.

Li, Y., Casey, S.C., and Felsher, D.W. (2014b). Inactivation of MYC reverses tumorigenesis. J Intern Med *276*, 52-60.

Liang, Y., Feng, Y., Zong, M., Wei, X.F., Lee, J., Feng, Y., Li, H., Yang, G.S., Wu, Z.J., Fu, X.D., and Feng, G.S. (2018). beta-catenin deficiency in hepatocytes aggravates hepatocarcinogenesis driven by oncogenic beta-catenin and MET. Hepatology *67*, 1807-1822.

Liu, C., Lu, H., Wang, H., Loo, A., Zhang, X., Yang, G., Kowal, C., Delach, S., Wang, Y., Goldoni, S., Hastings, W.D., Wong, K., Gao, H., Meyer, M.J., Moody, S.E., LaMarche, M.J., Engelman, J.A., Williams, J.A., Hammerman, P.S., Abrams, T.J., Mohseni, M., Caponigro, G., and Hao, H.X. (2021). Combinations with Allosteric SHP2 Inhibitor TNO155 to Block Receptor Tyrosine Kinase Signaling. Clin Cancer Res *27*, 342-354.

Liu, J.J., Li, Y., Chen, W.S., Liang, Y., Wang, G., Zong, M., Kaneko, K., Xu, R., Karin, M., and Feng, G.S. (2018). Shp2 deletion in hepatocytes suppresses hepatocarcinogenesis driven by oncogenic beta-Catenin, PIK3CA and MET. J Hepatol *69*, 79-88.

Liu, M., Guo, S., and Stiles, J.K. (2011). The emerging role of CXCL10 in cancer (Review). Oncol Lett *2*, 583-589.

Liu, P., Ge, M., Hu, J., Li, X., Che, L., Sun, K., Cheng, L., Huang, Y., Pilo, M.G., Cigliano, A., Pes, G.M., Pascale, R.M., Brozzetti, S., Vidili, G., Porcu, A., Cossu, A.,

Palmieri, G., Sini, M.C., Ribback, S., Dombrowski, F., Tao, J., Calvisi, D.F., Chen, L., and Chen, X. (2017). A functional mammalian target of rapamycin complex 1 signaling is indispensable for c-Myc-driven hepatocarcinogenesis. Hepatology *66*, 167-181.

Liu, X., and Qu, C.K. (2011). Protein Tyrosine Phosphatase SHP-2 (PTPN11) in Hematopoiesis and Leukemogenesis. J Signal Transduct *2011*, 195239.

Llovet, J.M., Bru, C., and Bruix, J. (1999). Prognosis of hepatocellular carcinoma: the BCLC staging classification. Semin Liver Dis *19*, 329-338.

Llovet, J.M., Zucman-Rossi, J., Pikarsky, E., Sangro, B., Schwartz, M., Sherman, M., and Gores, G. (2016). Hepatocellular carcinoma. Nat Rev Dis Primers *2*, 16018.

Luo, X., Liao, R., Hanley, K.L., Zhu, H.H., Malo, K.N., Hernandez, C., Wei, X., Varki, N.M., Alderson, N., Chu, C., Li, S., Fan, J., Loomba, R., Qiu, S.J., and Feng, G.S. (2016). Dual Shp2 and Pten Deficiencies Promote Non-alcoholic Steatohepatitis and Genesis of Liver Tumor-Initiating Cells. Cell Rep *17*, 2979-2993.

Ma, L., Hernandez, M.O., Zhao, Y., Mehta, M., Tran, B., Kelly, M., Rae, Z., Hernandez, J.M., Davis, J.L., Martin, S.P., Kleiner, D.E., Hewitt, S.M., Ylaya, K., Wood, B.J., Greten, T.F., and Wang, X.W. (2019). Tumor Cell Biodiversity Drives Microenvironmental Reprogramming in Liver Cancer. Cancer Cell *36*, 418-430 e416.

MacParland, S.A., Liu, J.C., Ma, X.Z., Innes, B.T., Bartczak, A.M., Gage, B.K., Manuel, J., Khuu, N., Echeverri, J., Linares, I., Gupta, R., Cheng, M.L., Liu, L.Y., Camat, D., Chung, S.W., Seliga, R.K., Shao, Z., Lee, E., Ogawa, S., Ogawa, M., Wilson, M.D., Fish, J.E., Selzner, M., Ghanekar, A., Grant, D., Greig, P., Sapisochin, G., Selzner, N., Winegarden, N., Adeyi, O., Keller, G., Bader, G.D., and McGilvray, I.D. (2018). Single cell RNA sequencing of human liver reveals distinct intrahepatic macrophage populations. Nat Commun *9*, 4383.

Mainardi, S., Mulero-Sanchez, A., Prahallad, A., Germano, G., Bosma, A., Krimpenfort, P., Lieftink, C., Steinberg, J.D., de Wit, N., Goncalves-Ribeiro, S., Nadal, E., Bardelli, A., Villanueva, A., and Bernards, R. (2018). SHP2 is required for growth of KRAS-mutant non-small-cell lung cancer in vivo. Nat Med *24*, 961-967.

Marra, F., and Tacke, F. (2014). Roles for chemokines in liver disease. Gastroenterology *147*, 577-594 e571.

Meex, R.C.R., and Watt, M.J. (2017). Hepatokines: linking nonalcoholic fatty liver disease and insulin resistance. Nat Rev Endocrinol *13*, 509-520.

Mendez-Lucas, A., Li, X., Hu, J., Che, L., Song, X., Jia, J., Wang, J., Xie, C., Driscoll, P.C., Tschaharganeh, D.F., Calvisi, D.F., Yuneva, M., and Chen, X. (2017). Glucose Catabolism in Liver Tumors Induced by c-MYC Can Be Sustained by Various PKM1/PKM2 Ratios and Pyruvate Kinase Activities. Cancer Res *77*, 4355-4364.

Miller, D.M., Thomas, S.D., Islam, A., Muench, D., and Sedoris, K. (2012). c-Myc and cancer metabolism. Clin Cancer Res *18*, 5546-5553.

Molina-Sanchez, P., Ruiz de Galarreta, M., Yao, M.A., Lindblad, K.E., Bresnahan, E., Bitterman, E., Martin, T.C., Rubenstein, T., Nie, K., Golas, J., Choudhary, S., Barcena-Varela, M., Elmas, A., Miguela, V., Ding, Y., Kan, Z., Grinspan, L.T., Huang, K.L., Parsons, R.E., Shields, D.J., Rollins, R.A., and Lujambio, A. (2020). Cooperation Between Distinct Cancer Driver Genes Underlies Intertumor Heterogeneity in Hepatocellular Carcinoma. Gastroenterology *159*, 2203-2220 e2214.

Murakami, H., Sanderson, N.D., Nagy, P., Marino, P.A., Merlino, G., and Thorgeirsson, S.S. (1993). Transgenic mouse model for synergistic effects of nuclear oncogenes and growth factors in tumorigenesis: interaction of c-myc and transforming growth factor alpha in hepatic oncogenesis. Cancer Res *53*, 1719-1723.

Neel, B.G., Gu, H., and Pao, L. (2003). The 'Shp'ing news: SH2 domain-containing tyrosine phosphatases in cell signaling. Trends Biochem Sci *28*, 284-293.

Nejak-Bowen, K.N., Thompson, M.D., Singh, S., Bowen, W.C., Jr., Dar, M.J., Khillan, J., Dai, C., and Monga, S.P. (2010). Accelerated liver regeneration and hepatocarcinogenesis in mice overexpressing serine-45 mutant beta-catenin. Hepatology *51*, 1603-1613.

Network., T.R. (2017). Comprehensive and Integrative Genomic Characterization of Hepatocellular Carcinoma. Cell *169*, 1327-1341 e1323.

Ohgaki, H., Sanderson, N.D., Ton, P., and Thorgeirsson, S.S. (1996). Molecular analyses of liver tumors in c-myc transgenic mice and c-myc and TGF-alpha double transgenic mice. Cancer Lett *106*, 43-49.

Ovejero, C., Cavard, C., Perianin, A., Hakvoort, T., Vermeulen, J., Godard, C., Fabre, M., Chafey, P., Suzuki, K., Romagnolo, B., Yamagoe, S., and Perret, C. (2004). Identification of the leukocyte cell-derived chemotaxin 2 as a direct target gene of beta-catenin in the liver. Hepatology *40*, 167-176.

Postic, C., and Magnuson, M.A. (2000). DNA excision in liver by an albumin-Cre transgene occurs progressively with age. Genesis *26*, 149-150.

Ran, H., Tsutsumi, R., Araki, T., and Neel, B.G. (2016). Sticking It to Cancer with Molecular Glue for SHP2. Cancer Cell *30*, 194-196.

Reed, K.R., Athineos, D., Meniel, V.S., Wilkins, J.A., Ridgway, R.A., Burke, Z.D., Muncan, V., Clarke, A.R., and Sansom, O.J. (2008). B-catenin deficiency, but not Myc deletion, suppresses the immediate phenotypes of APC loss in the liver. Proc Natl Acad Sci U S A *105*, 18919-18923.

Ren, Y., Chen, Z., Chen, L., Fang, B., Win-Piazza, H., Haura, E., Koomen, J.M., and Wu, J. (2010). Critical role of Shp2 in tumor growth involving regulation of c-Myc. Genes Cancer *1*, 994-1007.

Ruess, D.A., Heynen, G.J., Ciecielski, K.J., Ai, J., Berninger, A., Kabacaoglu, D., Gorgulu, K., Dantes, Z., Wormann, S.M., Diakopoulos, K.N., Karpathaki, A.F., Kowalska, M., Kaya-Aksoy, E., Song, L., van der Laan, E.A.Z., Lopez-Alberca, M.P., Nazare, M., Reichert, M., Saur, D., Erkan, M.M., Hopt, U.T., Sainz, B., Jr., Birchmeier, W., Schmid, R.M., Lesina, M., and Algul, H. (2018). Mutant KRAS-driven cancers depend on PTPN11/SHP2 phosphatase. Nat Med *24*, 954-960.

Ruiz de Galarreta, M., Bresnahan, E., Molina-Sanchez, P., Lindblad, K.E., Maier, B., Sia, D., Puigvehi, M., Miguela, V., Casanova-Acebes, M., Dhainaut, M., Villacorta-Martin, C., Singhi, A.D., Moghe, A., von Felden, J., Tal Grinspan, L., Wang, S., Kamphorst, A.O., Monga, S.P., Brown, B.D., Villanueva, A., Llovet, J.M., Merad, M., and Lujambio, A. (2019). beta-Catenin Activation Promotes Immune Escape and Resistance to Anti-PD-1 Therapy in Hepatocellular Carcinoma. Cancer Discov *9*, 1124-1141.

Russell, J.O., and Monga, S.P. (2018). Wnt/beta-Catenin Signaling in Liver Development, Homeostasis, and Pathobiology. Annu Rev Pathol *13*, 351-378.

Salghetti, S.E., Kim, S.Y., and Tansey, W.P. (1999). Destruction of Myc by ubiquitin-mediated proteolysis: cancer-associated and transforming mutations stabilize Myc. EMBO J *18*, 717-726.

Sanders, J.A., Schorl, C., Patel, A., Sedivy, J.M., and Gruppuso, P.A. (2012). Postnatal liver growth and regeneration are independent of c-myc in a mouse model of conditional hepatic c-myc deletion. BMC Physiol *12*, 1.

Sansom, O.J., Meniel, V.S., Muncan, V., Phesse, T.J., Wilkins, J.A., Reed, K.R., Vass, J.K., Athineos, D., Clevers, H., and Clarke, A.R. (2007). Myc deletion rescues Apc deficiency in the small intestine. Nature *446*, 676-679.

Schaub, F.X., Dhankani, V., Berger, A.C., Trivedi, M., Richardson, A.B., Shaw, R., Zhao, W., Zhang, X., Ventura, A., Liu, Y., Ayer, D.E., Hurlin, P.J., Cherniack, A.D., Eisenman, R.N., Bernard, B., Grandori, C., and Cancer Genome Atlas, N. (2018). Pan-cancer

Alterations of the MYC Oncogene and Its Proximal Network across the Cancer Genome Atlas. Cell Syst *6*, 282-300 e282.

Sears, R., Leone, G., DeGregori, J., and Nevins, J.R. (1999). Ras enhances Myc protein stability. Mol Cell *3*, 169-179.

Shachaf, C.M., Kopelman, A.M., Arvanitis, C., Karlsson, A., Beer, S., Mandl, S., Bachmann, M.H., Borowsky, A.D., Ruebner, B., Cardiff, R.D., Yang, Q., Bishop, J.M., Contag, C.H., and Felsher, D.W. (2004). MYC inactivation uncovers pluripotent differentiation and tumour dormancy in hepatocellular cancer. Nature *431*, 1112-1117.

Slowik, V., and Apte, U. (2017). Leukocyte Cell-Derived Chemotaxin-2: It's Role in Pathophysiology and Future in Clinical Medicine. Clin Transl Sci *10*, 249-259.

Spranger, S., Bao, R., and Gajewski, T.F. (2015). Melanoma-intrinsic beta-catenin signalling prevents anti-tumour immunity. Nature *523*, 231-235.

Sprinzl, M.F., Puschnik, A., Schlitter, A.M., Schad, A., Ackermann, K., Esposito, I., Lang, H., Galle, P.R., Weinmann, A., Heikenwalder, M., and Protzer, U. (2015). Sorafenib inhibits macrophage-induced growth of hepatoma cells by interference with insulin-like growth factor-1 secretion. J Hepatol *62*, 863-870.

Takahashi, A., Tsutsumi, R., Kikuchi, I., Obuse, C., Saito, Y., Seidi, A., Karisch, R., Fernandez, M., Cho, T., Ohnishi, N., Rozenblatt-Rosen, O., Meyerson, M., Neel, B.G., and Hatakeyama, M. (2011). SHP2 tyrosine phosphatase converts parafibromin/Cdc73 from a tumor suppressor to an oncogenic driver. Mol Cell *43*, 45-56.

Takami, T., Kaposi-Novak, P., Uchida, K., Gomez-Quiroz, L.E., Conner, E.A., Factor, V.M., and Thorgeirsson, S.S. (2007). Loss of hepatocyte growth factor/c-Met signaling pathway accelerates early stages of N-nitrosodiethylamine induced hepatocarcinogenesis. Cancer Res *67*, 9844-9851.

Tan, X., Behari, J., Cieply, B., Michalopoulos, G.K., and Monga, S.P. (2006). Conditional deletion of beta-catenin reveals its role in liver growth and regeneration. Gastroenterology *131*, 1561-1572.

Tartaglia, M., Martinelli, S., Cazzaniga, G., Cordeddu, V., Iavarone, I., Spinelli, M., Palmi, C., Carta, C., Pession, A., Arico, M., Masera, G., Basso, G., Sorcini, M., Gelb, B.D., and Biondi, A. (2004). Genetic evidence for lineage-related and differentiation stage-related contribution of somatic PTPN11 mutations to leukemogenesis in childhood acute leukemia. Blood *104*, 307-313.

Tartaglia, M., Mehler, E.L., Goldberg, R., Zampino, G., Brunner, H.G., Kremer, H., van der Burgt, I., Crosby, A.H., Ion, A., Jeffery, S., Kalidas, K., Patton, M.A., Kucherlapati, R.S., and Gelb, B.D. (2001). Mutations in PTPN11, encoding the protein tyrosine phosphatase SHP-2, cause Noonan syndrome. Nat Genet *29*, 465-468.

Tartaglia, M., Niemeyer, C.M., Fragale, A., Song, X., Buechner, J., Jung, A., Hahlen, K., Hasle, H., Licht, J.D., and Gelb, B.D. (2003). Somatic mutations in PTPN11 in juvenile myelomonocytic leukemia, myelodysplastic syndromes and acute myeloid leukemia. Nat Genet *34*, 148-150.

Thorgeirsson, S.S., and Santoni-Rugiu, E. (1996). Transgenic mouse models in carcinogenesis: interaction of c-myc with transforming growth factor alpha and hepatocyte growth factor in hepatocarcinogenesis. Br J Clin Pharmacol *42*, 43-52.

Tsutsumi, R., Masoudi, M., Takahashi, A., Fujii, Y., Hayashi, T., Kikuchi, I., Satou, Y., Taira, M., and Hatakeyama, M. (2013). YAP and TAZ, Hippo signaling targets, act as a rheostat for nuclear SHP2 function. Dev Cell *26*, 658-665.

Vacik, T., Stubbs, J.L., and Lemke, G. (2011). A novel mechanism for the transcriptional regulation of Wnt signaling in development. Genes Dev *25*, 1783-1795.

van Dijk, D., Sharma, R., Nainys, J., Yim, K., Kathail, P., Carr, A.J., Burdziak, C., Moon, K.R., Chaffer, C.L., Pattabiraman, D., Bierie, B., Mazutis, L., Wolf, G., Krishnaswamy, S., and Pe'er, D. (2018). Recovering Gene Interactions from Single-Cell Data Using Data Diffusion. Cell *174*, 716-729.e727.

Van Rooijen, N., and Sanders, A. (1994). Liposome mediated depletion of macrophages: mechanism of action, preparation of liposomes and applications. J Immunol Methods *174*, 83-93.

Vaseva, A.V., Blake, D.R., Gilbert, T.S.K., Ng, S., Hostetter, G., Azam, S.H., Ozkan-Dagliyan, I., Gautam, P., Bryant, K.L., Pearce, K.H., Herring, L.E., Han, H., Graves, L.M., Witkiewicz, A.K., Knudsen, E.S., Pecot, C.V., Rashid, N., Houghton, P.J., Wennerberg, K., Cox, A.D., and Der, C.J. (2018). KRAS Suppression-Induced Degradation of MYC Is Antagonized by a MEK5-ERK5 Compensatory Mechanism. Cancer Cell *34*, 807-822 e807.

Wang, E.Y., Yeh, S.H., Tsai, T.F., Huang, H.P., Jeng, Y.M., Lin, W.H., Chen, W.C., Yeh, K.H., Chen, P.J., and Chen, D.S. (2011). Depletion of beta-catenin from mature hepatocytes of mice promotes expansion of hepatic progenitor cells and tumor development. Proc Natl Acad Sci U S A *108*, 18384-18389.

Wei, J.C., Meng, F.D., Qu, K., Wang, Z.X., Wu, Q.F., Zhang, L.Q., Pang, Q., and Liu, C. (2015). Sorafenib inhibits proliferation and invasion of human hepatocellular carcinoma cells via up-regulation of p53 and suppressing FoxM1. Acta Pharmacol Sin *36*, 241-251.

Wen, L., Xin, B., Wu, P., Lin, C.H., Peng, C., Wang, G., Lee, J., Lu, L.F., and Feng, G.S. (2019). An Efficient Combination Immunotherapy for Primary Liver Cancer by Harmonized Activation of Innate and Adaptive Immunity in Mice. Hepatology *69*, 2518-2532.

Wong, C., Chen, C., Wu, Q., Liu, Y., and Zheng, P. (2015). A critical role for the regulated wnt-myc pathway in naive T cell survival. J Immunol *194*, 158-167.

Wong, G.S., Zhou, J., Liu, J.B., Wu, Z., Xu, X., Li, T., Xu, D., Schumacher, S.E., Puschhof, J., McFarland, J., Zou, C., Dulak, A., Henderson, L., Xu, P., O'Day, E., Rendak, R., Liao, W.L., Cecchi, F., Hembrough, T., Schwartz, S., Szeto, C., Rustgi, A.K., Wong, K.K., Diehl, J.A., Jensen, K., Graziano, F., Ruzzo, A., Fereshetian, S., Mertins, P., Carr, S.A., Beroukhim, R., Nakamura, K., Oki, E., Watanabe, M., Baba, H., Imamura, Y., Catenacci, D., and Bass, A.J. (2018). Targeting wild-type KRAS-amplified gastroesophageal cancer through combined MEK and SHP2 inhibition. Nat Med *24*, 968-977.

Wu, T., and Dai, Y. (2017). Tumor microenvironment and therapeutic response. Cancer Lett *387*, 61-68.

Wu, T.R., Hong, Y.K., Wang, X.D., Ling, M.Y., Dragoi, A.M., Chung, A.S., Campbell, A.G., Han, Z.Y., Feng, G.S., and Chin, Y.E. (2002). SHP-2 is a dual-specificity phosphatase involved in Stat1 dephosphorylation at both tyrosine and serine residues in nuclei. J Biol Chem *277*, 47572-47580.

Xiong, X., Kuang, H., Ansari, S., Liu, T., Gong, J., Wang, S., Zhao, X.Y., Ji, Y., Li, C., Guo, L., Zhou, L., Chen, Z., Leon-Mimila, P., Chung, M.T., Kurabayashi, K., Opp, J., Campos-Perez, F., Villamil-Ramirez, H., Canizales-Quinteros, S., Lyons, R., Lumeng, C.N., Zhou, B., Qi, L., Huertas-Vazquez, A., Lusis, A.J., Xu, X.Z.S., Li, S., Yu, Y., Li, J.Z., and Lin, J.D. (2019). Landscape of Intercellular Crosstalk in Healthy and NASH Liver Revealed by Single-Cell Secretome Gene Analysis. Mol Cell *75*, 644-660 e645.

Xu, M., Xu, H.H., Lin, Y., Sun, X., Wang, L.J., Fang, Z.P., Su, X.H., Liang, X.J., Hu, Y., Liu, Z.M., Cheng, Y., Wei, Y., Li, J., Li, L., Liu, H.J., Cheng, Z., Tang, N., Peng, C., Li, T., Liu, T., Qiao, L., Wu, D., Ding, Y.Q., and Zhou, W.J. (2019a). LECT2, a Ligand for Tie1, Plays a Crucial Role in Liver Fibrogenesis. Cell *178*, 1478-1492 e1420.

Xu, Z., Xu, M., Liu, P., Zhang, S., Shang, R., Qiao, Y., Che, L., Ribback, S., Cigliano, A., Evert, K., Pascale, R.M., Dombrowski, F., Evert, M., Chen, X., Calvisi, D.F., and Chen,

X. (2019b). The mTORC2-Akt1 Cascade Is Crucial for c-Myc to Promote Hepatocarcinogenesis in Mice and Humans. Hepatology *70*, 1600-1613.

Yamaji, S., Zhang, M., Zhang, J., Endo, Y., Bibikova, E., Goff, S.P., and Cang, Y. (2010). Hepatocyte-specific deletion of DDB1 induces liver regeneration and tumorigenesis. Proc Natl Acad Sci U S A *107*, 22237-22242.

Yang, J.D., and Heimbach, J.K. (2020). New advances in the diagnosis and management of hepatocellular carcinoma. BMJ *371*, m3544.

Yang, W., Wang, J., Moore, D.C., Liang, H., Dooner, M., Wu, Q., Terek, R., Chen, Q., Ehrlich, M.G., Quesenberry, P.J., and Neel, B.G. (2013). Ptpn11 deletion in a novel progenitor causes metachondromatosis by inducing hedgehog signalling. Nature *499*, 491-495.

Yochum, G.S., Cleland, R., and Goodman, R.H. (2008). A genome-wide screen for beta-catenin binding sites identifies a downstream enhancer element that controls c-Myc gene expression. Mol Cell Biol *28*, 7368-7379.

Yuan, L., Yu, W.M., Yuan, Z., Haudenschild, C.C., and Qu, C.K. (2003). Role of SHP-2 tyrosine phosphatase in the DNA damage-induced cell death response. J Biol Chem *278*, 15208-15216.

Zhang, Q., He, Y., Luo, N., Patel, S.J., Han, Y., Gao, R., Modak, M., Carotta, S., Haslinger, C., Kind, D., Peet, G.W., Zhong, G., Lu, S., Zhu, W., Mao, Y., Xiao, M., Bergmann, M., Hu, X., Kerkar, S.P., Vogt, A.B., Pflanz, S., Liu, K., Peng, J., Ren, X., and Zhang, Z. (2019). Landscape and Dynamics of Single Immune Cells in Hepatocellular Carcinoma. Cell *179*, 829-845 e820.

Zheng, C., Zheng, L., Yoo, J.K., Guo, H., Zhang, Y., Guo, X., Kang, B., Hu, R., Huang, J.Y., Zhang, Q., Liu, Z., Dong, M., Hu, X., Ouyang, W., Peng, J., and Zhang, Z. (2017a). Landscape of Infiltrating T Cells in Liver Cancer Revealed by Single-Cell Sequencing. Cell *169*, 1342-1356 e1316.

Zheng, K., Cubero, F.J., and Nevzorova, Y.A. (2017b). c-MYC-Making Liver Sick: Role of c-MYC in Hepatic Cell Function, Homeostasis and Disease. Genes (Basel) *8*.